

Combined analyses of long-term (1990-2015) water quality and plankton dynamics of Upper Klamath Lake (Phase II)



Prepared by:

Jens M. Nielsen¹, Jacob Kann², Michael T. Brett¹

Prepared for:

Klamath Tribes Natural Resources Department

Chiloquin, Oregon

July 2018

¹Department of Civil and Environmental Engineering, University of Washington, Seattle, Washington 98105, USA

²Aquatic Ecosystem Sciences, 295 East Main St., Ashland, OR 97520, USA

Combined analyses of long-term (1990-2015) water quality and plankton dynamics of Upper Klamath Lake (Phase II)

Prepared by:

Jens M. Nielsen¹, Jacob Kann², Michael T. Brett¹

Prepared for:

Klamath Tribes Natural Resources Department

P.O. Box 436

Chiloquin, OR

October 15, 2017

¹Department of Civil and Environmental Engineering, University of Washington, Seattle, Washington 98105, USA

²Aquatic Ecosystem Sciences, 295 East Main St., Ashland, OR 97520, USA

Suggested citation:

Nielsen, J. M., Kann, J., and Brett M. T. 2018. Combined analyses of long-term (1990-2015) water quality and plankton dynamics of Upper Klamath Lake (Phase II). Prepared by Aquatic Ecosystem Sciences LLC and University of Washington for the Klamath Tribes Natural Resources Department. 107p.

Executive Summary

This report summarizes the water quality and plankton dynamics, particularly for chlorophyll-a and the dominant cyanobacteria species *Aphanizomenon flos-aquae* in Upper Klamath Lake (UKL). The report focuses on the Klamath Tribes' long-term limnological monitoring program using data from 1990-2015 from 9 stations that were consistently monitored throughout the time period. A primary task of this effort was the combination and comparative analyses of the water quality, phytoplankton and zooplankton databases. These comparative analyses are needed to understand the underlying processes that drive algal biomass and plankton populations and are essential when predicting how ecosystems respond to environmental perturbations. The analyses also include seasonal and long-term trend analyses and multivariate assessments of the combined datasets.

Here, we combine three separate lake monitoring databases containing data from 1990-2015 for water quality, and phytoplankton and zooplankton composition which were previously standardized separately (Phase I Report; Kann et al. 2015). Our goal was to provide an overview and description of both the seasonal and long-term dynamics of the most important water quality factors and plankton species. By coupling the water quality and plankton data we then determine how the growth and decline of the annual cyanobacterial bloom influences lake water quality and the dynamics of other plankton species in the lake. This includes analyses of the phenology (e.g., annual bloom timing) of the most important plankton species and water quality parameters'. Furthermore, we use multivariate statistics, such as multiple linear regression models, two-way cluster analyses and Mann-Kendall trend tests to better understand the dominant factors that influence the lake's limnological dynamics.

Major findings

- The seasonal plankton patterns in UKL are highly consistent. However, the timing and magnitude of the *Aphanizomenon flos-aquae* bloom and resulting poor water quality varies temporally from year to year.
- Chlorophyll-a concentration and Cyanophyta biovolume, which in the summer represents >99 percent of the total algal biomass are highly correlated, confirming that chlorophyll-a is a very good predictor of total phytoplankton biomass in UKL. Furthermore, chlorophyll-a is also a good predictor of the cyanobacteria *Aphanizomenon flos-aquae* because of this single species' dominance during the June to September growing season. Analyses of phenology (timing of bloom onset, peak timing and decline) also support the observation of a strong relationship between chlorophyll-a and total Cyanobacteria (i.e., *Aphanizomenon flos-aquae*).
- Because chlorophyll-a was a good proxy for total phytoplankton a regression analysis was developed to allow interpolation of the total phytoplankton biomass for 4 years with missing phytoplankton data (i.e., 2000-2003). However, chlorophyll-a does not fully capture extremes (high data points) in the algae data. This regression model works well to predict *Aphanizomenon flos-aquae* biovolume from June to October, when that species is the dominant phytoplankton species.

- Phenology analyses of the plankton data showed that warmer spring temperatures result in an earlier phytoplankton bloom. This pattern was reflected in phenology analyses of chlorophyll a (when using June-October data). This pattern was also reflected in the phenology analyses of the *Aphanizomenon flos-aquae* data, as evident in both the timing of the onset and timing of the peak of the bloom.
- Years with an earlier phytoplankton bloom tended to have lower dissolved oxygen concentrations in late summer. This suggests that an early bloom onset may contribute to more stressful habitat conditions for endangered suckers.
- Mann-Kendall trend analyses showed a decreasing trend in total chlorophyll-a and nitrogen concentrations. However, some phytoplankton taxa such as several diatom species and the toxin producing *Microcystis aeruginosa* appear to have increased in abundance from 1990 to 2015.
- We found few long-term increases or decreases in the phenology of chlorophyll-a, total nitrogen and total phosphorus concentrations. In other words, the dates of the *Aphanizomenon* bloom onset and bloom peak do not occur consistently earlier or later now compared to the early 1990s.
- *Daphnia* increase in abundance in the early summer similar to the main cyanobacteria *Aphanizomenon flos-aquae*. Despite the apparent positive correlation between *Daphnia* and *Aphanizomenon flos-aquae*, *Daphnia* typically appear several weeks earlier in the season suggesting co-existence of these two species and not necessarily that *Aphanizomenon flos-aquae* is a primary dietary resource for *Daphnia*.
- The times series for the diatom bloom and *Daphnia* population development suggests the diatom bloom usually peaks a month prior to the spring increase in *Daphnia* and then declines markedly when *Daphnia* reach high biomass levels. These patterns suggest diatoms drive the initial spring upswing in *Daphnia* biomass, and then *Daphnia* at least partially cause the diatom bloom to collapse. Declining silica concentrations and increasing water temperatures may also play an important role in the June decline in diatom biomass.
- The increase in *Daphnia* coinciding with the decline in diatoms is also associated with a clear-water phase that directly precedes the onset of *Aphanizomenon* and increase in heterocyst biomass occurring in late-May and early-June. These patterns suggest that increasing temperatures along with increased water column light foster desirable growth conditions for *Aphanizomenon*, especially considering the high light/energy requirement for nitrogen fixation.
- Similarly, *Aphanizomenon flos-aquae* governs phytoplankton and zooplankton species richness seasonally, with high *Aphanizomenon* biomass suppressing plankton species richness. Multivariate analyses of phytoplankton community similarity analyses confirmed the regulating role *Aphanizomenon flos-aquae* has for other plankton species.
- A second *Aphanizomenon* peak occurring in late summer (August and September) in some but not all years, suppresses phytoplankton species richness in UKL until this bloom declines. In Agency Lake (AL) the second *Aphanizomenon* peak is much less pronounced.

- Multivariate analyses were implemented using various seasonal (e.g., April-May for diatoms or 15 May to 10 June for bloom onset) means for a given year of the long-term database. Multiple linear regression analyses indicate that diatom biomass was associated with cooler and windier conditions during the spring months, as well as decreasing soluble reactive phosphorus concentrations indicating uptake. A similar trend was found with soluble reactive phosphorus during the *Aphanizomenon* bloom onset period, and higher biomass in general was associated with a more stable water column. Although other variables such as nitrogen to phosphorus ratios and the light extinction coefficient were often significant in the models, it was difficult to differentiate between cause and effect since, for example, the positive association with light extinction (high extinction = lower light) for most models likely illustrates the effect of biomass accrual on water column light rather than the effect of light on bloom development, even though graphical analysis indicated a consistent year-to-year clear-water phase prior to *Aphanizomenon* onset.
- Hierarchical clustering and redundancy analyses both indicate that years with higher than normal temperatures (e.g., 2014 and 2015) also had higher levels of *Microcystis*, and years with higher relative thermal resistance to mixing were associated with higher than average *Aphanizomenon flos-aquae* biomass. In contrast, years that had higher spring abundances of diatoms, Cryptophyta and Chlorophyta generally occurred during colder and also more mixed years. Finally two-way and seasonal two-way cluster analyses indicated that high temperature and soluble reactive phosphorus was associated with high biomass of *Microcystis aeruginosa*, and higher than normal diatom abundance seemed to occur in years with relatively high wind speeds and thus a higher water column mixing, which likely promotes both nutrient and diatom resuspension in the spring

Database updates

- Data from three separate monitoring databases of water quality (1990-2016), phytoplankton and zooplankton for the 1990-2015 time period were combined. This combined database contains twice monthly observations from all stations from 1990-2015 (1990-2016 for water quality) and is available as an appendix in CSV format. In cases where more than one measurement occurred within the same bimonthly interval (two weeks), an average value was calculated for that period
- A correction to the chlorophyll data from 2008-2016 was implemented in the combined database, following comparative analyses of chlorophyll-a estimates before and after a laboratory change from spectrophotometric to fluorometric methodology (Appendix III in Kann 2018).
- As part of the standardization of the database, adjacent stations PM and FB were combined for data consistency. The combined data for these stations is now presented as the station “UKL out” which represents the water quality and plankton dynamics close to Pelican Marina at the southern-most part of UKL near the outflow.
- Analyses also indicate that zooplankton biomass estimates from 1998-2003 are very low and we urge caution regarding the use of biomass and abundance data from those years. Our analyses seem to indicate a systematic under estimation of both abundance

and biomass from these years. It is suggested that analyses which incorporate biomass or abundance data from the zooplankton be restricted to data from 1990-1999 and 2004-2016. However, we note that the percent biomass data appear to be valid for the entire period as this data is not influenced by the systematic underestimation.

- A regression model was developed to predict total phytoplankton biomass for the missing years 2000-2003 based on chlorophyll-a biomass. This regression model can similarly be used to predict Cyanobacteria (mainly *Aphanizomenon flos-aquae*) biovolume for the period June-October when this species comprises >99% of the phytoplankton community biomass.

General future recommendations

- The long-term Mann-Kendall analyses indicated interesting long-term patterns, such as declining chlorophyll-a, total phosphorus and total nitrogen concentrations during the monitoring period (1990-2016). However, a time-series with only 27 years data is still only capable of detecting relatively short-term (annual to less than decadal) climatic cycles. Thus, in order to be able to capture potential long-term biological responses to future climatic changes continuation of UKL monitoring is essential.
- Our findings suggest that *Daphnia* feed on other species than the dominant *Aphanizomenon flos-aquae*. For example, Cryptophyta biomass was negatively related to *Daphnia* biomass, and recent dietary assessments using fatty acid analyses support this observation (M.T. Brett, unpublished data) and furthermore, the majority of the *Aphanizomenon* are filamentous and likely to be too large to be edible for *Daphnia*. It is also evident from our data analyses that *Daphnia* commonly increase in numbers earlier in summer prior to the onset of the *Aphanizomenon flos-aquae* bloom. However, to fully estimate the importance of diatoms, Cryptophytes and other available algae for the diet of *Daphnia* it is suggested that phytoplankton production estimates would be a useful future analysis to further assess the importance of the understory phytoplankton as a food source for herbivorous zooplankton. Such information would help better elucidate the most important trophic dynamics in the plankton in UKL.
- Continued monitoring to increase sample size for inter-annual models is recommended, as is additional modelling efforts to describe planktonic controlling factors in Upper Klamath Lake. These models should incorporate site effects as well as non-linear functions.

Contents

Executive Summary.....	iii
List of Tables.....	viii
INTRODUCTION.....	1
Primary Goals.....	1
METHODS.....	2
Data Sources.....	2
Sample Collection Methodology	3
Climate Data.....	6
Statistical Methods	6
Characterizing Phenology	7
Multivariate analyses.....	8
RESULTS/DISCUSSION	10
Chlorophyll-a and total phytoplankton regression model	10
Supporting climate data	11
General characteristics of the combined data.....	16
Seasonal trends and general species characteristics	19
Phytoplankton species in UKL and AL.....	19
Seasonal cycle of the total phytoplankton	19
Phytoplankton species	27
Zooplankton.....	34
Combined seasonal cycles of plankton and major water quality parameters	43
Species richness.....	45
Mann-Kendall analyses of long-term trends	47
Long-term changes of specific key variables	50
Mann-Kendall estimates of multiple time-series.....	50
Long-term relationships between water quality, chlorophyll-a, and <i>Aphanizomenon flos-aquae</i>	51
Monthly correlations among key variables	57
Phenology models to assess factors influencing the bloom onset, peak and collapse.....	65
Mann-Kendall trend analyses of phenology estimates	69
Temperature and phytoplankton phenology	71
Plankton trophic interactions— <i>Daphnia</i> and phytoplankton	75
Multivariate Analyses.....	77
Multiple linear regression models	77

Hierachal clustering analyses	82
Redundancy analyses.....	82
Two-way cluster analyses.....	84
SUMMARY	86
Spring temperature regulates summer bloom phenology	86
The influence of phenology on oxygen levels in Upper Klamath Lake	87
The consequences of changing phenology on the plankton food web	87
<i>Daphnia</i> and cyanobacteria co-existence.	87
The importance of long-term temperature regimes in Upper Lake Klamath	88
REFERENCES	89

List of Tables

Table 1. Seasonal sampling frequency for Upper Klamath Lake primary stations, 1990-2015. Blue shading denotes the core sampling season occurring May-October for primary stations with additional samples covering the winter months available for UKL_OUT. Sampling for CP begins in 1997.	5
Table 2. Limnological parameters sampled in Upper Klamath Lake, 1990-2015.....	5
Table 3: P-values of Mann-Kendall trend analyses based on mean biomass or biovolume data for each month and for the period April to October, from 1990-2015 (2004-2015 for zooplankton) for Agency Lake. Red denotes statistically decreasing trends while blue denotes statistically increasing trends ($p<0.05$).	48
Table 4. P values of Mann-Kendall long-term trend analyses based on mean biomass or biovolume data for each month and for the period April to October, from 1990-2015 (2004-2015 for zooplankton) for UKL, and combined for all months. Red denotes statistically decreasing trends while blue denotes statistically increasing trends ($p<0.05$) with the value of the test statistics is also presented.	49
Table 5: Phenology correlations between the major variables in the main part of Upper Klamath Lake. Pairwise correlations were done for the onset measurements of all variables, the peak timing decline and length of season, respectively. Data show the r^2 for all pairwise correlations, with blue denoting all significant positive correlations ($p<0.05$).	69
Table 6: Mann-Kendall trend analyses of phenology estimates of onset, peak timing, decline and length of season for all major variables measured at stations in the main part of Upper Klamath Lake. Significant p-values are denoted in red for $p<0.05$, and light red for $p < 0.10$, and in this case all negative as shown by the negative Tau value.	70
Table 7. Regional Mann-Kendall trend test for chlorophyll-a estimated for all individual stations.	70
Table 8. Model summary of the diatom model using dissolved nutrient and physical data.....	78
Table 9. Model summary of the bloom onset model using dissolved nutrients and physical data:.....	79
Table 10. Model summary of the Chl-a bloom onset model using ratio and physical data:	80
Table 11. Model summary of the bloom peak model using dissolved nutrients and physical data:	80
Table 12. Model summary of the bloom peak model using nutrient ratio and physical data:	81

List of Figures

Figure 1: Location of UKL and primary long-term sampling stations. The analyses presented here utilized data from AS, AN in Agency Lake (AL), NB, WB, ML, ER, SB, MN in the main part of Upper Klamath Lake (UKL). PM and FB were combined into a single station named UKL OUT.....	4
Figure 2. Spatial-temporal sampling matrix for Upper Klamath Lake primary stations, 1990-2015.	4
Figure 3: Schematic of phenology metrics obtained by the phenology modeling	8
Figure 4: Linear model based on type II regression of logged values of chlorophyll-a (mg [DW/L]) and log total phytoplankton (biovolume [mm^3/L]). Regression model: log total phytoplankton = 0.9276*log chlorophyll-a-0.9513, p<0.01, $r^2=0.68$	11
Figure 5: Temporal changes of the A) Pacific Decadal Oscillation (black), Upper Klamath Lake modeled air temperature (light blue) from 1900-2015, where solid lines are loess smoothed data for each time-series, B) modeled spring air temperature (light blue) and mean spring water temperature (dark blue) from 1990-2015 and C) spring precipitation (grey) and summer Lake elevation (black) from 1990-2015.....	12
Figure 6. Correlations among monthly means of air temperature for the time periods 1990-2015 measured from Station 725895 - Klamath Falls airport.	14
Figure 7: Overview of warm (red) and cold (blue) air temperature anomalies from Station 725895 - Klamath Falls airport.....	15
Figure 8: Overview of above (red) or below (blue) wind speeds, from Station 725895 - Klamath Falls airport. The wind metric WSPD_MEAN4_MAX is the daily maximum of the four-hour running mean wind speed.....	16
Figure 9: nMDS of monthly Total phosphorus data from all years and each station, with the AL stations in red and the main UKL stations in blue.....	17
Figure 10: nMDS of monthly Total Nitrogen data from all years and all stations, with the AL stations in red and main the UKL stations in blue.....	17
Figure 11: nMDS of monthly chlorophyll-a data from all years for each station, with the AL stations in red and main the UKL stations in blue.....	18
Figure 12: nMDS of station Total phytoplankton from all years and each station, with AL stations in red and the 7 main UKL stations in blue.....	18
Figure 13: Seasonal dynamics of mean of total phosphorus ($\mu\text{g}/\text{L}$) (a,c) UKL and (b,d) AL. Note: The data for AL in January consistent of only 1 measurement and should be treated with caution. Note: Y-axis are the same for a,c and b,d, respectively to allow comparison between UKL and AL. Boxplot is based on all individual data from each station and year.....	20
Figure 14: Seasonal dynamics of mean of total Soluble reactive phosphorus ($\mu\text{g}/\text{L}$) (a,c) UKL and (b,d) AL. Note: Y-axis are the same for a,c and b,d, respectively to allow comparison between UKL and AL. Boxplot is based on all individual data from each station and year.....	20
Figure 15: Seasonal dynamics of mean of total nitrogen ($\mu\text{g}/\text{L}$) (a,c) UKL and (b,d) AL. Note: Y-axis are the same for a,c and b,d, respectively to allow comparison between UKL and AL. Boxplot is based on all individual data from each station and year.....	21
Figure 16: Seasonal dynamics of mean of dissolved oxygen (mg/L) from (a,c) UKL and (b,d) AL stations. Note: Y-axis are the same for a,c and b,d, respectively to allow comparison between UKL and AL. Boxplot is based on all individual data from each station and year.....	21

Figure 17: Seasonal dynamics of mean pH from (a,c) UKL and (b,d) AL stations. Note: Y-axis are the same for a,c and b,d, respectively to allow comparison between UKL and AL. Boxplot is based on all individual data from each station and year.....	22
Figure 18: Seasonal dynamics of mean of chlorophyll-a biomass from (a, c) UKL and (b,d) AL. Note difference in scale of y-axis between line plots (a,c) and boxplots (b,d) . Boxplot is based on all individual data from each station and year.....	22
Figure 19: Square rooted phytoplankton species biovolume [mm ³ /L] from Upper Klamath Lake for all years and all stations, based on bi-monthly data. Note the break in scale for <i>Aphanizomenon flos-aquae</i>	23
Figure 20: Square rooted phytoplankton species biovolume [mm ³ /L] from Agency Lake for all years and all stations, based on bi-monthly data. Note the break in scale for <i>Aphanizomenon flos-aquae</i>	24
Figure 21: Seasonal dynamics of mean total phytoplankton biovolume from (a,c) UKL and (b,d) AL. Note difference in scale of y-axis between line plots and boxplots. Boxplot is based on all individual data from each station and year.....	25
Figure 22: Seasonal dynamics of mean of total Cyanophyta biovolume from (a,c) UKL and (b,d) AL. Note difference in scale of y-axis between line plots and boxplots. Boxplot is based on all individual data from each station and year.....	26
Figure 23: Seasonal dynamics of mean of total diatoms biovolume from (a,c) UKL and (b,d) AL. Note difference in scale of y-axis between line plots and boxplots. Please note the spike in the average April diatom biomass for AL is mainly due to a single very high value (339 mm ³ /l) which is above the y-axis limit in the boxplot for AL. Boxplots were based on all individual data from each station and year... ..	28
Figure 24: Seasonal dynamics of mean of total Cryptophyta biovolume from (a,c) UKL and (b,d) AL. Note difference in scale of y-axis between line plots and boxplots. Boxplot is based on all individual data from each station and year.....	28
Figure 25: Seasonal dynamics of mean of total Chlorophyta biovolume from (a,c) UKL and (b,d) AL. Note difference in scale of y-axis between line plots and boxplots. Boxplot is based on all individual data from each station and year.....	29
Figure 26: Seasonal dynamics of mean of <i>Aphanizomenon flos-aquae</i> . Biovolume from (a,c) UKL and (b,d) AL. Note difference in scale of y-axis between line plots and boxplots. Boxplot is based on all individual data from each station and year.....	29
Figure 27: Seasonal dynamics of mean of <i>Aphanizomenon flos-aquae</i> heterocysts. Biovolume from (a,c) UKL and (b,d) AL. Note difference in scale of y-axis between line plots and boxplots. Boxplot is based on all individual data from each station and year.....	30
Figure 28: Seasonal dynamics of mean of <i>Aphanizomenon flos-aquae</i> akinetes. Biovolume from (a,c) UKL and (b,d) AL. Note difference in scale of y-axis between line plots and boxplots. Boxplot is based on all individual data from each station and year.....	30
Figure 29: Seasonal dynamics of mean of <i>Microcystis aeruginosa</i> biovolume from (a,c) UKL and (b,d) AL. Note difference in scale of y-axis between line plots and boxplots. Boxplot is based on all individual data from each station and year.....	31
Figure 30: Seasonal dynamics of mean of <i>Tribonema</i> sp. biovolume from (a,c) UKL and (b,d) AL. Note difference in scale of y-axis between line plots and boxplots. Boxplot is based on all individual data from each station and year.....	31
Figure 31: Seasonal dynamics of mean of <i>Stephanodiscus niagarae</i> biovolume from (a,c) UKL and (b,d) AL. Note difference in scale of y-axis between line plots and boxplots. Boxplot is based on all individual data from each station and year.....	32
Figure 32: Seasonal dynamics of mean of <i>Asterionella formosa</i> from (a,c) UKL and (b,d) AL. Note difference in scale of y-axis between line plots and boxplots. Boxplot is based on all individual data from each station and year.....	32

Figure 33: Seasonal dynamics of mean of <i>Fragilaria</i> sp. from (a,c) UKL and (b,d) AL. Note difference in scale of y-axis between line plots and boxplots. Boxplot is based on all individual data from each station and year.....	33
Figure 34: Seasonal dynamics of mean of <i>Synedra</i> sp. from (a,c) UKL and (b,d) AL. Note difference in scale of y-axis between line plots and boxplots. Boxplot is based on all individual data from each station and year.....	33
Figure 35: Seasonal dynamics of mean of <i>Cryptomonas</i> sp. from (a,c) UKL and (b,d) AL. Note difference in scale of y-axis between line plots and boxplots. Boxplot is based on all individual data from each station and year.....	34
Figure 36: Square rooted zooplankton species biomass from Upper Klamath Lake for all years and all stations, based on bi-monthly data. Note the brake in scale for <i>Daphnia</i> sp.....	35
Figure 37: Square rooted zooplankton species biomass from Agency Lake for all years and all stations, based on bi-monthly data. Note the brake in the scale for <i>Daphnia</i> sp.....	36
Figure 38: Seasonal dynamics of mean of <i>Daphnia</i> sp. biomass from (a,c) UKL and (b,d) AL. Note difference in scale of y-axis between line plots and boxplots.	37
Figure 39: Seasonal dynamics of mean of <i>Leptodiaptomus ashlandi</i> biomass from (a,c) UKL and (b,d) AL. Note difference in scale of y-axis between line plots and boxplots.	37
Figure 40: Seasonal dynamics of mean of <i>Chydorus sphaericus</i> biomass from (a,c) UKL and (b,d) AL. Note difference in scale of y-axis between line plots and boxplots.....	38
Figure 41: Seasonal dynamics of mean of <i>Diacyclops thomasi</i> biomass from (a,c) UKL and (b,d) AL. Note difference in scale of y-axis between line plots and boxplots.....	38
Figure 42: Seasonal dynamics of mean of Calanoid copepodid biomass from (a,c) UKL and (b,d) AL. Note difference in scale of y-axis between line plots and boxplots.....	39
Figure 43: Seasonal dynamics of mean of <i>Leptodora kindtii</i> biomass from (a,c) UKL and (b,d) AL. Note difference in scale of y-axis between line plots and boxplots.....	39
Figure 44: Seasonal dynamics of mean of Copepoda nauplii biomass from (a,c) UKL and (b,d) AL. Note difference in scale of y-axis between line plots and boxplots.....	40
Figure 45: Seasonal dynamics of mean of <i>Euchlanis</i> sp. biomass from (a,c) UKL and (b,d) AL. Note difference in scale of y-axis between line plots and boxplots.	40
Figure 46: Seasonal dynamics of mean of <i>Epischura nevadensis</i> biomass from (a,c) UKL and (b,d) AL. Note difference in scale of y-axis between line plots and boxplots.....	41
Figure 47: Seasonal dynamics of mean of Cyclopoid copepodid biomass from (a,c) UKL and (b,d) AL. Note difference in scale of y-axis between line plots and boxplots.....	41
Figure 48: Seasonal dynamics of mean of <i>Keratella</i> sp. biomass from (a,c) UKL and (b,d) AL. Note difference in scale of y-axis between line plots and boxplots.	42
Figure 49: Seasonal dynamics of mean of <i>Synchaeta</i> sp. biomass from (a,c) UKL and (b,d) AL. Note difference in scale of y-axis between line plots and boxplots.	42
Figure 50: Upper Klamath Lake wide mean annual seasonal cycle of A) the biomass ($\mu\text{g/L}$) of chlorophyll-a (black), total phosphorus (grey) and total nitrogen (blue), B) total dissolved oxygen (black) and pH (blue), C) Soluble reactive phosphorus (black), Silica (grey) and Total inorganic nitrogen (blue), D) the biovolume (mm^3/L) of total phytoplankton (black line), Cyanophyta (green), diatoms (blue), Cryptophyta (red) and other phytoplankton taxa, E) Biomass (mg/L) of <i>Daphnia</i> sp. (black) and total copepods (blue), and F) species richness of phytoplankton (black) and zooplankton (blue).	43
Figure 51. Seasonal dynamics of Secchi disk (black) and diatoms (blue) for individual stations and averaged for all stations. Note that Secchi y-axis is reverted	44

Figure 52: Spatial overview of phytoplankton richness based on mean number of phytoplankton species across all years. Data interpolated from all stations (denoted in black). Scale is the same for each month.....	46
Figure 53: Spatial overview of <i>Aphanizomenon flos-aquae</i> biovolume [mm ³ /L] across all years. Data extrapolated from all stations in UKL and AL (denoted in black). Scale is the same for each month..	46
Figure 54: UKL long-term annual plot of mean chlorophyll-a, total phosphorus, total nitrogen, <i>Aphanizomenon flos-aquae</i> , <i>Microcystis aeruginosa</i> and diatoms averaged for the April to October time period. Red denotes below the overall long-term median biomass or biovolume for a specific time-series, and blue denotes above the long-term median. Trend statistics are presented in	50
Figure 55: A) Temporal dynamics of chlorophyll-a (black) and total phosphorus (red) in UKL and B) the correlation of yearly mean values (April-October) of chlorophyll-a and total phosphorus concentration ($r^2 = 0.36$, $p < 0.01$).....	51
Figure 56: A) Temporal dynamics of chlorophyll-a (black) and total nitrogen (red) in UKL and B) the correlation of yearly mean values (April-October) of chlorophyll-a and total nitrogen concentration ($r^2 = 0.64$, $p < 0.01$).	52
Figure 57: A) Temporal dynamics of <i>Aphanizomenon flos-aquae</i> (black) and total phosphorus (red) in UKL and B) the correlation of yearly mean values (April-October) of <i>Aphanizomenon flos-aquae</i> and total phosphorus concentration ($r^2 = 0.31$, $p < 0.01$).	53
Figure 58: A) Temporal dynamics of <i>Aphanizomenon flos-aquae</i> (black) and total nitrogen (red) in UKL and B) the correlation of yearly mean values (April-October) of <i>Aphanizomenon flos-aquae</i> and total nitrogen concentration ($r^2 = 0.46$, $p < 0.01$).	54
Figure 59: A) Temporal dynamics of chlorophyll-a (black) and dissolved oxygen (red) in UKL and B) the correlation of the mean values (August-September) of chlorophyll-a and dissolved oxygen.	55
Figure 60: Relationship between DO and pH for a) August-September data and b) a monthly lag between DO (Aug) and pH (July).	56
Figure 61: Correlation between total phosphorus and chlorophyll-a for each month.....	58
Figure 62: Correlation between total nitrogen and chlorophyll-a for each month.....	59
Figure 63: Correlation between total nitrogen and total-phosphorus for each month.....	60
Figure 64: Correlation between the nitrogen to phosphorus ratio and total-chlorophyll-a for each month.	61
Figure 65: Correlation between soluble reactive phosphorus and chlorophyll-a for each month.....	62
Figure 66: Correlation between total phosphorus and <i>Aphanizomenon flos-aquae</i> for each month.....	63
Figure 67: Correlation between total nitrogen and <i>Aphanizomenon flos-aquae</i> for each month.....	64
Figure 68: Correlation between chlorophyll-a and <i>Aphanizomenon flos-aquae</i> for each month.....	65
Figure 69: Phenology estimates onset, peak timing and decline, of A) chlorophyll-a, B) <i>Aphanizomenon flos-aquae</i> , C) total nitrogen concentration, D) <i>Daphnia</i> , E) total phosphorus concentration and F) soluble reactive phosphorus concentration in Upper Klamath Lake (Data from 7 stations in the main part of the lake).....	67
Figure 70: Estimates of the length of the season (number of days between onset and decline phenology estimates), of A) chlorophyll-a (grey), <i>Aphanizomenon flos-aquae</i> (green) and <i>Daphnia</i> (orange) and B) total phosphorus concentration (grey), total nitrogen concentration (green) and soluble reactive phosphorus concentration (orange) in Upper Klamath Lake (Data from 7 stations in the main part of the lake).	68
Figure 71: Air temperature in April-May showed a clear negative relationship with both the timing of the maximum peak and the start of the bloom in UKL, a pattern visible both in the chlorophyll-a and <i>Aphanizomenon flos-aquae</i> data.....	72

Figure 72: a) showing the long-term trend and b) correlation ($r^2 = 0.37$, $p < 0.01$) of the August - September mean of dissolved oxygen (black) and the estimated onset of the chlorophyll-a bloom (red) for UKL	72
Figure 73: a) showing the long-term trend and b) correlation ($r^2 = 0.37$, $p < 0.01$) of the August-September mean of DO (black) and the timing of the chlorophyll-a bloom peak, (red) for UKL 73	
Figure 74: a) showing the long-term trend and b) correlation ($r^2 = 0.39$, $p < 0.01$) of the minimum dissolved oxygen (black) from the period (April-October) and onset of the chlorophyll-a bloom (red) for UKL	73
Figure 75: a) showing the long-term trend and b) correlation ($r^2 = 0.38$, $p < 0.01$) of the minimum dissolved oxygen (black) from the period (April-October) and peak timing of the chlorophyll-a bloom (red) for UKL	74
Figure 76: Relationship between the timing of the chlorophyll-a onset and the total chlorophyll-a summer biomass (June-September).....	74
Figure 77 : Change <i>Daphnia</i> biomass in relation to A) <i>Aphanizomenon flos-aquae</i> biovolume ($r^2 = 0.36$, $p < 0.01$) in summer, B) relationship between <i>Aphanizomenon flos-aquae</i> and <i>Daphnia</i> peak timing ($r^2 = 0.27$, $p < 0.05$), relationship between summer <i>Daphnia</i> biomass and C) summer Cryptophyta biovolume ($r^2 = 0.34$, $p < 0.01$) and D) phytoplankton community dissimilarity ($r^2 = 0.38$, $p < 0.01$). Note that in B the black line denotes a 1:1 relationship to show the apparent offset in peak timing between <i>Daphnia</i> and <i>Aphanizomenon flos-aquae</i>	76
Figure 78: Relationship between A) the decline of the bloom and the summer <i>Daphnia</i> biomass, B) the chlorophyll-a and <i>Daphnia</i> peak timings, C) the chlorophyll-a decline and the Bray-Curtis dissimilarity index and D) the decline of the <i>Aphanizomenon flos-aquae</i> bloom and the phytoplankton Bray-Curtis dissimilarity index. Note that in B the black line is the 1:1 line and thus denotes if <i>Daphnia</i> peak before or after the chlorophyll-a bloom.	77
Figure 79. Overview of the time period for which chlorophyll-a data was used for the multiple linear regression models to assess the <i>Aphanizomenon flos-aquae</i> bloom onset.	79
Figure 80: nMDS of the major phytoplankton composition for each year, with cluster 1 (green), 2 (red) and 3 (black) as partitioned by the hierachal clustering analysis (PERMANOVA, $p < 0.01$)	82
Figure 81: Redundancy analyses showing the relationship between major phytoplankton groups and the primary physical and chemical parameters in the main part of UKL. Data based on annual specific means values (see method for full details). Yearly phytoplankton clusters based on the hierachal clustering analyses are denoted in red, green and black, respectively.....	83
Figure 82: Two-way cluster analysis of the data for the major variables (dendrogram on top, label on x-axis) for each year (y-axis, dendrogram on right). Black lines show major cluster separations.....	84
Figure 83: Two-way cluster analysis, based on season specific average values for the major variables in UKL (dendrogram on top, label on x-axis) for each year (y-axis, dendrogram on right). Black lines show major cluster separations.	86

INTRODUCTION

Eutrophic freshwater lakes are highly sensitive to increasing temperatures (Kosten et al. 2012) and summer dominance by cyanobacteria is often a key characteristic of these systems (Ger 2014). Upper Lake Klamath (UKL) in south central Oregon is a shallow hyper-eutrophic lake with a seasonal cycle of diatoms dominating in the spring, followed by a transition to intense summer dominance by cyanobacteria blooms. The summer blooms in UKL are strongly dominated by the diazotrophic *Aphanizomenon flos-aquae* and during some summers subsequent appearance of toxicigenic *Microcystis aeruginosa* (Kann and Smith 1999; Kann 2017; Eldridge et al. 2013). Paleolimnological evidence indicates that *Aphanizomenon flos-aquae* (as indicated by *Aphanizomenon flos-aquae* akinetes preserved in lake sediments) did not appear in UKL until the latter part of the 19th century and increased substantially after that time as a result of watershed and hydrological alterations (Bradbury et al., 2004; Eilers et al. 2004). The high biomass of *Aphanizomenon flos-aquae* has a negative impact on water quality and thus the habitat for endangered endemic fishes, e.g., the Lost River (*Deltistes luxatus*) and shortnose (*Chasmistes brevirostris*) suckers (Rasmussen 2011; USFWS 2012). *Daphnia pulicaria*, the most abundant zooplankton in UKL, are thought to be an important dietary resource for larval and juvenile fish, including endangered sucker species in UKL. The conservation of native and endangered sucker species is a primary conservation focus (Day et al. 2017). Recruitment failure over the last 30 years severely threatens the survival of these long-lived fishes (Hewett et al. 2017), and since 1988 these species have been recognized as endangered by both IUCN (International Union of Conservation of Nature) and USFWS (U.S. Fish and Wildlife Service) (Day et al. 2017).

Diminishing water quality, particularly during mid- to late-summer, as a direct consequence of high cyanobacteria biomass can cause spikes in pH (Kann and Smith 1999) and unionized ammonia, and sags in dissolved oxygen concentrations all of which frequently exceed critical water quality thresholds for sucker survival in UKL (Kann and Welch 2005). Fish kills and redistribution of adult suckers in UKL have been associated primarily with low dissolved oxygen (Perkins et al. 2000; Banish et al. 2009) due to bloom declines occurring during the latter part of the summer (Kann and Welch 2005). While previous studies have identified various controlling factors for algal blooms and water quality in UKL (e.g., Eldridge et al. 2013; Kann 2017), the current analysis is intended to evaluate chemical, physical and potentially biological factors that regulate and promote periods of poor water quality, as well as factors that govern plankton community dynamics both seasonally and long-term. By incorporating the inherent variability in inter-annual and seasonal climatic factors and bloom periodicity, and by increasing statistical power to detect potential effects through a large number of samples, long-term datasets provide a means to quantify the complex interactions that are prevalent in many ecosystems (e.g., Lindenmayer et al. 2012; Dodds et al. 2012).

Primary Goals

The long-term monitoring of water quality, and phytoplankton and zooplankton communities by The Klamath Tribes of Oregon, that now includes 26 years of data, provides the opportunity to

conduct a combined analysis of the plankton ecology and water quality dynamics for UKL and Agency Lake (AL) (Figure 1). Specifically, in this report we,

- Combine three separate databases of lake monitoring data from 1990-2015 for water quality, phytoplankton and zooplankton composition. (These raw data are available as an appendix in CSV format).
- Describe the seasonal lake dynamics of the major chemical, physical and biological variables, and characterize the spatial and temporal variability in UKL.
- Assess how climate perturbations influence the timing (i.e., phenology) of the bloom initiation and magnitude of the seasonal phytoplankton cycle.
- Determine how the growth and decline of the annual cyanobacterial bloom influences lake water quality and the dynamics of other plankton species in the lake.
- Evaluate long-term trends in dominant plankton species, chlorophyll-a, and major water quality parameters.
- Evaluate major drivers of bloom phenology and water quality dynamics using multivariate techniques.

The analyses presented here focuses on chlorophyll-a and the most dominant phytoplankton and zooplankton taxa/species, such as *Aphanizomenon flos-aquae*, various diatoms, and *Daphnia pulicaria*. Analyses of other data are also presented when relevant.

METHODS

Data Sources

The Klamath Tribes have conducted monitoring at 15 stations since 1990; however, this report focusses on the 9 primary stations that were analyzed consistently throughout the entire 1990-2015 period (Figure 1). These stations are: AS and AN in Agency Lake (AL), and UKL_OUT, NB, WB, ML, ER, SB, MN in the main part of Upper Klamath Lake (UKL). The station CP is considered a primary station but was not sampled until 1997 and is thus not included in our long-term analyses. UKL_OUT represents the combined data from the two stations FB and PM to fully capture the temporal patterns of the outlet of UKL, including sampling during the winter months. These two stations are closely situated but are generally sampled at different times of the year (Figure 2; Table 1). FB was only consistently sampled until 1997, intermittently between 1998 and 2006, and consistently during the winter months from 2011 to 2015 (Figure 2). In general, PM was consistently sampled during the April-October sampling period.

Our initial analyses showed that temporal physical, chemical and biological patterns differed between the AL stations and UKL stations (See Results section on spatial differences), thus for the majority of our analyses we examined these two areas separately, something that had also been done previously (Jassby and Kann 2010; Kann 2017). Data used in this report are primarily based on water column averages from twice monthly sampling. For long-term time-series analyses, such as the phenology calculations, we used data from the April-October period where sampling was relatively consistent for all years. The three data resources (water quality, phytoplankton and zooplankton databases) were merged and used for the analyses in this report. Prior to merging the databases, a thorough standardization of the plankton data, including

comparison of laboratory consistency was done in Phase I (Kann et al. 2015), allowing robust analyses of the entire sampling period (1990-2015).

Sample Collection Methodology

Methods followed The Klamath Tribes' established procedures for field collection and laboratory analysis of water quality parameters (see The Klamath Tribes 2014; 2013 for a complete description of these methods). Limnological data (Table 2) were collected approximately biweekly from the end of April through October¹ at 10 standardized stations in UKL and AL (Figure 1; Figure 2). Detailed descriptions of the UKL water quality sampling program from which the primary water quality data were obtained are presented in a series of annual data reports (e.g., Kann et al 2017) and in The Klamath Tribes Standard Operating Procedures (SOP) for UKL Water Quality Field Sampling (The Klamath Tribes 2014; 2013).

Phytoplankton samples were collected concomitant with the depth-integrated water quality samples and decanted to opaque polyethylene bottles and preserved with Acid-Lugol's solution (APHA 1985) to obtain a final preservative concentration of 1% (1 ml Lugol's/100 ml's of sample). Although the laboratory methodology for phytoplankton biomass varied over time (see Kann et al. 2015 for details), the primary methods utilized were the Utermöhl method (Utermöhl 1958, Lund et al 1958, APHA 1989, Rott 1981, Willen 1976) and two permanent mounting methods for preparing algal samples for counting: 1) based on APHA Standard Methods (1992), 10200.D.2; and McNabb (1960), and 2) an HPMA permanent mounting method for preparing algal samples for counting (Crumpton 1987, St. Amand 1990). In all cases cell volumes (biovolume) were determined by utilizing cell dimensions and volumetric equations for shapes most resembling the species form (e.g., Willen 1976; Bergquist 1985, Olrik et al. 1998, Hillebrand et al. 1999, and St. Amand 1990). The total biovolume of each species was then computed as cell abundance (individuals L⁻¹) multiplied by average individual volume (μm^3). Final biovolume estimates are reported as mm³ L⁻¹, which approximates wet weight biomass in mg L⁻¹.

As outlined in Kann (1998) crustacean zooplankton and rotifers were sampled at each location through 2002 using a 12 L Schindler-Patalas trap with a 64 μm mesh. Beginning in 2003 a 30 L Schindler-Patalas trap with a 64 μm mesh was used (Klamath Tribes 2013). A depth-integrated sample was obtained by taking one sample from between the surface to 1 m depth interval (target depth 0.5 m), one from between the 1 m above bottom to bottom interval (target depth 0.5 m off-bottom), and then combining the two samples for a total of 24 L filtered (60 L for 2003 and onwards). The exception to this was the deeper Eagle Ridge site (ER) where a third sample was collected from the midpoint of the water column (approximately 3 m) for a total of 36 L filtered (90 L for 2003), but only through 2003².

¹ As noted above the Fremont Bridge (FB) station at the outlet of UKL was sampled prior to April and after October, and based on analyses showing that PM and FB values follow a 1:1 trajectory values for both stations are included here as the combined station (UKL_OUT).

² Beginning in 2004 the integration protocol at ER was similar to other stations.

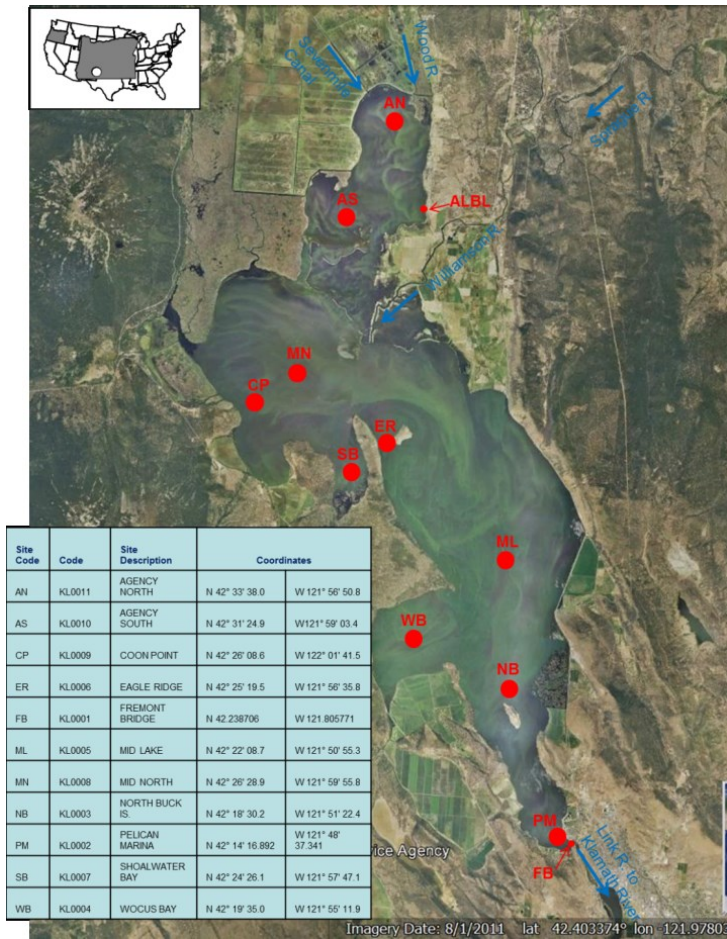


Figure 1: Location of UKL and primary long-term sampling stations. The analyses presented here utilized data from AS, AN in Agency Lake (AL), NB, WB, ML, ER, SB, MN in the main part of Upper Klamath Lake (UKL). PM and FB were combined into a single station named UKL OUT.

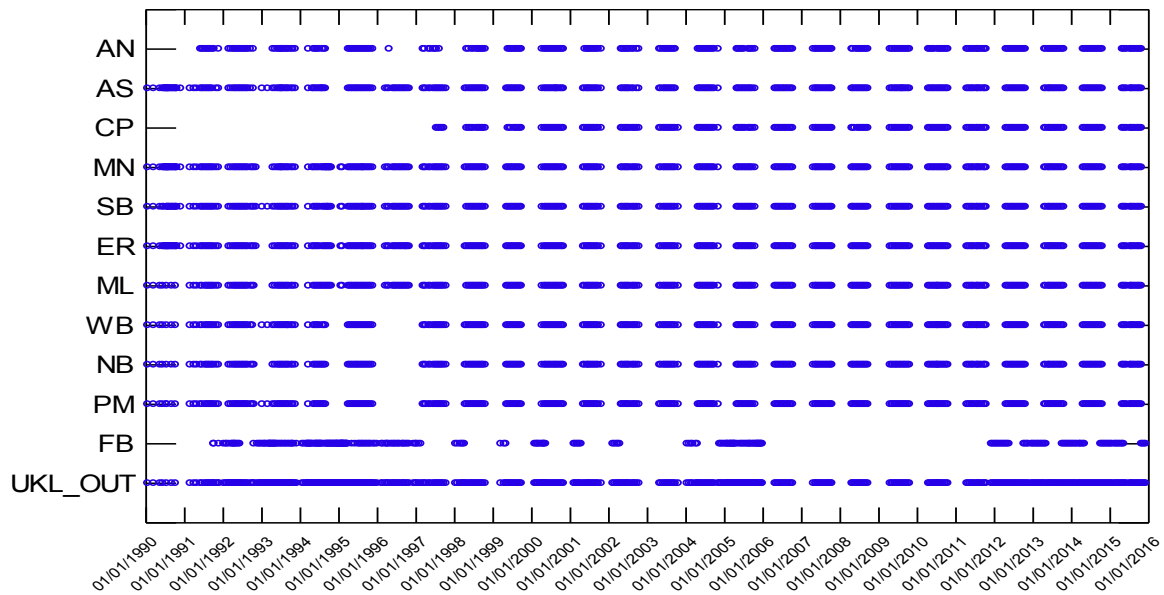


Figure 2. Spatial-temporal sampling matrix for Upper Klamath Lake primary stations, 1990-2015.

Table 1. Seasonal sampling frequency for Upper Klamath Lake primary stations, 1990-2015. Blue shading denotes the core sampling season occurring May-October for primary stations with additional samples covering the winter months available for UKL_OUT. Sampling for CP begins in 1997.

Month	UKL_OUT	FB	PM	NB	WB	ML	ER	SB	MN	CP	AS	AN	Total
1	29	30	2	1	2	2	2	3	2	0	2	0	75
2	35	35	2	2	2	3	3	3	3	0	2	1	91
3	44	40	6	5	6	6	6	7	6	0	7	4	137
4	55	37	23	23	23	24	26	24	26	14	26	20	321
5	63	21	49	48	48	49	49	49	49	36	49	44	554
6	64	13	53	53	53	55	57	56	57	39	57	50	607
7	68	12	59	58	57	60	63	61	65	43	66	54	666
8	63	13	51	51	51	53	57	57	58	39	58	49	600
9	61	12	49	49	50	53	55	56	57	40	52	45	579
10	53	25	36	36	35	41	45	44	46	26	39	31	457
11	29	24	5	5	5	5	7	7	7	1	6	5	106
12	24	25	0	0	0	0	0	0	0	0	0	0	49
Total	588	287	335	331	332	351	370	367	376	238	364	303	4,242

Table 2. Limnological parameters sampled in Upper Klamath Lake, 1990-2015.

Parameter	Abbreviation/Unit	Profile ^a	Grab ^b
Temperature	T (°C)	X	
Dissolved Oxygen	DO (mg/L)	X	
pH	pH	X	
Specific Conductivity	(µSiemens/cm)	X	
Secchi Transparency	Secchi (m)		
Light (Photosynthetically Active Radiation)	PAR (uEm ⁻² s ⁻¹)	X	
Total Phosphorus	TP (µg/L)		X
Soluble Reactive phosphorus	SRP (µg/L)		X
Total Nitrogen	TN (µg/L)		X
Ammonia Nitrogen	NH ₄ -N (µg/L)		X
Nitrate-Nitrite Nitrogen	NO ₃ ⁺ NO ₂ -N (µg/L)		X
Silica	SiO ₂ (µg/L)		X
Chlorophyll <i>a</i>	CHL (µg/L)		X
Phytoplankton Species Composition and Biomass ^c	(mm ³ /L)		X
Zooplankton Species Composition and Biomass ^c	(mg/L)		X

a Profile = collected with multi-parameter WQ probe at multiple depths in water column

b Grab = depth-integrated water column sample collected with “tube sampler” except for zooplankton which was collected with a Schindler-Patalis Trap

Due to the very shallow nature of UKL and AL (mean depth \approx 2.4 m), the collection method provided a representative water column sample to pair with the phytoplankton and water quality samples. Zooplankton samples were narcotized with carbonated water prior to preservation in an ethanol-glycerin solution (Pennak 1989). Laboratory methods were similar over the 1990-2015 period, with individual species abundance determined from the depth-integrated sample at each site and date. Species measurements of individual species were used to convert to dry weight biomass according to Dumont et al. (1975), McCauley (1984), Culver et al. (1985), and Lawrence et al. (1987). Rotifer biomass was estimated by approximating to a geometric figure, according to several standard references: Bergquist (1985), Olrik et al. (1998), Hillebrand et al. (1999), and St. Amand (1990). As noted above, due to plankton analysis by several laboratories over the 1990-2015 period, a comprehensive standardization was undertaken prior to merging the three databases (see Kann et al. 2015 for greater detail).

Climate Data

Additional environmental data, for air temperature and wind data from the metrological *Station 725895 - Klamath Falls Airport* (<https://www.ncdc.noaa.gov/cdo-web/datasets/LCD/stations/WBAN:94236/detail>), positioned in the city of Klamath Falls were used to categorize general climate patterns expected to influence the biological processes in UKL and AL. The base dataset for wind speed (hourly wind speed measurements from the ISD-Lite dataset for station 725895 at the Klamath Falls Airport) over the period 1990 through 2015 was augmented between 2001-05-01 and 2002-02-28 with hourly measurements from the ULCD dataset for station at the Klamath Falls Airport due to missing observations for zero wind speed in the ISD-Lite dataset. In addition, a standardization of all wind speed measurements reported at less than 1.5 m/s was performed by setting those values to zero due to a change in the reporting limit for “calm” conditions that occurred around 1997. Subsequent to computation of daily climate statistics the rolling mean of the previous seven days was computed prior to merging with the water quality and plankton datasets. Similarly, we included data on the Pacific Decadal Oscillation (PDO, Mantua et al. 1997) as a measure of large scale climate perturbations for the Pacific Northwest Region (http://research.jisao.washington.edu/data_sets/). Long-term air temperature and precipitation data used for trend analysis were obtained from the Oregon State University PRISM model outputs (<http://www.prism.oregonstate.edu>).

Statistical Methods

Several statistical methods were used to analyze the relationships between water quality, climate, other relevant abiotic factors, and the phytoplankton and zooplankton data. We used linear regression or non-parametric Theil-Sen slope analyses to assess relationships between variables. The Theil-Sen slope estimate represents the median slope computed from the slopes of all lines through the pairwise sample points (Jassby et al. 2002). Associated tests for significance were computed using Kendall’s rank correlation coefficient (τ). We used Mann-Kendall trend tests to assess for long-term increases or decreases in the phytoplankton and zooplankton abundances. Mann-Kendall trend and regional Mann-Kendall analyses were performed for individual time-series and for a group of time-series (e.g., several related

phytoplankton species). Similarly, we used a regional Mann-Kendall trend test to analyze the long-term trend for a parameter for multiple stations.

Characterizing Phenology

Measurements of the timing of the annual phytoplankton bloom, hereafter phenology, are an effective method to understand how environmental factors impact yearly bloom dynamics. Obtaining robust phenology metrics is challenging and calculations are sensitive to the choice of method(s) (Thackerey et al. 2008). Here, all calculations were done on samples from the April to October period for plankton in UKL and AL in order to have the most consistent time-series and to avoid phenology calculations that were influenced by missing data in early months (Jan-Mar). We restricted our analyses to major parameters such as TP, TN, chlorophyll-a, *Aphanizomenon flos-aquae* and *Daphnia*, which all showed consistent seasonal cycles for many years in the database.

For early occurring species (e.g., diatoms) the general data coverage from April to October does not cover the bloom initiation, and thus calculations were limited to the estimation of peak abundance. Because total chlorophyll-a primarily represents *Aphanizomenon flos-aquae*, after the diatom bloom collapse in May, we additionally performed phenology analyses of chlorophyll-a from June and onwards which also allowed us to use chlorophyll-a to estimate phenology metrics for *Aphanizomenon flos-aquae* during years when phytoplankton samples were not processed. This also provided an additional assessment of the extent to which chlorophyll-a captures *Aphanizomenon flos-aquae* dynamics.

Our analyses centered on the following phenology metrics which are measured in day of the year (number of days since the start of the year a.k.a. Julian days), and included estimates of the timing of the onset, position of the main peak, decline, the length of the growing season (the difference between onset and decline), and finally the magnitude of the peak measured in biomass or biovolume (Figure 3). Phenology estimates of onset, peak timing and decline for *Daphnia* were calculated for all years in the time period; however, maximum peak biomass estimates were based on 1990-1999 and 2004-2015 data, but not calculated for the period 1998-2003 when the zooplankton biomass data were abnormally low³.

We used spline approximations to fit the phenology models for UKL (White et al. 1997, Forkel and Wutzler 2015). Using a smoothing of individual points, spline approximations are good for capturing the phenology of a water quality parameter or plankton species, however, because of the smoothing such models are not suitable for capturing actual peak values. Thus, we used spline models to characterize the onset, peak timing, decline and length of season. While the peak biomass or biovolume values were simply measured as the maximum point during a full growing season. Phenology analyses were restricted to the 7 stations in UKL (AN and AS excluded) which all showed similar temporal dynamics. A similar phenology interpolation method, linear trend analyses (Fockel et al. 2015) was also initially considered but since this method produced overall similar results to the spline method, we restricted our analyses to using spline approximations.

³ In general, abnormally low abundance and biomass values in the zooplankton dataset between 1998 and 2003 could not be confirmed so are not utilized in most analyses.

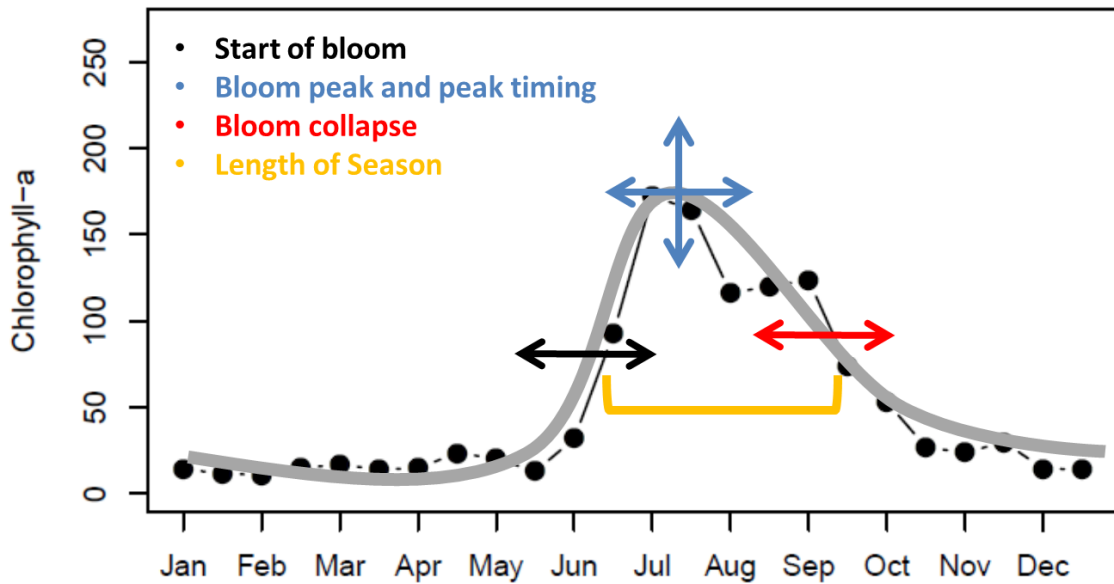


Figure 3: Schematic of phenology metrics obtained by the phenology modeling

We also explored other methods to establish phenology estimates. A threshold method was initially considered to establish the bloom onset, peak timing and magnitude. Threshold methods are suitable for capturing abundance increases in a particular species however determination of onset is dependent on the specific threshold values used (Brody et al. 2013). This works well for parameters (e.g., chlorophyll-a) where threshold values are fairly well known, however is more difficult when threshold values are difficult to estimate. A common extension of threshold phenology method is using a measure of a given percent above a baseline value of the annual phytoplankton abundance or biomass. However, this method was not used here, where data was primarily available from April-October as this is not suitable for data that do not cover a full annual cycle, since baseline values will be heavily influenced by the phytoplankton abundances measured during the growing season. Because all models showed similar outcomes compared to the spline approximation method, we focused the analyses on the spline estimation phenology method (Fockel et al. 2015).

Multivariate analyses

Comparing and coupling multiple time-series data sets requires appropriate multivariate statistical methods. To identify potential factors responsible for changes in the plankton time-series data, a range of associated ecological (e.g., other plankton species) and chemical and physical data (temperature, oxygen, nutrient, and climate indices) were used as potential explanatory variables. Calculations of physical (e.g., thermal resistance to mixing, Wetzel and Likens 1991; Kann and Welch 2005) and biological indices (e.g., species diversities) were used as additional metrics for the multivariate analyses of the plankton dynamics of UKL.

To assess diversity, we calculated the Shannon diversity index (H), a measure of species richness (Shannon 1948), for each zooplankton and water sample, as well as the microscopy phytoplankton data according to,

$$H = - \sum_{j=1}^S p_i \ln p_i$$

where p_i is the proportion of each prey item and S is the number of prey species in the sample. To estimate species turnover, used as a proxy for measuring the stability of the phytoplankton community, we calculated Bray-Curtis similarities (Bray & Curtis 1957) for each month of the growing season and estimated the mean change in species composition for a given year. Bray-Curtis similarities were calculated using the formula:

$$Simm(i, j) = 1 - \frac{\sum_{k=0}^{n-1} y_{i,k} - y_{j,k}}{\sum_{k=0}^{n-1} y_{i,k} + y_{j,k}}$$

Where, i and j are the pairwise sites and k are the species abundances for the n number of species y . A $Simm$ value of 1 denotes complete overlap of species between sites and zero denotes complete separation between sites.

Prior to the multivariate analyses, the data was transformed using a \log_{10} transformation. In the case of a few parameters that included zero a value of 0.01 was substituted. The log transformation was used to meet assumptions for comparison of multivariate data, which standardizes the data within sampling units allowing comparison across the biological, chemical and physical data.

Multiple linear regression models were used to model the relationship between two or more explanatory variables and a response variable. Models were computed initially with complete models consisting of all variables deemed relevant for the particular response variable. We then used forward and backward selection to estimate the most parsimonious model based on the Akaike Information Criterion (AIC). The most parsimonious model was then reported. Before model selection, explanatory variables were tested for collinearity by estimating the variance inflation factors (VIF). A threshold VIF value of 10 was used to exclude variables with high collinearity. For example, total nitrogen and total phosphorus often correlated substantially (resulting in a high VIF value), and thus one of these variables was excluded. Multiple linear regressions were used to explain the variation in the annual values of diatoms, chlorophyll-a, as a proxy for the initiation and peak of the *Aphanizomenon flos-aquae* bloom. We used a range of explanatory variables to estimate the variance in these four response variables. Commonly, we used explanatory variables estimated in the same time period as the response variable, i.e., for diatoms we used explanatory factors measured in the spring, data measured in mid-May to early June for the bloom initiation model, and for the bloom peak model, data measured in July.

Multivariate analyses, specifically non-metric multidimensional scaling (nMDS) were used to identify co-variation among multiple species or stations. Hierarchical clustering analyses using Ward's minimum variance method (Legendre & Legendre 2012) was applied to differentiate

the annual phytoplankton, physical or chemical composition into major clusters. Clusters of annual groups were tested for significance using permutational multivariate ANOVA (PERMANOVA, Euclidian distance, 999 permutations; Anderson 2001, Anderson & Walsh 2013). For the phytoplankton data we used annual mean data for Chrysophyta, Cryptophyta, *Aphanizomenon flos-aquae*, diatoms, and *Microcystis aeruginosa*.

To assess common patterns among major phytoplankton groups we constructed redundancy analysis (RDA) models based on Bray-Curtis distances (Zuur et al. 2007) using phytoplankton data as the response variables and physical and/or chemical parameters as explanatory or independent variables. The most parsimonious RDA model was chosen based on forward selection and 999 permutations. The reported F-value was derived from the permutation procedure. Again we used the phytoplankton data for Chrysophyta, Cryptophyta, *Aphanizomenon flos-aquae*, diatoms, and *Microcystis aeruginosa*, while for the nutrient data we used soluble reactive phosphorus, total inorganic nitrogen, total nitrogen, total ammonia and total phosphorus concentrations, as well as the nitrogen to phosphorus (TN:TP) and the total inorganic nitrogen to soluble reactive phosphorus (TIN:SRP) ratios. For the physical data we used monthly averages for water temperature, light attenuation, relative thermal resistance to mixing (RTRM), the mean 7-day air temperature, and the mean 7-day wind speed. These data groupings were chosen as they were consistently measured throughout the time period 1990-2015. In addition to single cluster analyses, we also used two-way Cluster analysis using Ward's minimum variance method to visualize synchronous patterns in the multivariate data of years and covariation in the different input variables. Additionally, and based on the initial results of the multivariate analyses, an RDA model and a two-way cluster analysis for specific monthly values were constructed to better understand the main factors influencing the bloom during the main growing season. Here we used the mean data for diatoms for the April-May period, and *Microcystis aeruginosa* for the Jul-Oct period, while the other algae biomasses were calculated over the main growing season (Jun-Sep). In this model all explanatory variables were taken from the spring period (Apr-Jun). All plots and statistical analyses were performed in R (R Cran 2015), and phenology models were fitted using the package "greenbrown" (Fockel et al. 2015) while the "vegan" package (Oksanen 2013) was used for the multivariate statistical analyses.

RESULTS/DISCUSSION

Chlorophyll-a and total phytoplankton regression model

First, we tested to what extent the chlorophyll-a measurements captured the independent microscopy measurements of total phytoplankton biovolumes. This was also done to establish approximate estimates of phytoplankton biovolume for the four years (2000-2003) when phytoplankton data were missing. Overall there was a strong relationship between measurements of chlorophyll-a biomass and total phytoplankton as shown by the regression model ($\log \text{total phytoplankton} = 0.9276 * \log \text{chlorophyll-a} - 0.9513$, $p < 0.01$, $r^2 = 0.68$, Figure 4). This allowed reasonable prediction of total phytoplankton and thus cyanobacteria for the

years when data were missing (2000-2003). We recommend that this regression model is suitable to model total phytoplankton and thus, also Cyanobacteria during the summer period (June-September) when *Aphanizomenon flos-aquae* usually comprises 99% of the total phytoplankton biovolume.

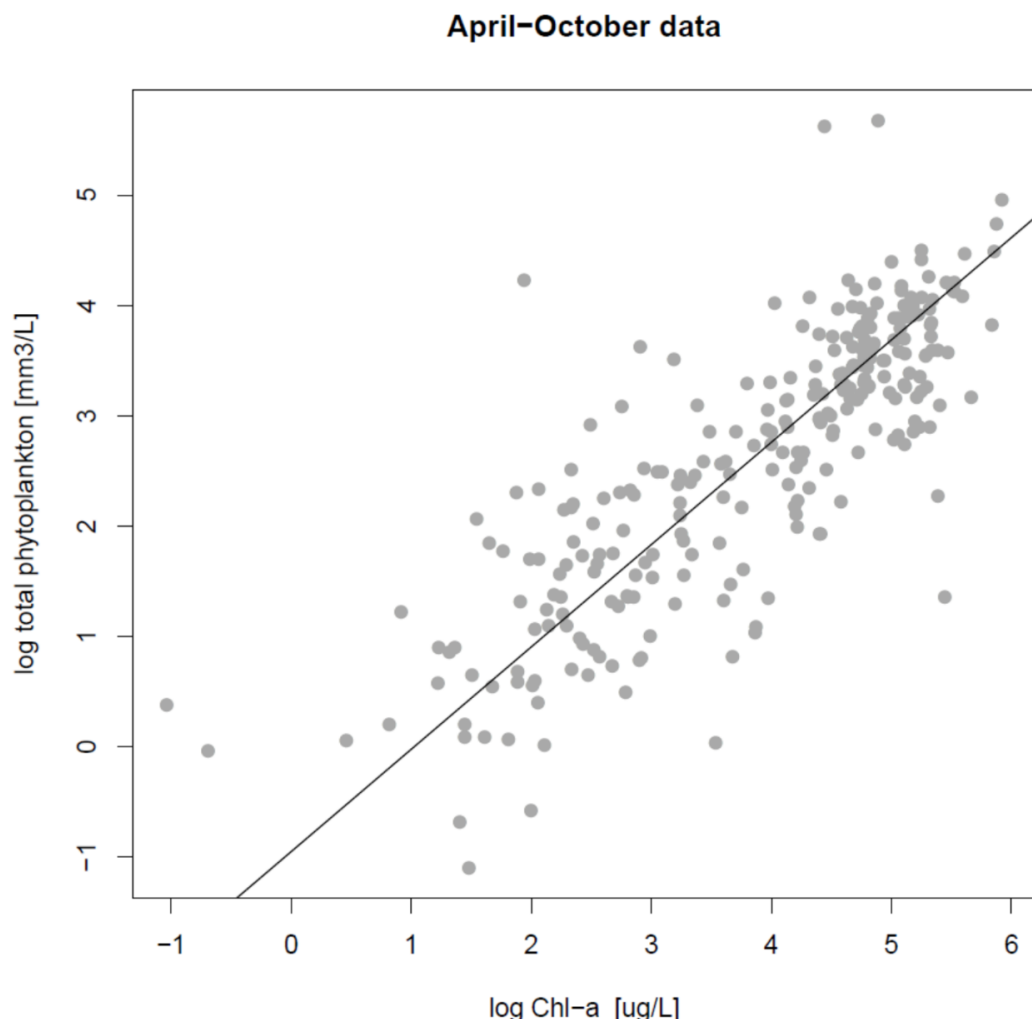


Figure 4: Linear model based on type II regression of logged values of chlorophyll-a (mg [DW/L]) and log total phytoplankton (biovolume [mm^3/L]). Regression model: **log total phytoplankton = 0.9276*log chlorophyll-a - 0.9513**, $p<0.01$, $r^2=0.68$.

Supporting climate data

Climatic variation influences ecosystem processes on a range of spatial and temporal scales (Doney 2012). How changes to the ambient climate have influenced the biota in UKL requires understanding of both short term (seasonal and inter annual) and longer decadal changes. The climate in the Pacific Northwest is influenced by long-term decadal processes such as the Pacific Decadal Oscillation (Mantua et al. 1997). This includes the Upper Klamath basin where the air temperature regime is significantly correlated to the PDO ($r^2=0.25$, $p<0.01$, Figure 5). However, as evidenced by the r^2 value, local environmental forcing also plays an

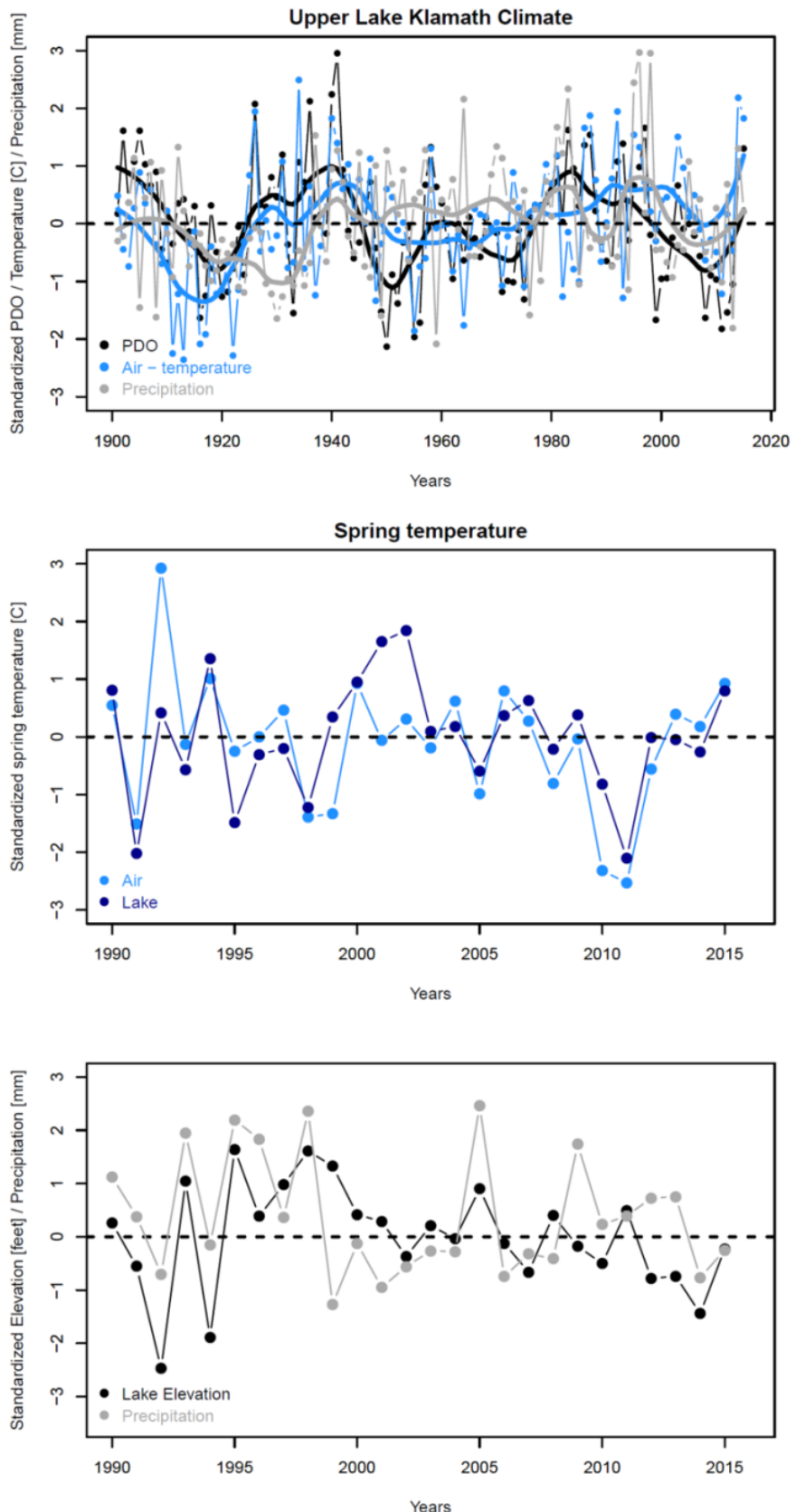


Figure 5: Temporal changes of the **A**) Pacific Decadal Oscillation (black), Upper Klamath Lake modeled air temperature (light blue) from 1900-2015, where solid lines are loess smoothed data for each time-series, **B)** modeled spring air temperature (light blue) and mean spring water temperature (dark blue) from 1990-2015 and **C)** spring precipitation (grey) and summer Lake elevation (black) from 1990-2015.

important role. The standardized PDO was generally positive during the first ten years of the study period (1990-1999), negative from ~2000-2010, and negative but rising from 2011-2015.

Mean lake temperature was positively correlated to the modeled PRISM air temperature data (<http://www.prism.oregonstate.edu/>) in spring ($r^2=0.38$, $p<0.01$), and negatively correlated to precipitation ($r^2=0.21$, $p<0.01$; Figure 5B-C). Lake elevation is actively managed to supply irrigation water downstream, and thus summer lake elevation was not significantly correlated with spring water temperature ($r^2=0.05$, $p=n.s.$; Figure 5B-C) or spring precipitation ($r^2=-0.1$, $p=n.s.$).

UKL water temperature changes rather quickly due to its shallow depth, and consequently temperature fluctuations between adjacent months tend not to be highly correlated, indicating that short term temperature regimes are important in governing intra-annual lake phytoplankton development. When analyzing the UKL air temperature data we commonly found a significant correlation between adjacent months; however, this pattern was rarely apparent over longer time scales (Figure 6). Although some specific years could be described as generally warm (e.g., 1992, 1996, 2014, or 2015) or cold (1991, 1993, or 2011), or windy (e.g., 1991, 1993, or 2010), a common pattern was relatively shorter cold and warm periods within the same year (Figure 7) as well as variable wind speeds (Figure 8). For example, year 2000 had higher than average spring temperatures, while from July onwards temperatures were below average. Likewise, 1997 was a relatively calm year overall, while 2015 was calm in May and June, windy in July and August, and calm in September and October (Figure 8).

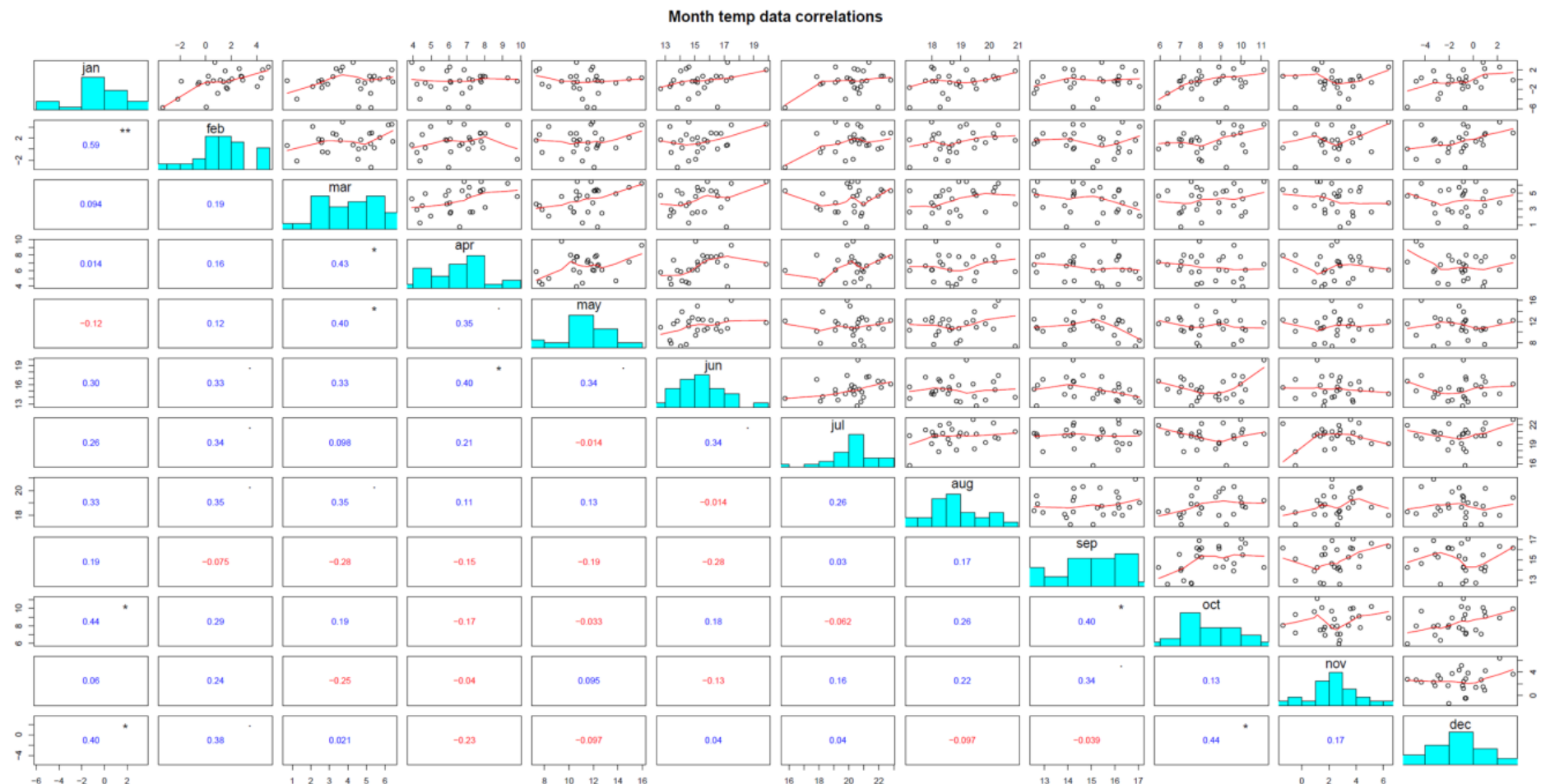


Figure 6. Correlations among monthly means of air temperature for the time periods 1990-2015 measured from Station 725895 - Klamath Falls airport.

TEMP_MEAN

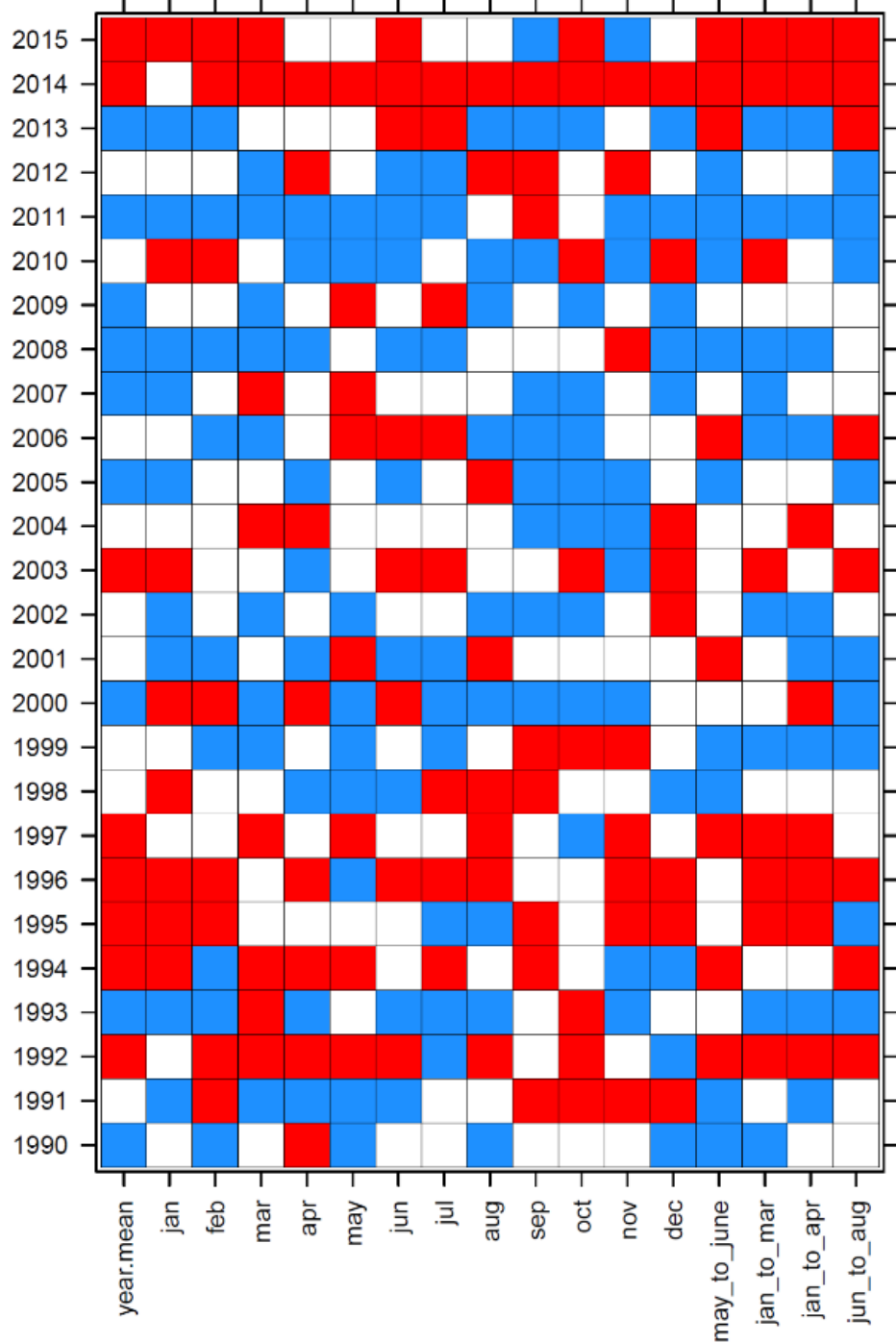


Figure 7: Overview of warm (red) and cold (blue) air temperature anomalies from Station 725895 - Klamath Falls airport.

WSPD_MEAN4_MAX

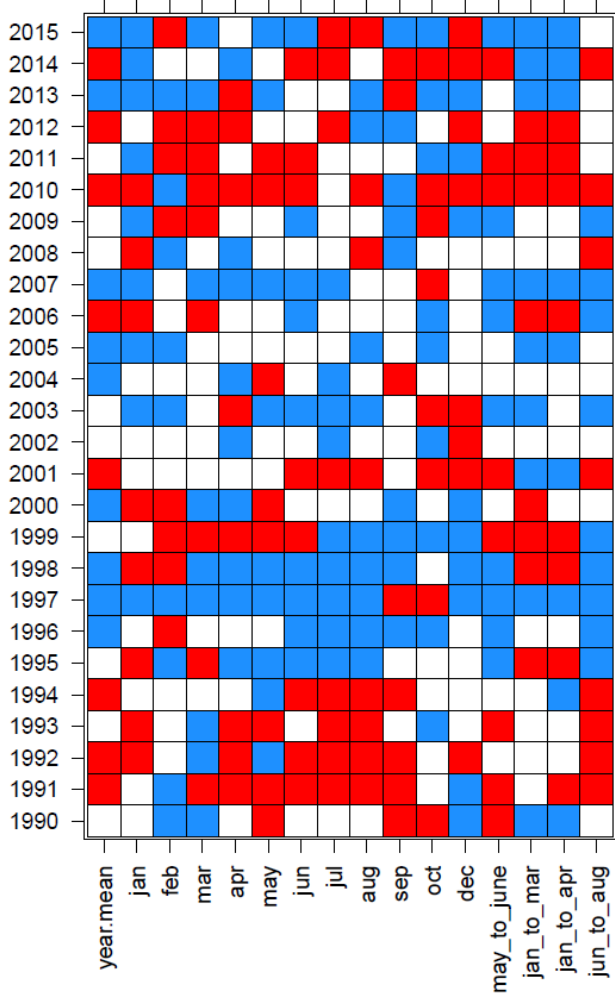


Figure 8: Overview of above (red) or below (blue) wind speeds, from Station 725895 - Klamath Falls airport. The wind metric WSPD_MEAN4_MAX is the daily maximum of the four-hour running mean wind speed.

General characteristics of the combined data

Spatial differences in primary water quality and plankton variables

Data were consistently collected from UKL and AL at 9 stations. Overall seasonal dynamics tend to be similar for all 9 stations however there were some distinct differences. This was confirmed by nMDS analyses for these stations and the major chemical (total nitrogen, total phosphorus) and biological constituents (chlorophyll-a and total phytoplankton). A consistent outcome from the nMDS analyses was the differences between the AL stations AS and AN, compared to the rest of UKL (Figure 9 to Figure 12). Thus, unless otherwise specified, subsequent statistical analyses were grouped into AL comprising AS and AN, and the 7 other stations (UKL_OUT, NB, WB, ML, ER, SB, MN) representing the main area of UKL.

Furthermore, due to the differences between AL and the main part of UKL, phenology analyses were performed on average values from the 7 main stations, excluding the AL stations. Although AL stations were the most different, the bay stations WB and SB also stood out for TP, TN and chlorophyll-a.

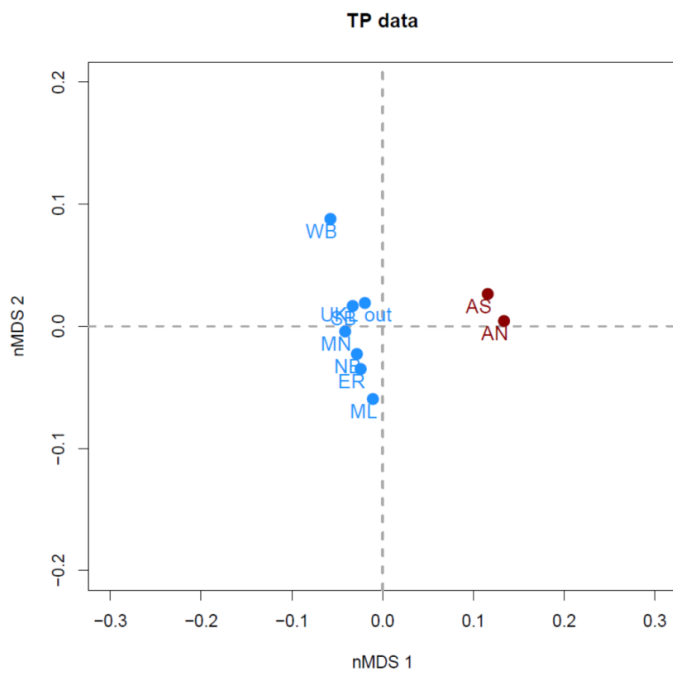


Figure 9: nMDS of monthly Total phosphorus data from all years and each station, with the AL stations in red and the main UKL stations in blue.

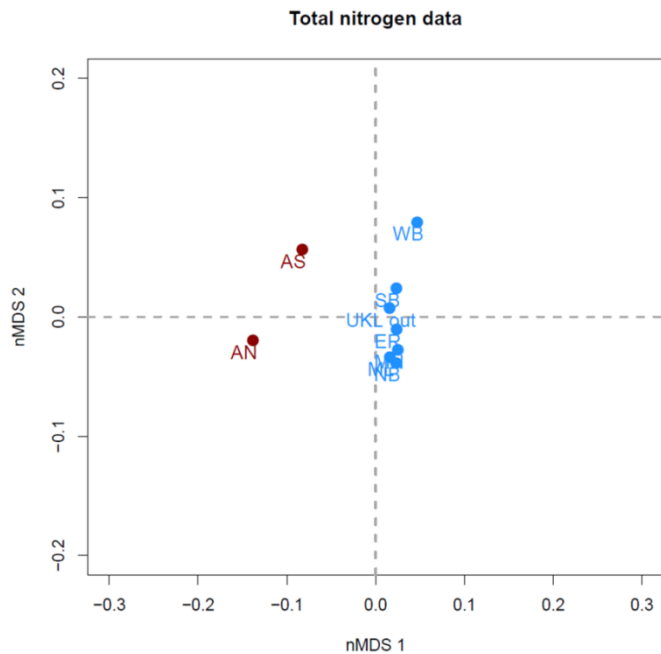


Figure 10: nMDS of monthly Total Nitrogen data from all years and all stations, with the AL stations in red and main the UKL stations in blue.

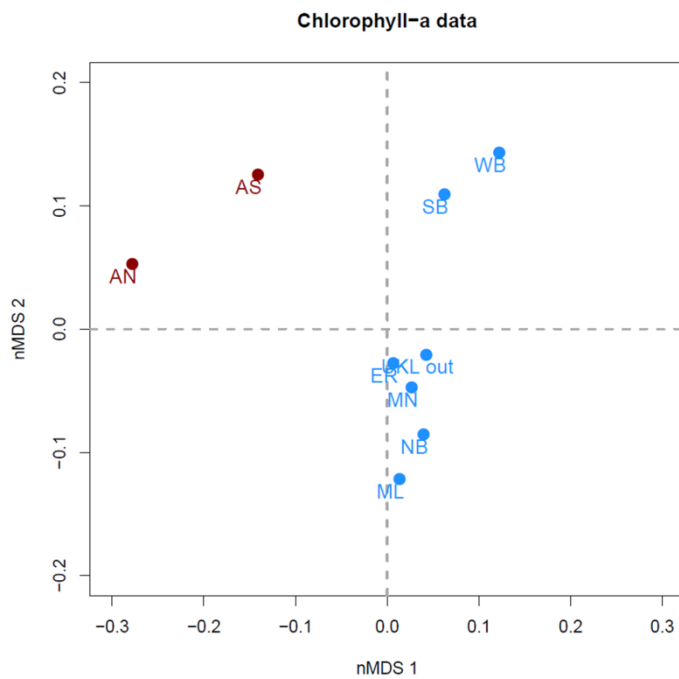


Figure 11: nMDS of monthly chlorophyll-a data from all years for each station, with the AL stations in red and main the UKL stations in blue.

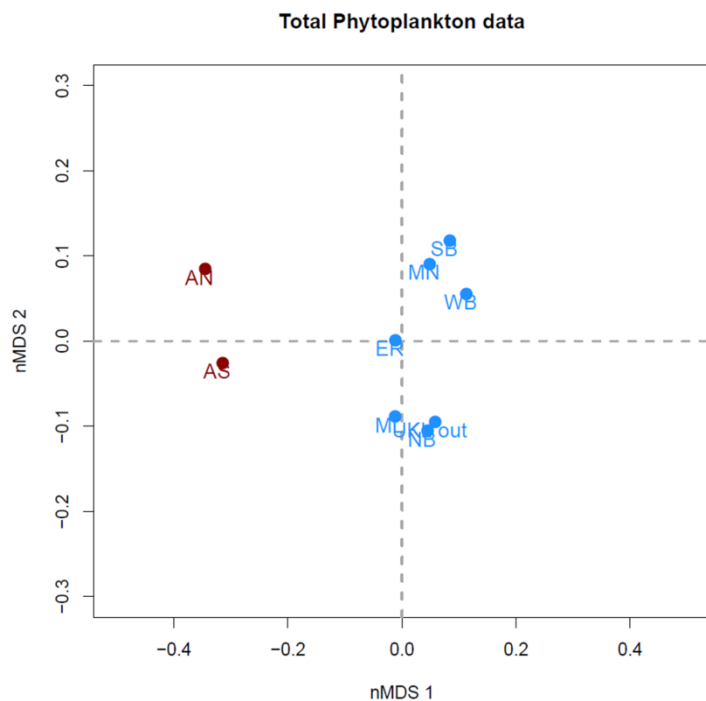


Figure 12: nMDS of station Total phytoplankton from all years and each station, with AL stations in red and the 7 main UKL stations in blue.

Seasonal trends and general species characteristics

Both UKL and AL showed consistent seasonal patterns. All temporal plots for AL and UKL were based on mean values for the entire time period (1990-2015), except for the zooplankton where we used data from 2004-2015 due to the low biomass values reported for 1998-2003 and because the 2004-2015 data were processed by a single laboratory. Boxplot data were based on all individual samples collected twice per month for each station. However, while the data are generally reported twice per month there are several gaps. Especially during Jan-Mar and Nov-Dec when sampling was sporadic at the majority of stations and was most commonly restricted to the UKL OUT stations. Nonetheless, UKL OUT provides a good description of the general trends of the major variables in the lake between late-fall and early-spring, which is outside of the period of consistent sampling at the core UKL stations (Table 1).

Total phosphorus, SRP and total nitrogen all increased in June and subsequently declined in late summer. However, there was an earlier increase in AL nutrient concentrations compared to UKL (Figure 12-14) as also noted previously (Kann 2017). Similarly, phosphorus, SRP and nitrogen levels also seemed to decline earlier in AL compared to UKL. Despite the distinct seasonal pattern, boxplots also showed substantial year to year variation in phosphorus, SRP and nitrogen concentrations. Dissolved oxygen showed a general declines in mid-summer and an increase in late-summer in UKL and AL, while the boxplots of all yearly data again showed substantial year to year variation (Figure 16).

Chlorophyll-a also showed a distinct increase in early June followed by a decline usually in mid-July to August for UKL and slightly earlier for AL (Figure 18). Data from UKL also showed a tendency for an extended Chl-a plateau in Aug-Sep after an initial decline in July. This pattern was visible at most stations in UKL but less visible for the AL stations where the peak lasted substantially less time and commonly declined by late July.

Phytoplankton species in UKL and AL

A range of phytoplankton species were observed in the lake during the 1990-2015 period. By far the most dominant species in both UKL and AL is *Aphanizomenon flos-aquae* which strongly dominates the phytoplankton community from June to September, commonly accounting for >99% of the total phytoplankton biomass. Other common species include various species of diatoms especially in the spring (Figure 19, Figure 20). A total of 130 and 103 phytoplankton species were observed in UKL and AL, respectively, across the entire time period of 1990-2015, but most species were observed only in low biomasses or for short time periods each year.

Seasonal cycle of the total phytoplankton

The seasonal cycle of the total phytoplankton biovolume showed a small increase in May and then a substantial increase in June during the main summer growing season. Similar to the chlorophyll-a data the phytoplankton peak persisted longer in UKL compared to AL where the bloom was usually more protracted (Figure 21). The phytoplankton is comprised primarily of cyanobacteria (Figure 22), especially in the summer, while diatoms dominate in April and

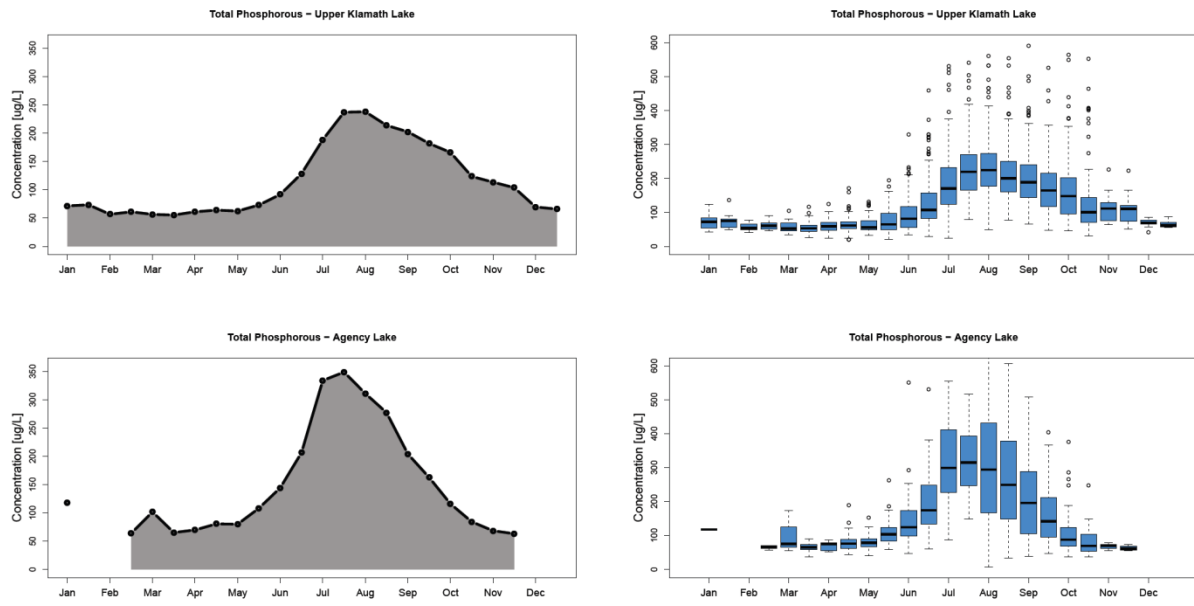


Figure 13: Seasonal dynamics of mean of total phosphorus ($\mu\text{g/L}$) (a,c) UKL and (b,d) AL. Note: The data for AL in January consistent of only 1 measurement and should be treated with caution. Note: Y-axis are the same for a,c and b,d, respectively to allow comparison between UKL and AL. Boxplot is based on all individual data from each station and year.

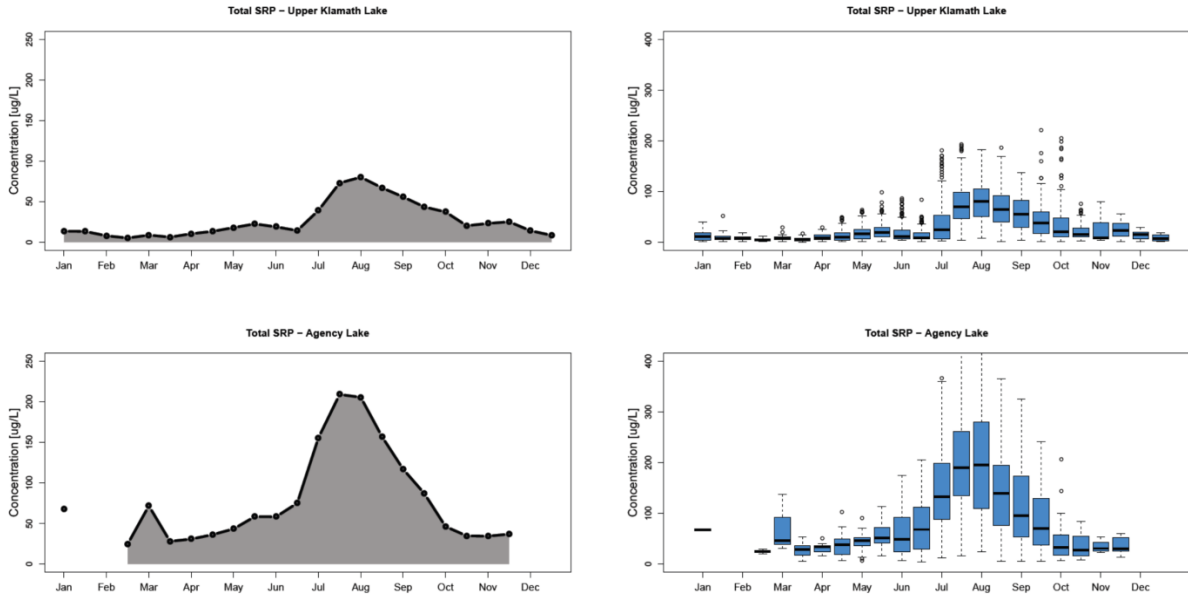


Figure 14: Seasonal dynamics of mean of total Soluble reactive phosphorus ($\mu\text{g/L}$) (a,c) UKL and (b,d) AL. Note: Y-axis are the same for a,c and b,d, respectively to allow comparison between UKL and AL. Boxplot is based on all individual data from each station and year.

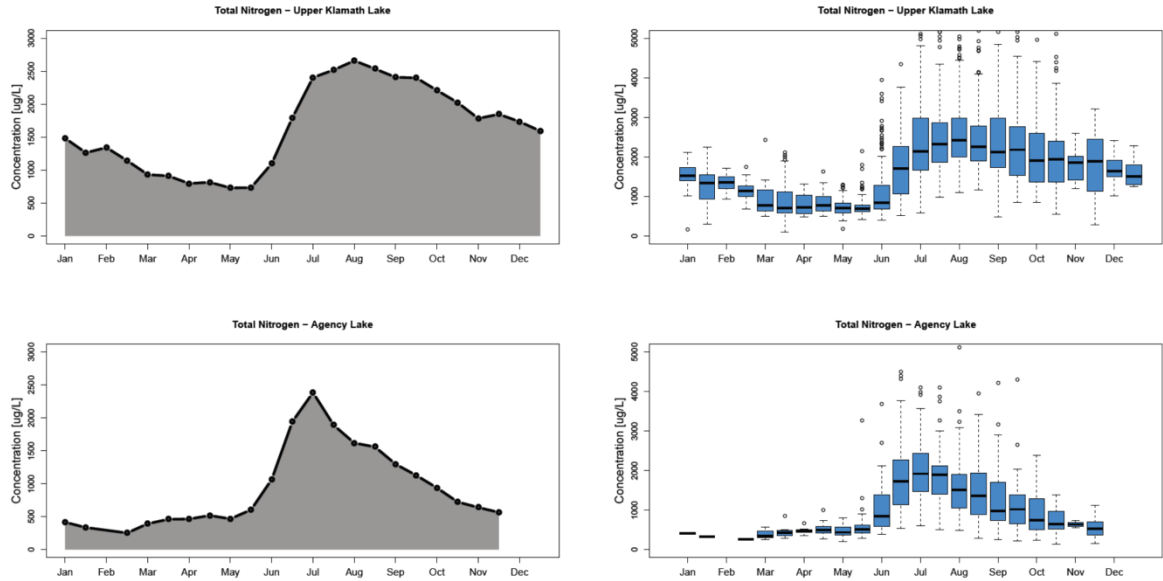


Figure 15: Seasonal dynamics of mean of total nitrogen ($\mu\text{g/L}$) (a,c) UKL and (b,d) AL. Note: Y-axis are the same for a,c and b,d, respectively to allow comparison between UKL and AL. Boxplot is based on all individual data from each station and year.

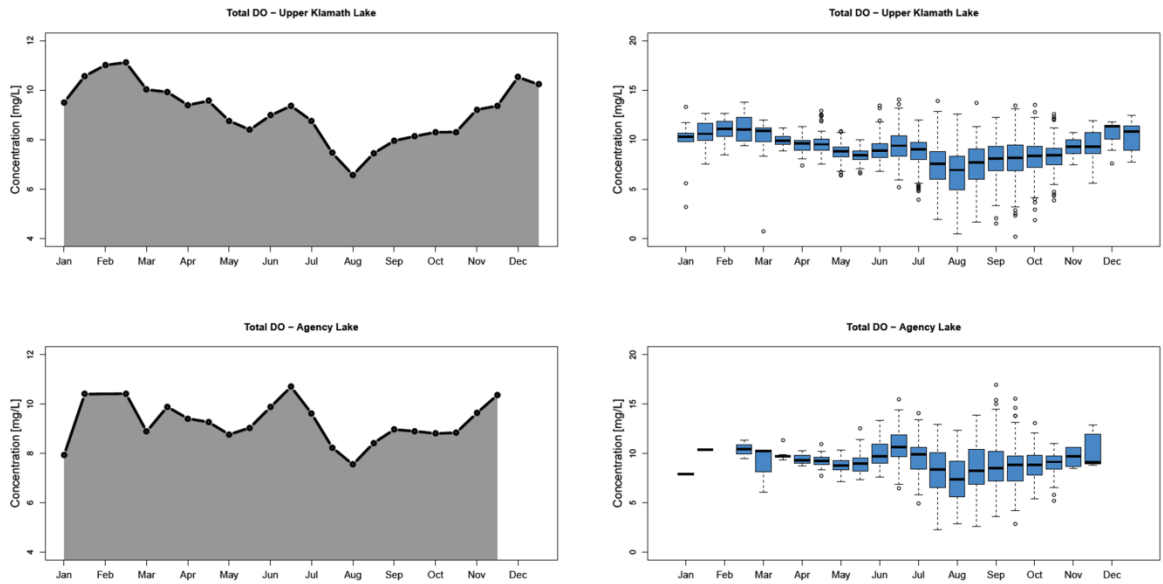


Figure 16: Seasonal dynamics of mean of dissolved oxygen (mg/L) from (a,c) UKL and (b,d) AL stations. Note: Y-axis are the same for a,c and b,d, respectively to allow comparison between UKL and AL. Boxplot is based on all individual data from each station and year.

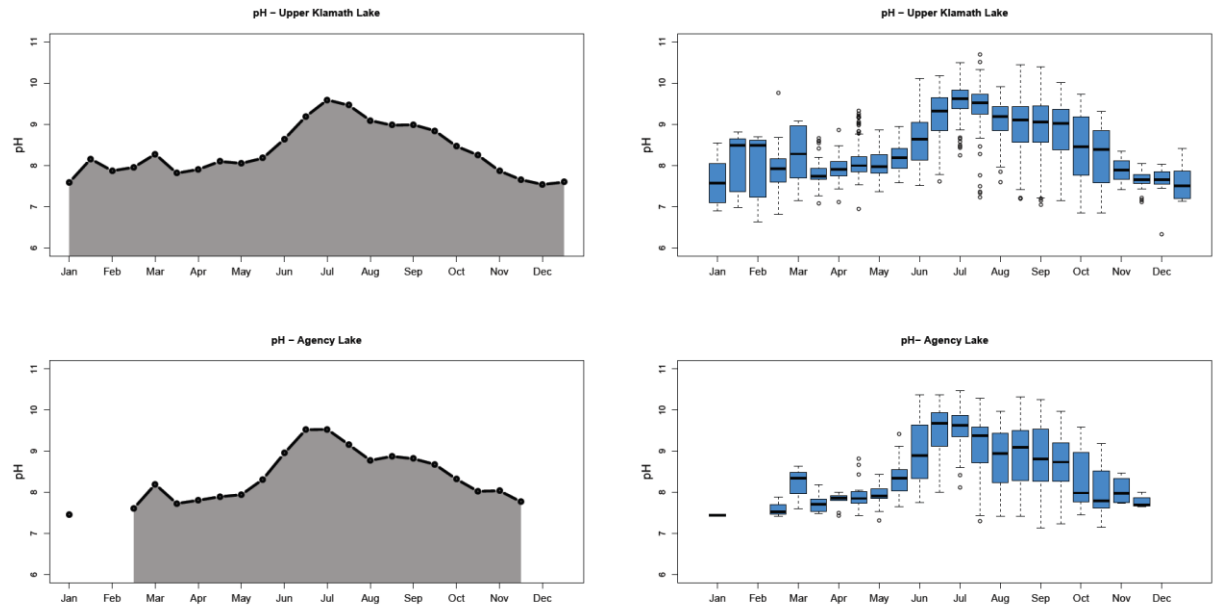


Figure 17: Seasonal dynamics of mean pH from **(a,c)** UKL and **(b,d)** AL stations. Note: Y-axis are the same for a,c and b,d, respectively to allow comparison between UKL and AL. Boxplot is based on all individual data from each station and year.

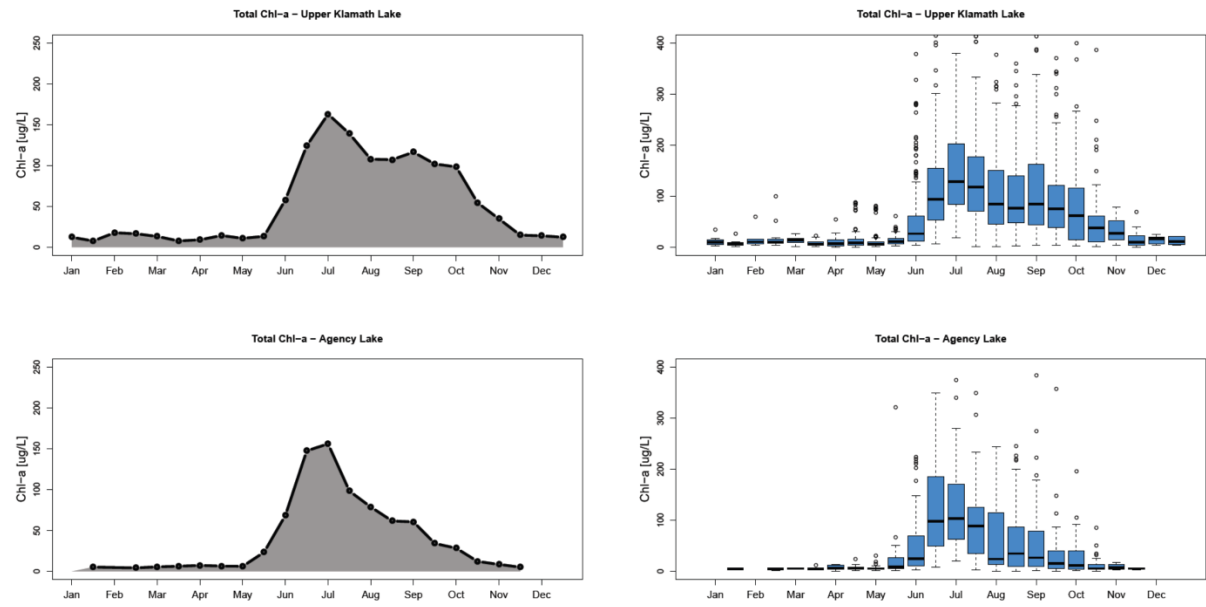


Figure 18: Seasonal dynamics of mean of chlorophyll-a biomass from **(a, c)** UKL and **(b,d)** AL. Note difference in scale of y-axis between line plots (a,c) and boxplots (b,d). Boxplot is based on all individual data from each station and year.

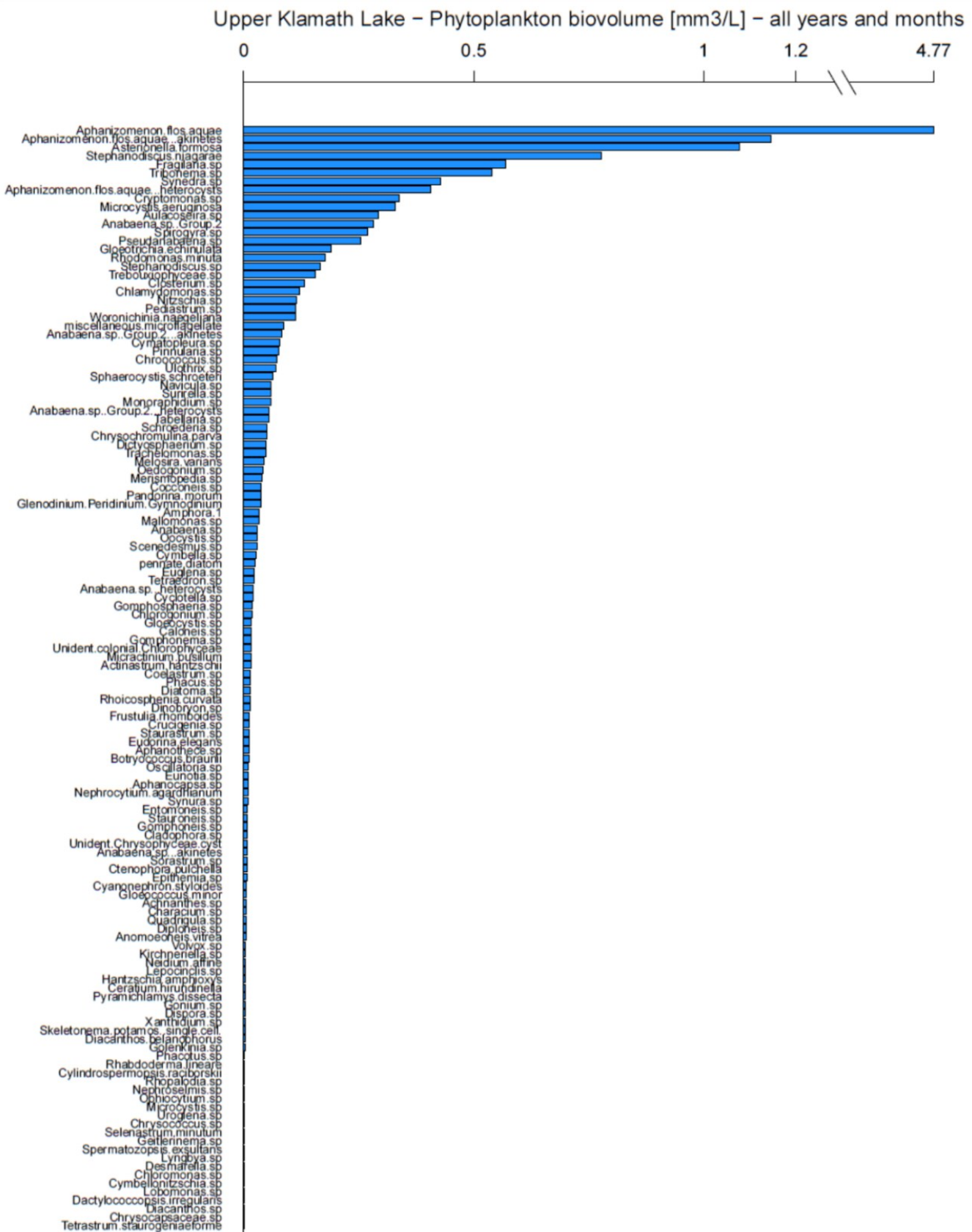


Figure 19: Square rooted phytoplankton species biovolume [mm³/L] from Upper Klamath Lake for all years and all stations, based on bi-monthly data. Note the break in scale for *Aphanizomenon flos-aquae*.

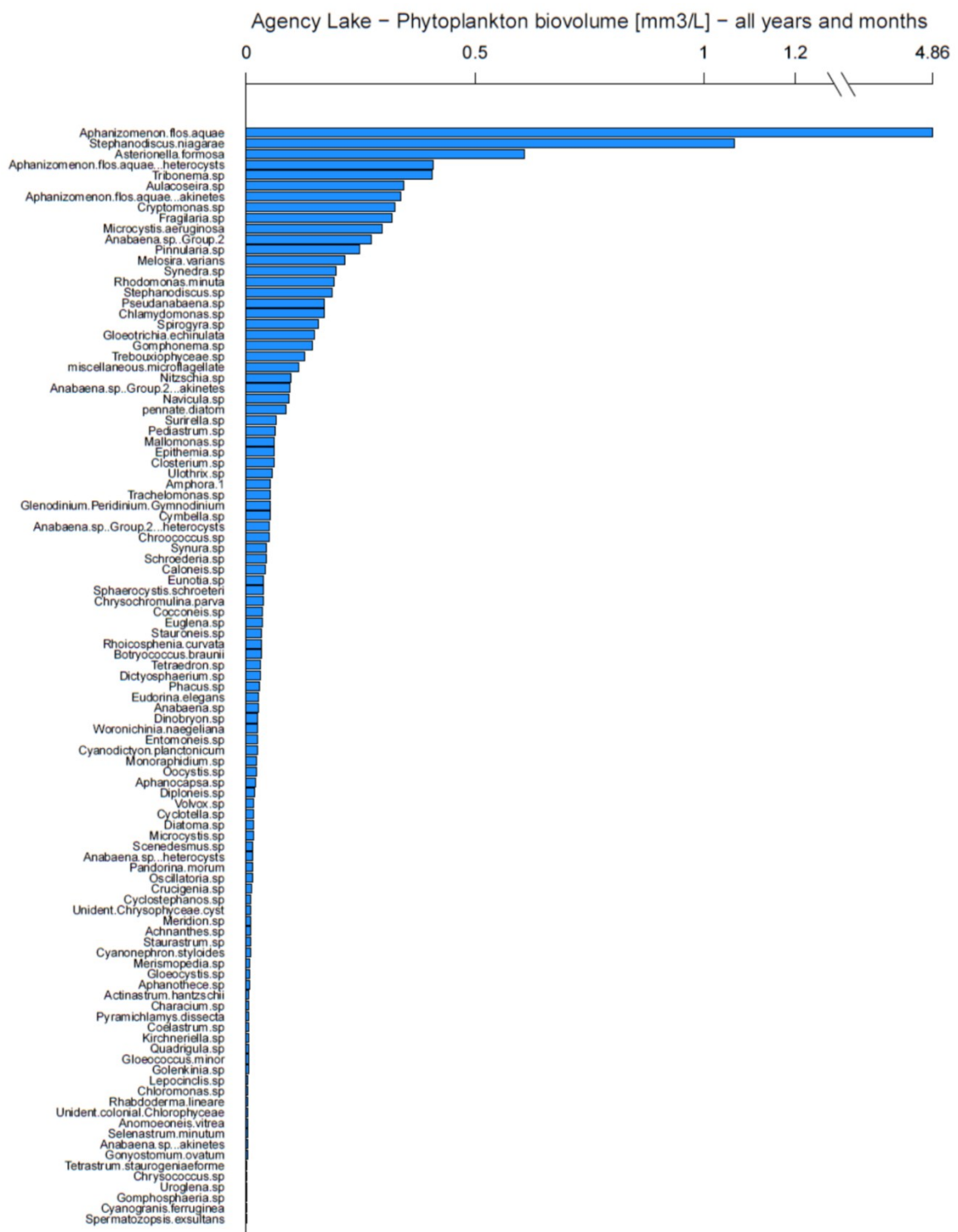


Figure 20: Square rooted phytoplankton species biovolume [mm³/L] from Agency Lake for all years and all stations, based on bi-monthly data. Note the break in scale for *Aphanizomenon flos-aquae*.

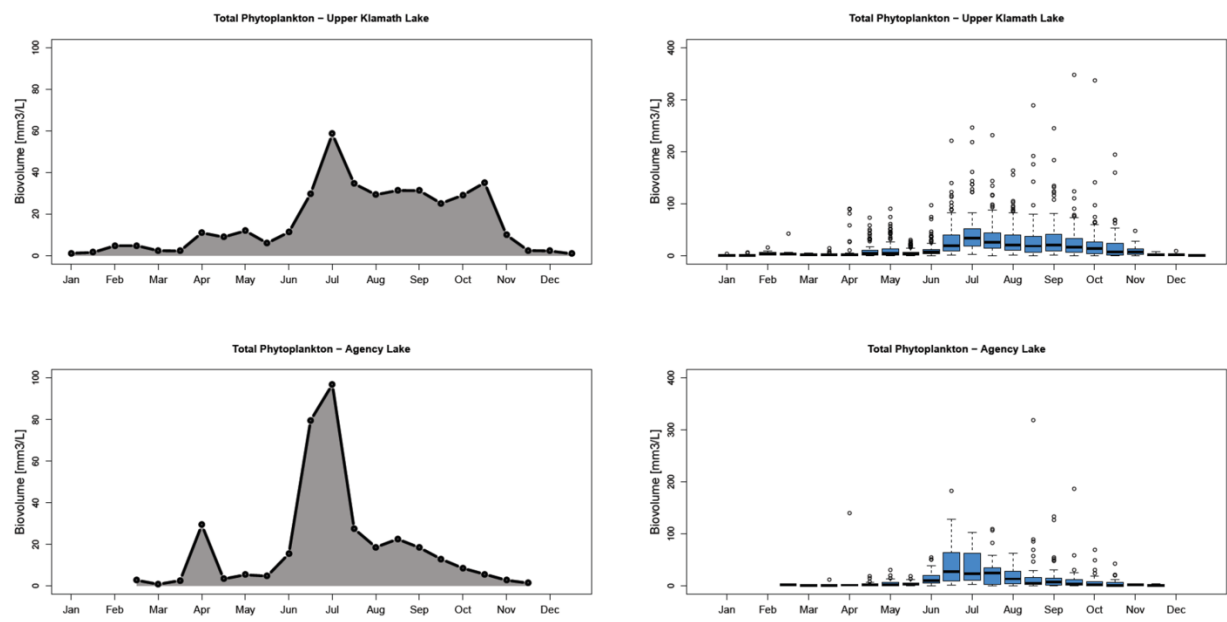


Figure 21: Seasonal dynamics of mean total phytoplankton biovolume from (a,c) UKL and (b,d) AL. Note difference in scale of y-axis between line plots and boxplots. Boxplot is based on all individual data from each station and year.

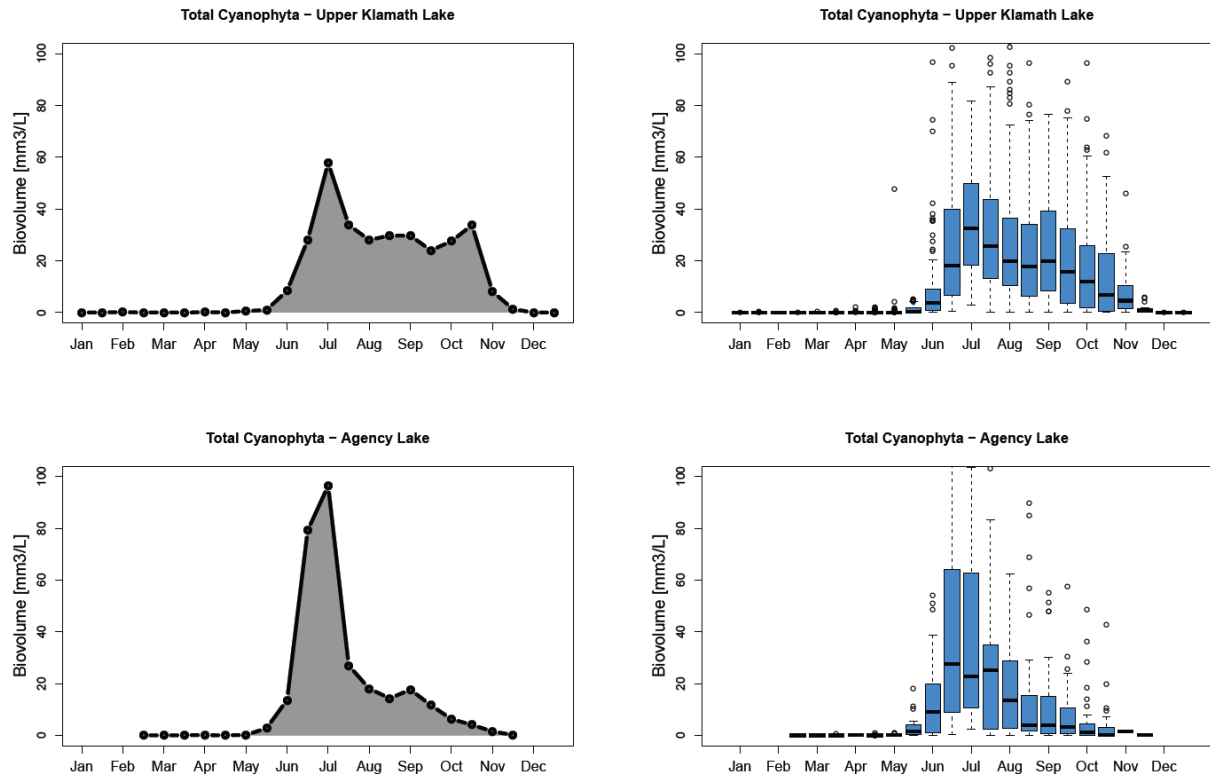


Figure 22: Seasonal dynamics of mean of total Cyanophyta biovolume from **(a,c)** UKL and **(b,d)** AL. Note difference in scale of y-axis between line plots and boxplots. Boxplot is based on all individual data from each station and year.

May (Figure 23). In AL the peak in the average April diatom biomass for AL in Figure 23 is mainly due to a single very high value ($339 \text{ mm}^3/\text{l}$), which is also apparent for the total phytoplankton in Figure 21. Other algae taxa present in the lake include Cryptophyta and Chlorophyta which are present in lower abundance during most of the year (Figure 24, Figure 25).

Phytoplankton species

Aphanizomenon flos-aquae is the most dominant Cyanophyta species. In both UKL and AL the bloom usually initiated in June, however, the bloom commonly declines much faster in AL than in UKL, and in UKL the bloom persists well into October in some years (Figure 26). Concomitant with the June rise in biomass, *Aphanizomenon* heterocysts also increased (Figure 27) indicating nitrogen fixation occurring during periods of seasonal low total nitrogen and total inorganic nitrogen concentrations (see Figure 50, below) as well as seasonal low values of phosphorus to nitrogen ratios (both total and inorganic forms; e.g., Kann 2017).

Aphanizomenon akinete biomass substantially increased during the fall, consistent with reduced growth conditions for *Aphanizomenon* and the final seasonal decline in biomass.

Another important species is the late summer blooming *Microcystis aeruginosa* which is at times abundant and can produce toxins (Figure 29). Such toxic blooms of the non-diazotrophic *Microcystis* tend to follow the decline in *Aphanizomenon* when there is abundant nitrogen generally in the form of ammonia (Eldridge et al. 2013; Kann 2017).

Besides *Aphanizomenon* and *Microcystis*, a range of other species are also present in the lake, including several species of diatoms and cryptophytes which are abundant primarily in the spring and fall. *Tribonema* sp. *Stephanodiscus niagarae*, *Asterionella Formosa*, *Fragilaria* sp. and *Synedra* are some of the main diatom species which peak from March to June (Figure 30-34). Throughout the April to October period, mainly before and after the main *Aphanizomenon flos-aquae* peak, Cryptophyta, including the most common *Cryptomonas* sp. (Figure 35), were also present at notable biomasses. It is likely that the various species of diatoms and cryptophytes provide valuable dietary resources to the zooplankton community in the lake, despite their low biomass compared to *Aphanizomenon flos-aquae*. However, without information on their productivity it is difficult to assess their importance to the general planktonic food web in UKL and AL.

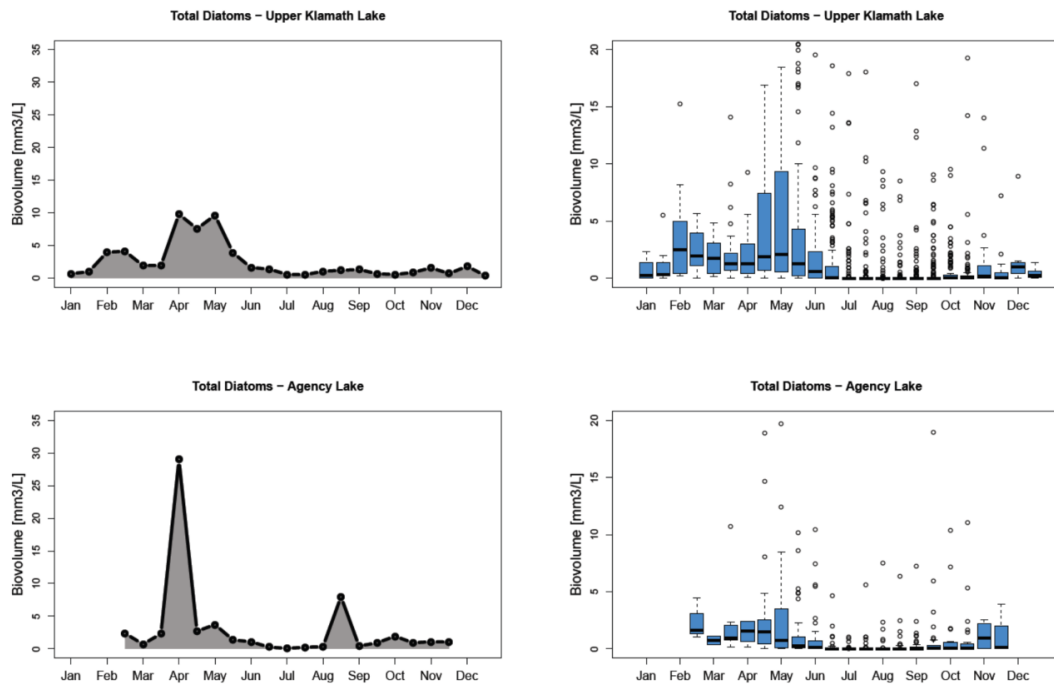


Figure 23: Seasonal dynamics of mean of total diatoms biovolume from (a,c) UKL and (b,d) AL. Note difference in scale of y-axis between line plots and boxplots. Please note the spike in the average April diatom biomass for AL is mainly due to a single very high value ($339 \text{ mm}^3/\text{l}$) which is above the y-axis limit in the boxplot for AL. Boxplots were based on all individual data from each station and year.

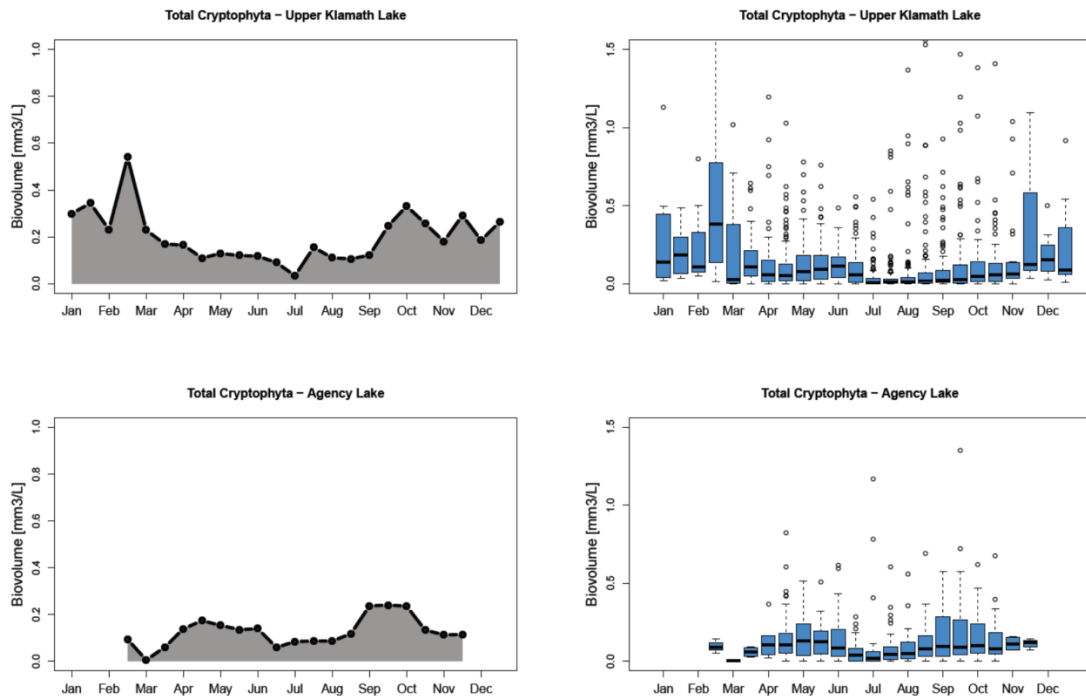


Figure 24: Seasonal dynamics of mean of total Cryptophyta biovolume from (a,c) UKL and (b,d) AL. Note difference in scale of y-axis between line plots and boxplots. Boxplot is based on all individual data from each station and year.

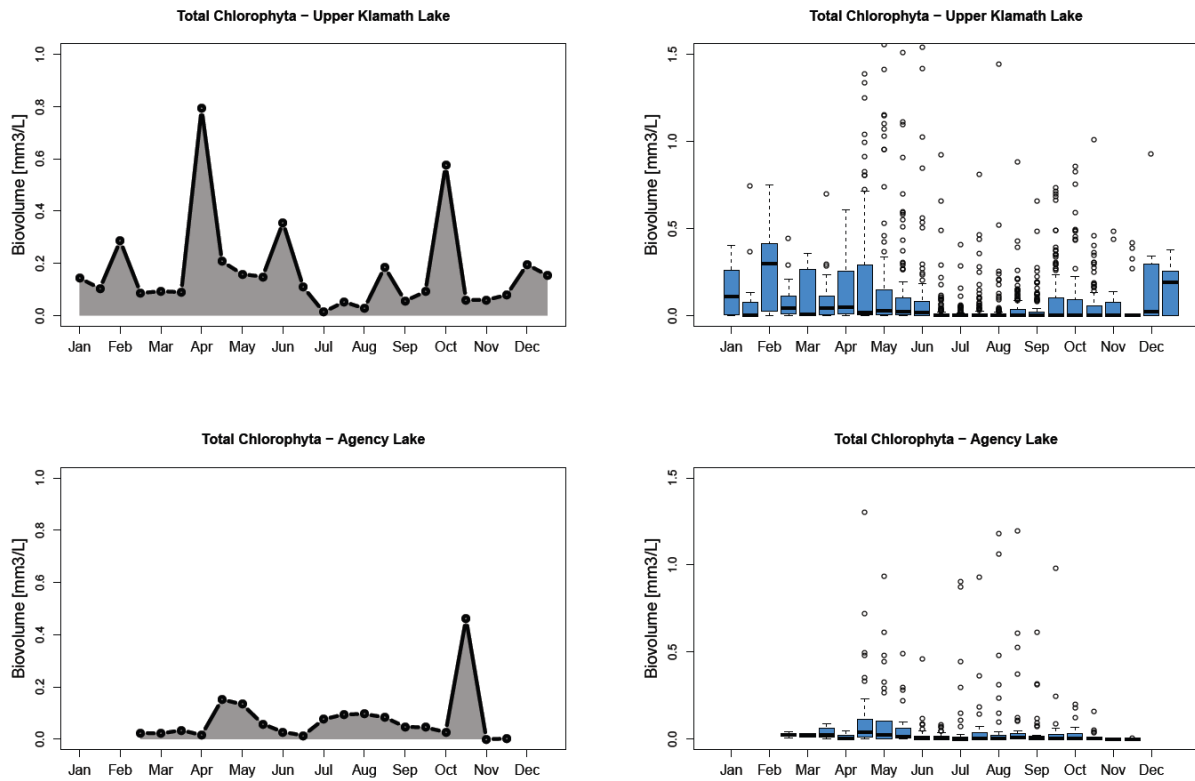


Figure 25: Seasonal dynamics of mean of total Chlorophyta biovolume from (a,c) UKL and (b,d) AL. Note difference in scale of y-axis between line plots and boxplots. Boxplot is based on all individual data from each station and year.

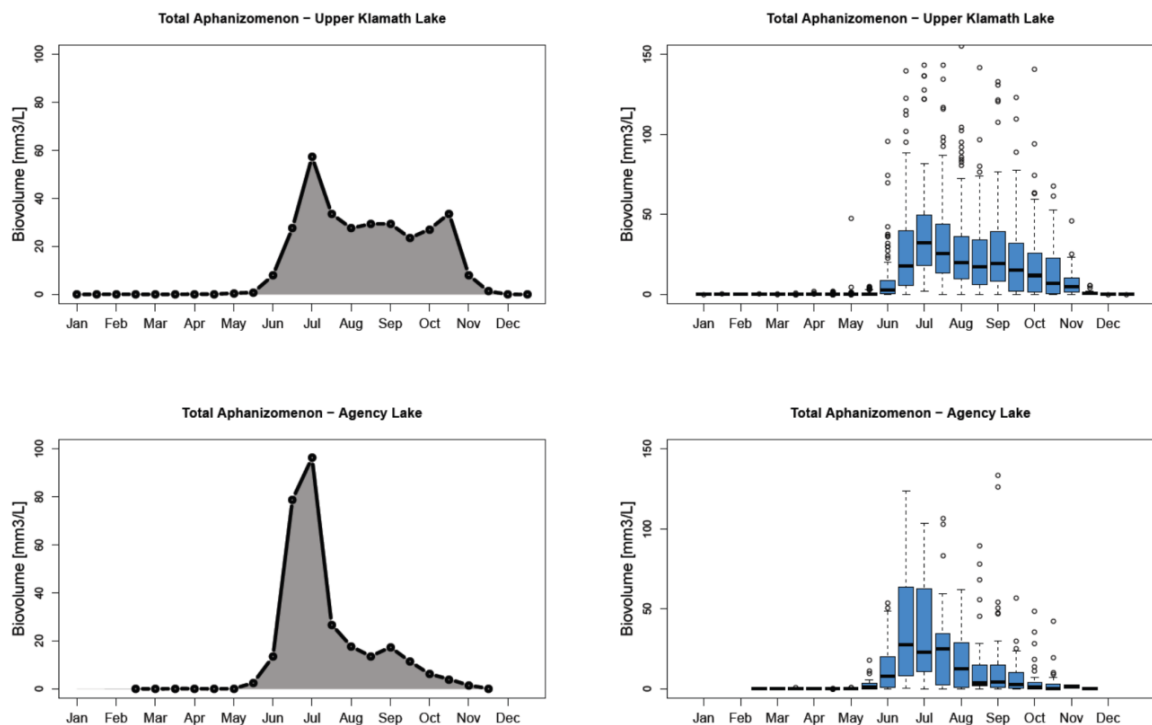


Figure 26: Seasonal dynamics of mean of *Aphanizomenon flos-aquae*. Biovolume from (a,c) UKL and (b,d) AL. Note difference in scale of y-axis between line plots and boxplots. Boxplot is based on all individual data from each station and year.

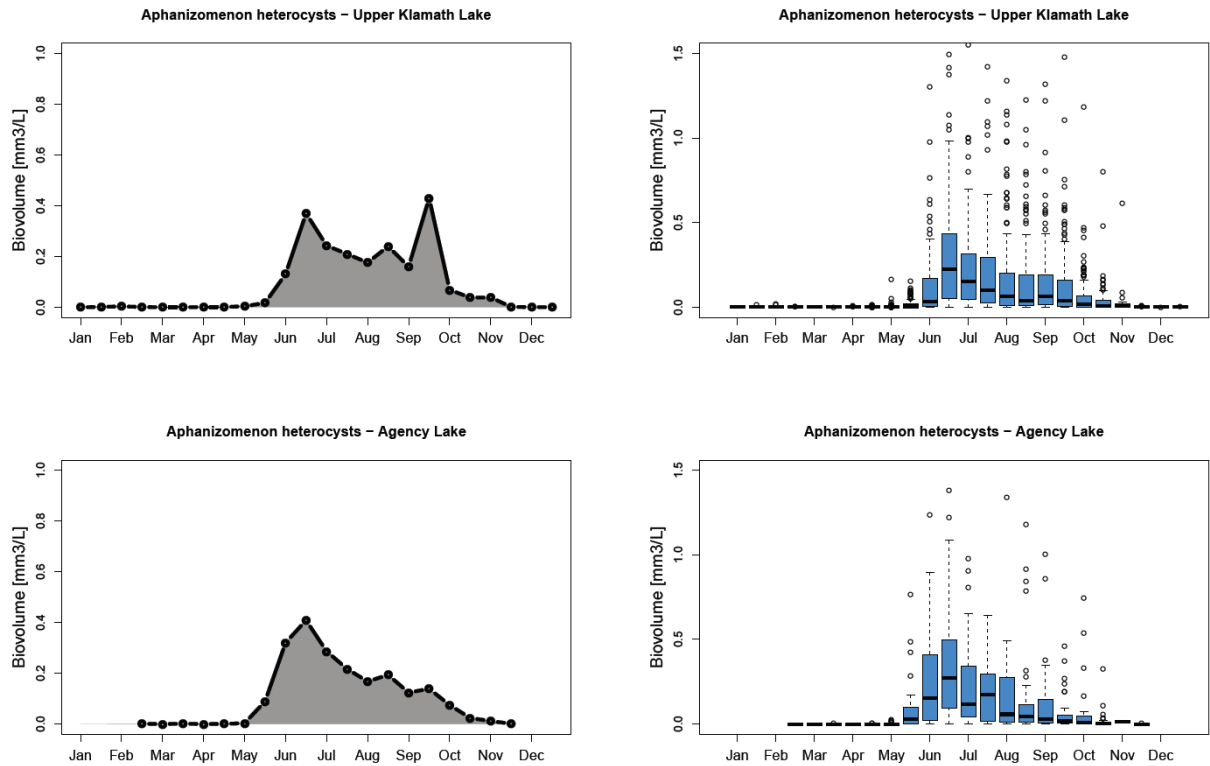


Figure 27: Seasonal dynamics of mean of *Aphanizomenon flos-aquae* heterocysts. Biovolume from (a,c) UKL and (b,d) AL. Note difference in scale of y-axis between line plots and boxplots. Boxplot is based on all individual data from each station and year.

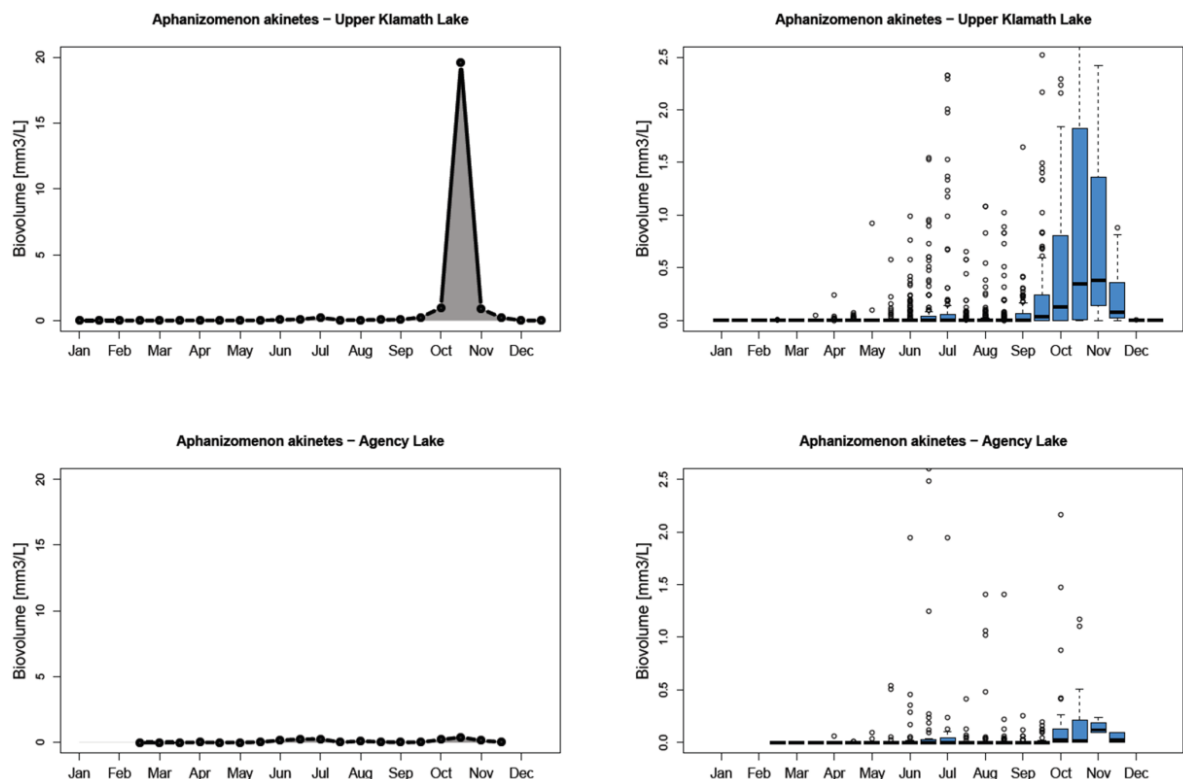


Figure 28: Seasonal dynamics of mean of *Aphanizomenon flos-aquae* akinetes. Biovolume from (a,c) UKL and (b,d) AL. Note difference in scale of y-axis between line plots and boxplots. Boxplot is based on all individual data from each station and year.

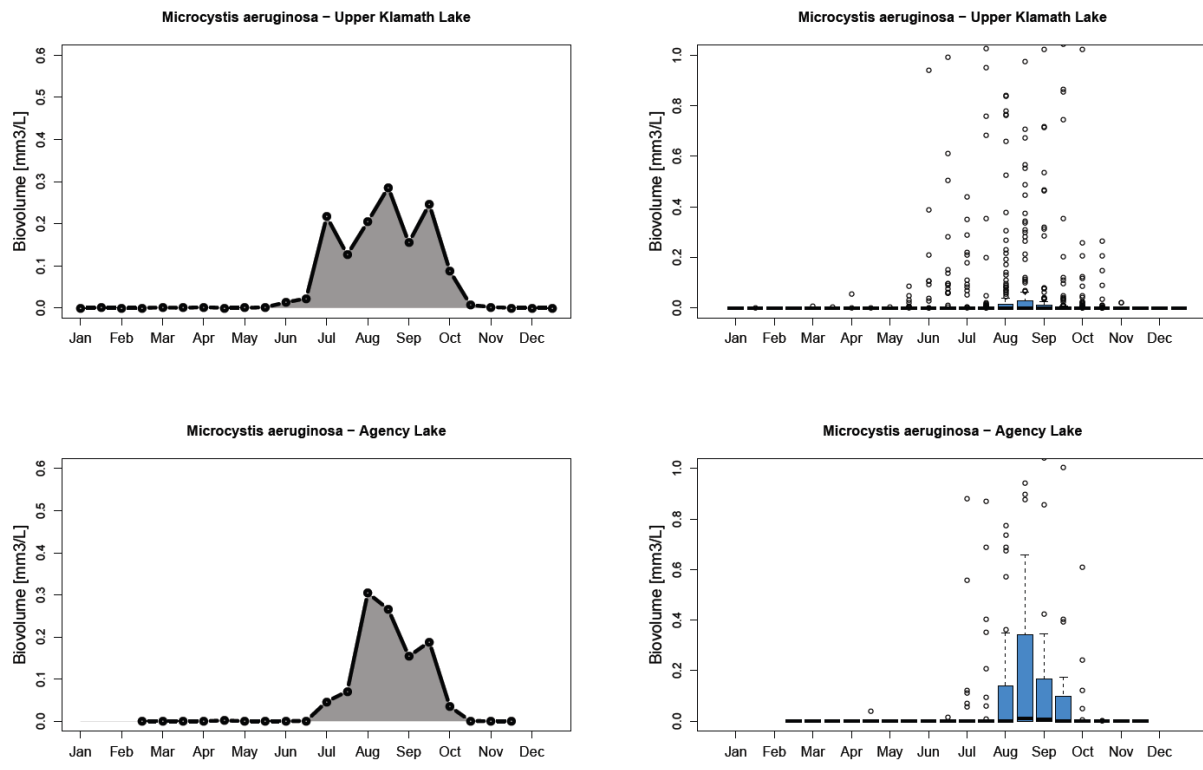


Figure 29: Seasonal dynamics of mean of *Microcystis aeruginosa* biovolume from (a,c) UKL and (b,d) AL. Note difference in scale of y-axis between line plots and boxplots. Boxplot is based on all individual data from each station and year.

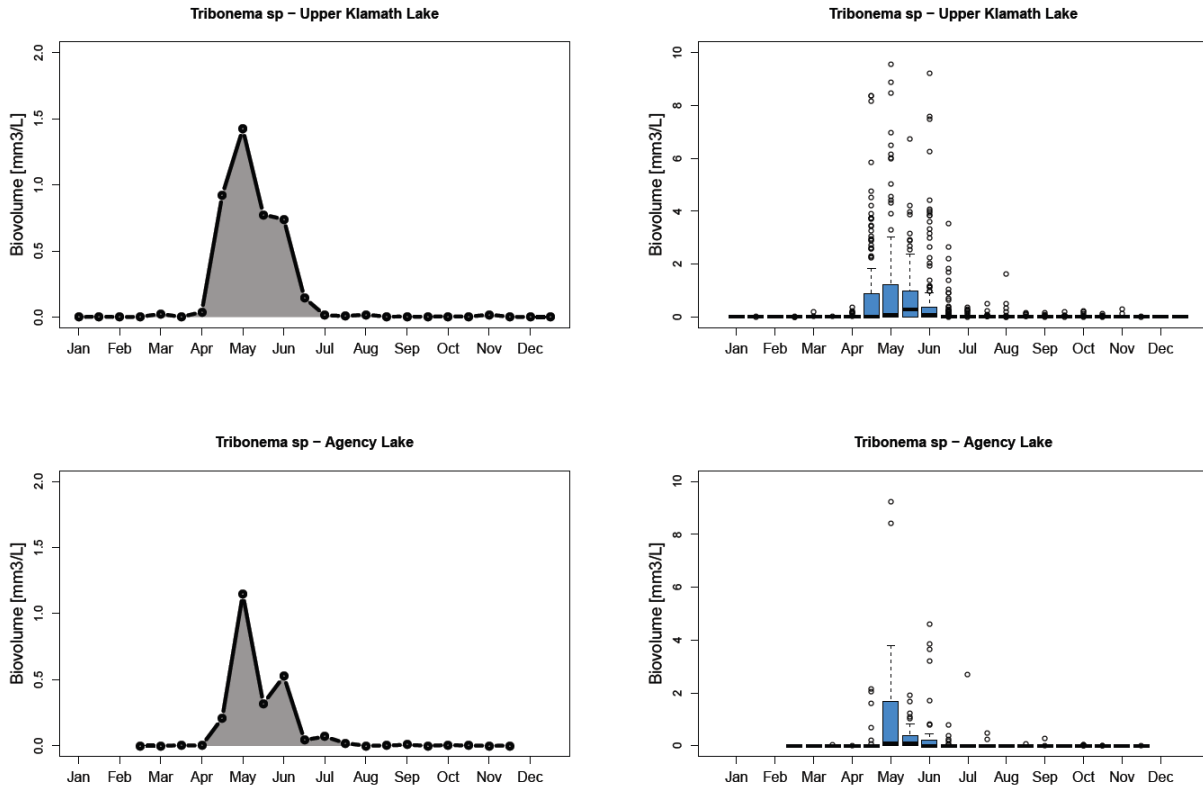


Figure 30: Seasonal dynamics of mean of *Tribonema* sp. biovolume from (a,c) UKL and (b,d) AL. Note difference in scale of y-axis between line plots and boxplots. Boxplot is based on all individual data from each station and year.

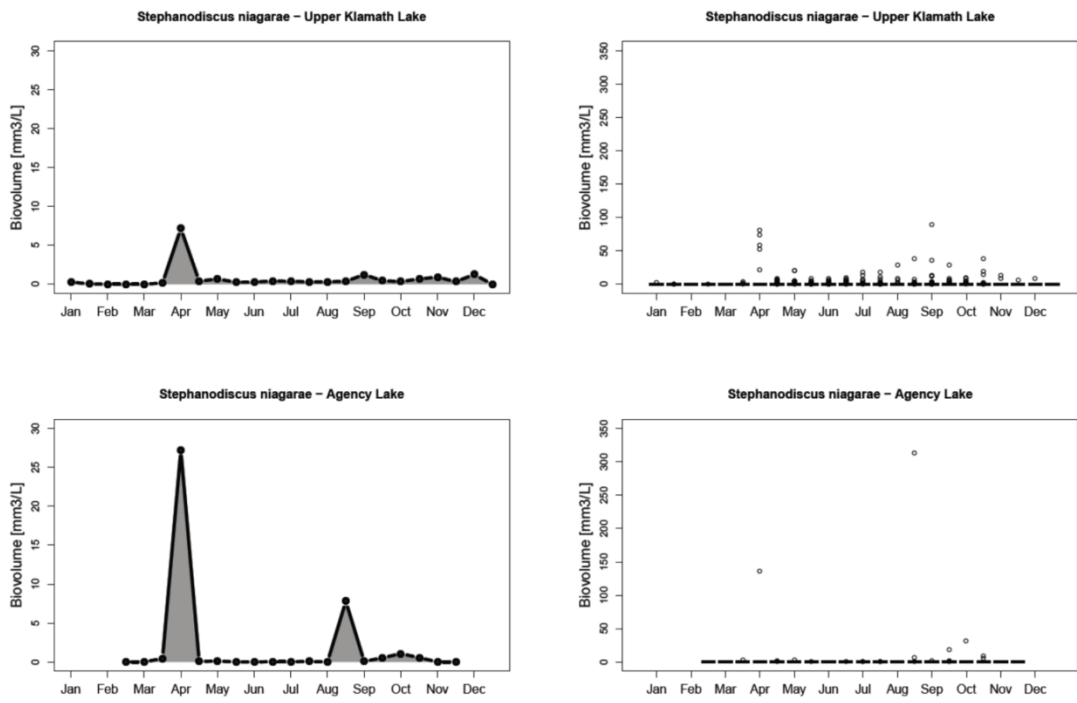


Figure 31: Seasonal dynamics of mean of *Stephanodiscus niagarae* biovolume from (a,c) UKL and (b,d) AL. Note difference in scale of y-axis between line plots and boxplots. Boxplot is based on all individual data from each station and year.

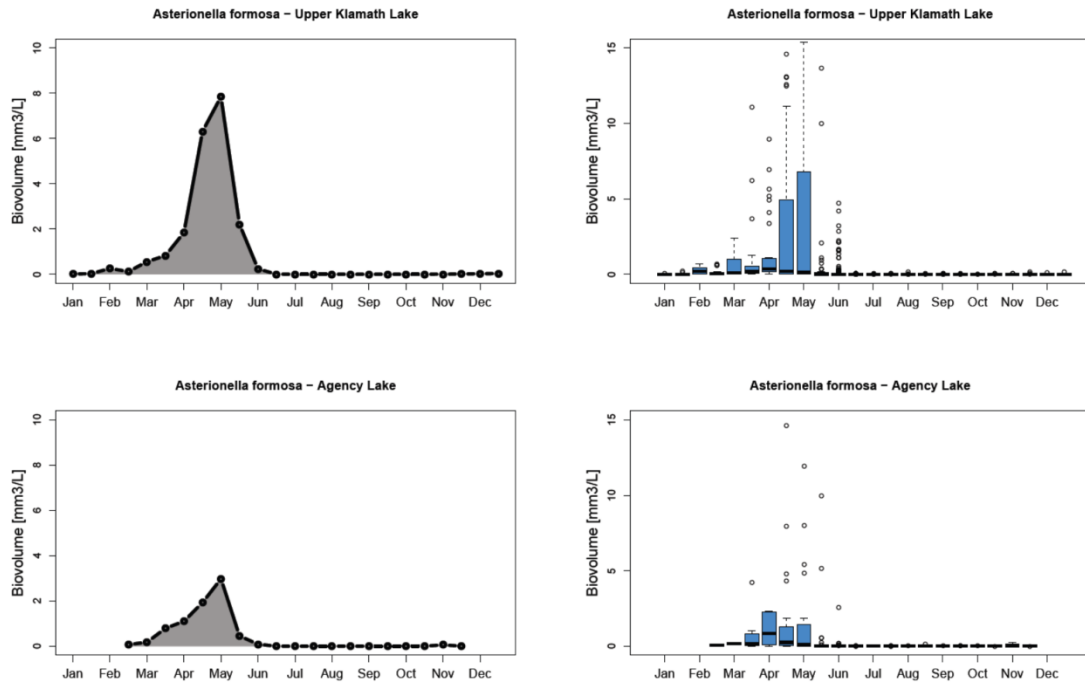


Figure 32: Seasonal dynamics of mean of *Asterionella formosa* from (a,c) UKL and (b,d) AL. Note difference in scale of y-axis between line plots and boxplots. Boxplot is based on all individual data from each station and year.

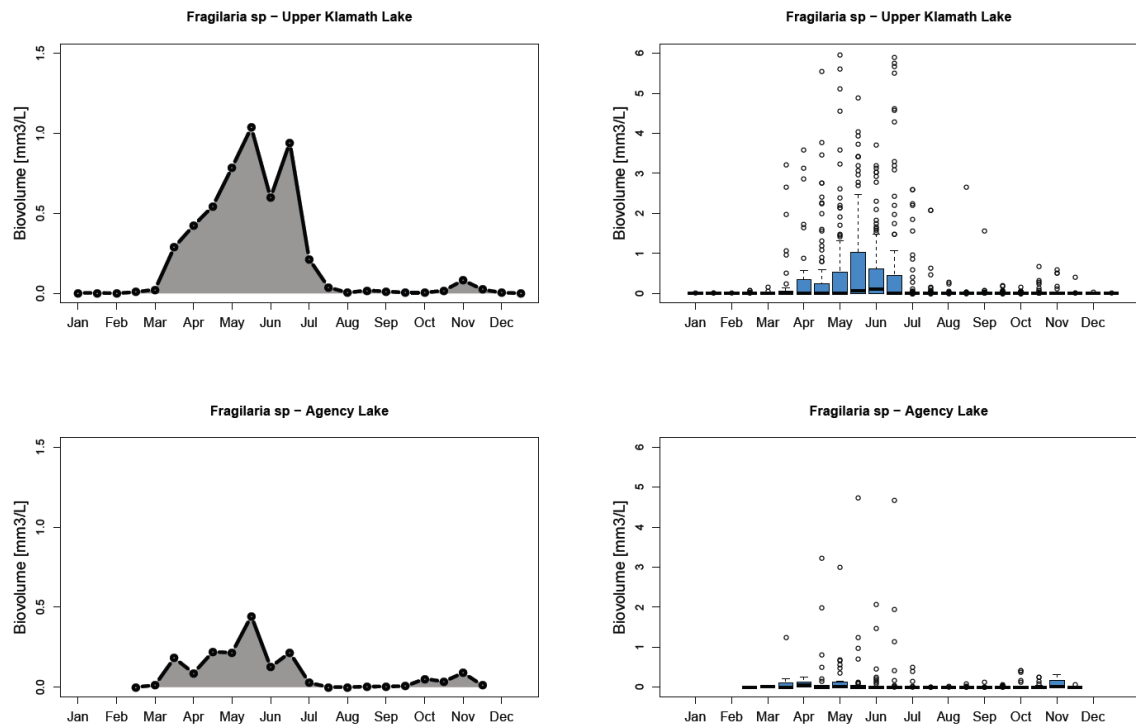


Figure 33: Seasonal dynamics of mean of *Fragilaria* sp. from (a,c) UKL and (b,d) AL. Note difference in scale of y-axis between line plots and boxplots. Boxplot is based on all individual data from each station and year.

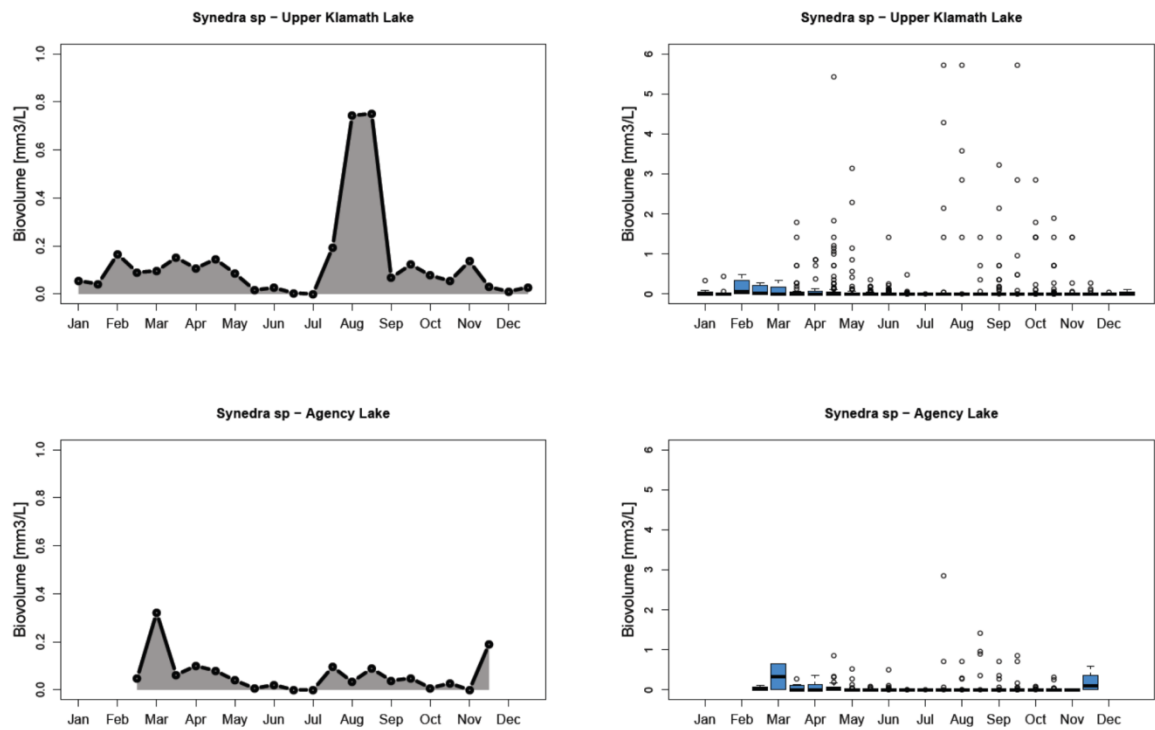


Figure 34: Seasonal dynamics of mean of *Synedra* sp. from (a,c) UKL and (b,d) AL. Note difference in scale of y-axis between line plots and boxplots. Boxplot is based on all individual data from each station and year.

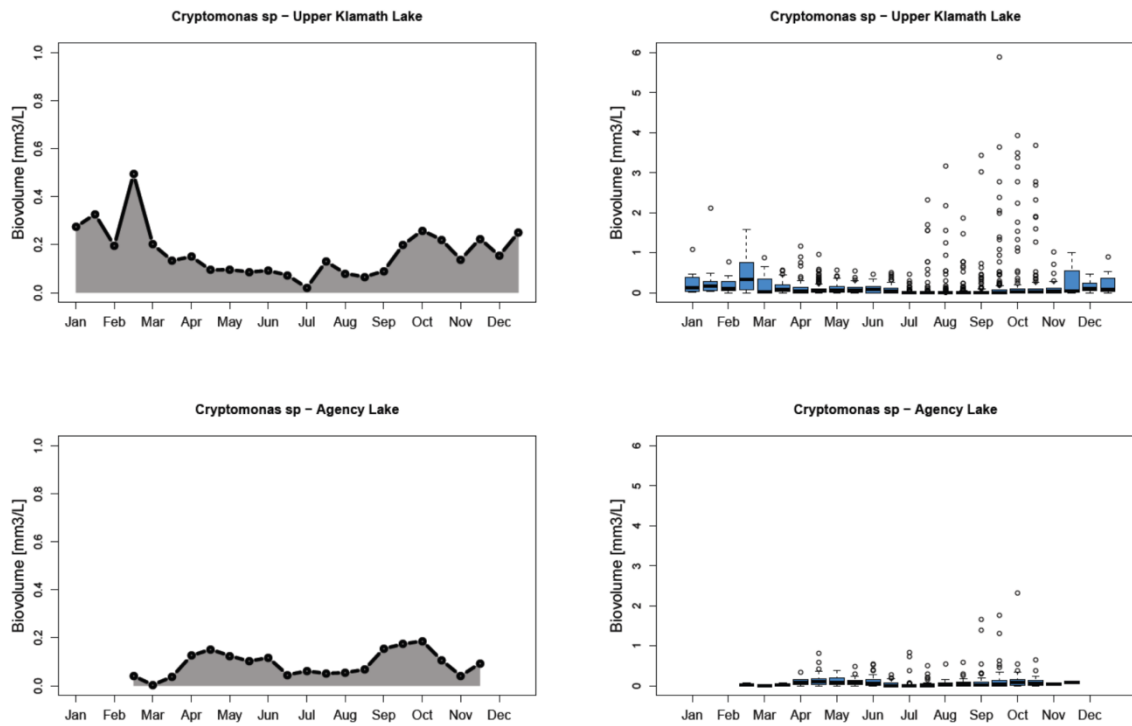


Figure 35: Seasonal dynamics of mean of *Cryptomonas* sp. from (a,c) UKL and (b,d) AL. Note difference in scale of y-axis between line plots and boxplots. Boxplot is based on all individual data from each station and year.

Zooplankton

A wide range of zooplankton species (or genera) were identified in UKL (Figure 36) and AL (Figure 37), however, the lakes are generally dominated by a relatively few species and primarily by *Daphnia pulicaria*. A total of 44 and 41 zooplankton species were observed in UKL and AL, respectively, across the entire time period of 1990-2015 but most species were observed at low biomasses. The most dominant zooplankton was comprised of *Daphnia* species which were abundant during most of the growing season. An increase in *Daphnia* abundance typically occurs in late April or early May, extending into June, and starting right after the diatom bloom (Figure 38). The seasonal pattern is consistent in both UKL and AL. Boxplots for both AL and UKL also show that despite the clear seasonal increase during the growing season, substantial variation among stations and years is common.

The calanoid copepod *Leptodiaptomus ashlandi* showed similar patterns in both AL and UKL (Figure 39), being dominant in the spring before declining and remaining low until mid to late August before a smaller fall increase. The cyclopoid copepod *Diacyclops thomasi* (Figure 41), calanoid copepodids (Figure 42), cyclopoid copepodids (Figure 47) and Copepoda nauplii (Figure 44) showed a similar pattern being most abundant in the spring before declining in late May to early June as the *Daphnia* increased. The cladoceran *Leptodora kindtii* (Figure 43) and rotifer *Euchlanis* sp. (Figure 45) increased in late June, and peaked in July before declining sharply in August. The calanoid copepod *Epischura nevadensis* (Figure 46) showed a high August peak in AL and a more modest but still the high peak in UKL. The cladoceran *Chydorus sphaericus* (Figure 40) was primarily present in late summer during the months of

Sep-Oct. The microzooplankton rotifer genera *Keratella* (Figure 48) and *Synchaeta* (Figure 49) were most abundant in the spring, and declined in July before showing a small increase in the fall in AL, and in the winter in UKL. Besides *Daphnia*, *Euchlanis* sp. and *Leptodora kindtii*, the general pattern of the most common zooplankton species, including microzooplankton, were that they all occurred before and after the main *Aphanizomenon flos-aquae* and *Daphnia* peaks.

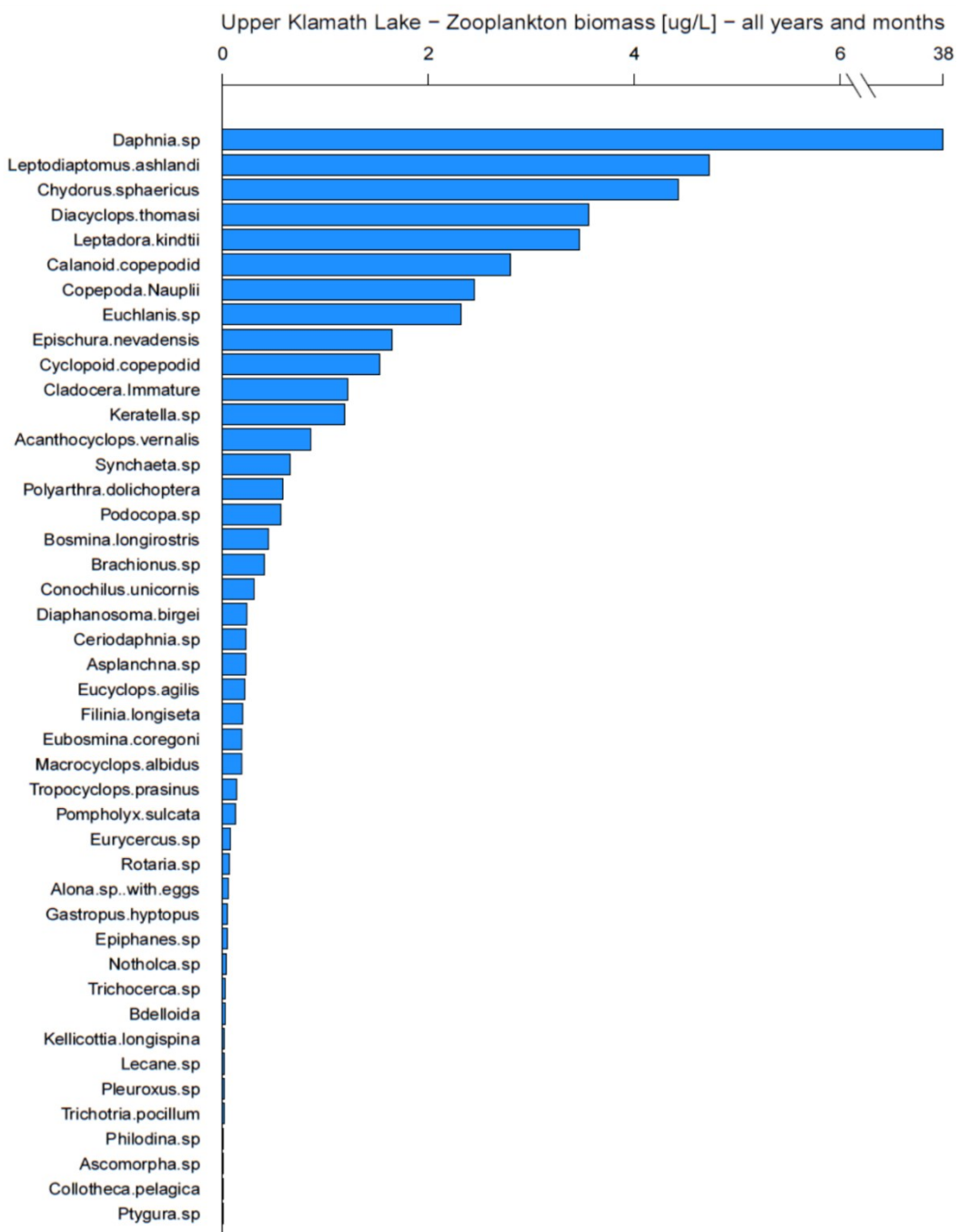


Figure 36: Square rooted zooplankton species biomass from Upper Klamath Lake for all years and all stations, based on bi-monthly data. Note the brake in scale for *Daphnia* sp.

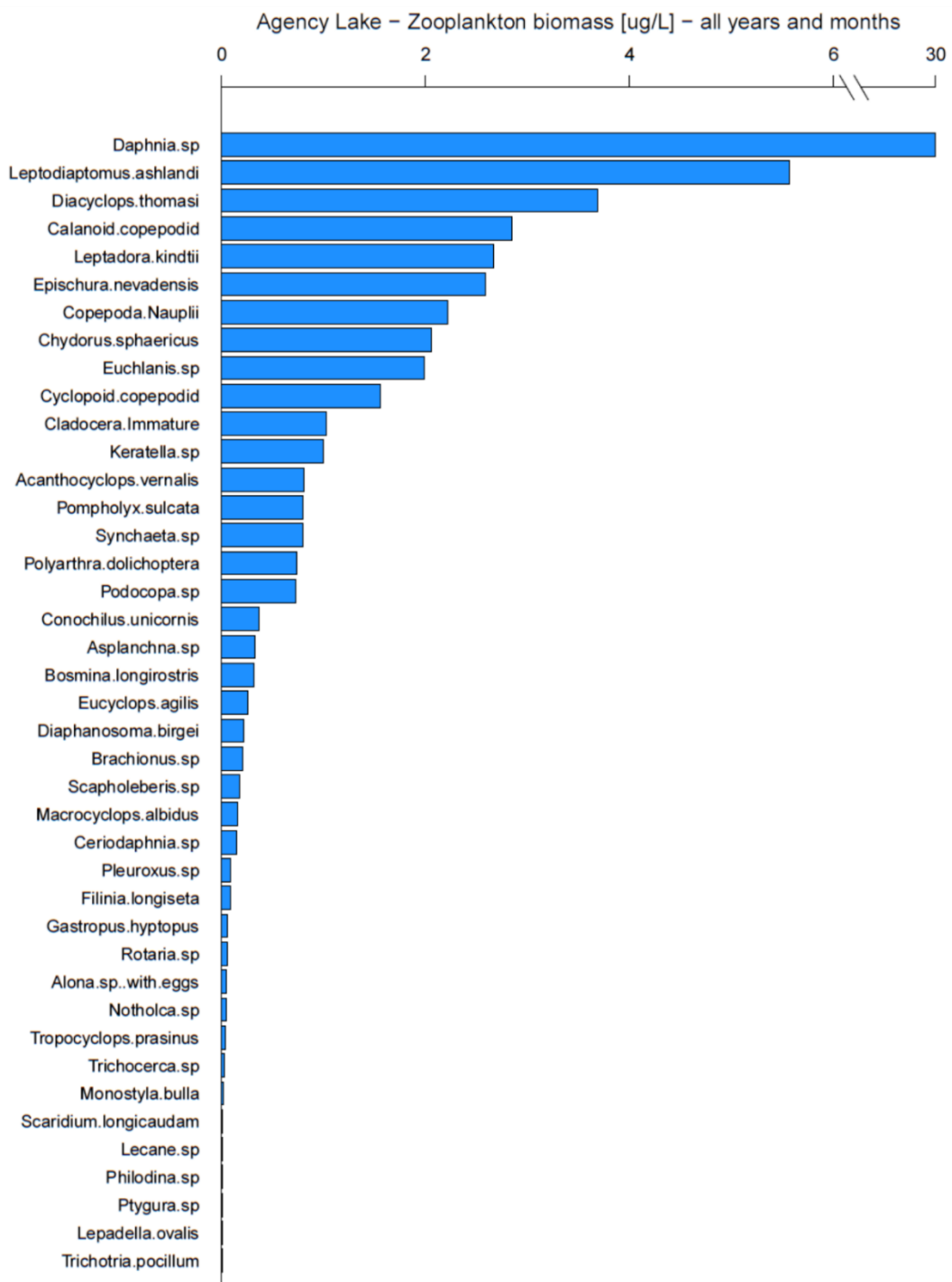


Figure 37: Square rooted zooplankton species biomass from Agency Lake for all years and all stations, based on bi-monthly data. Note the brake in the scale for *Daphnia* sp.

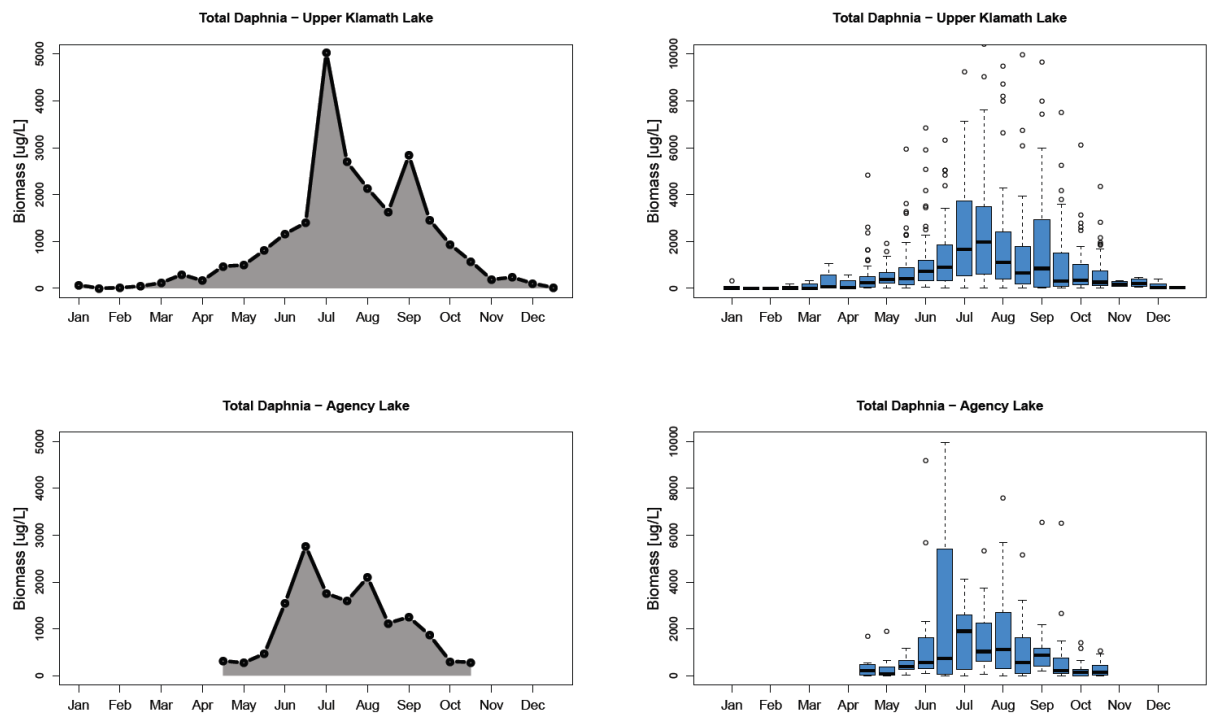


Figure 38: Seasonal dynamics of mean of *Daphnia* sp. biomass from (a,c) UKL and (b,d) AL. Note difference in scale of y-axis between line plots and boxplots.

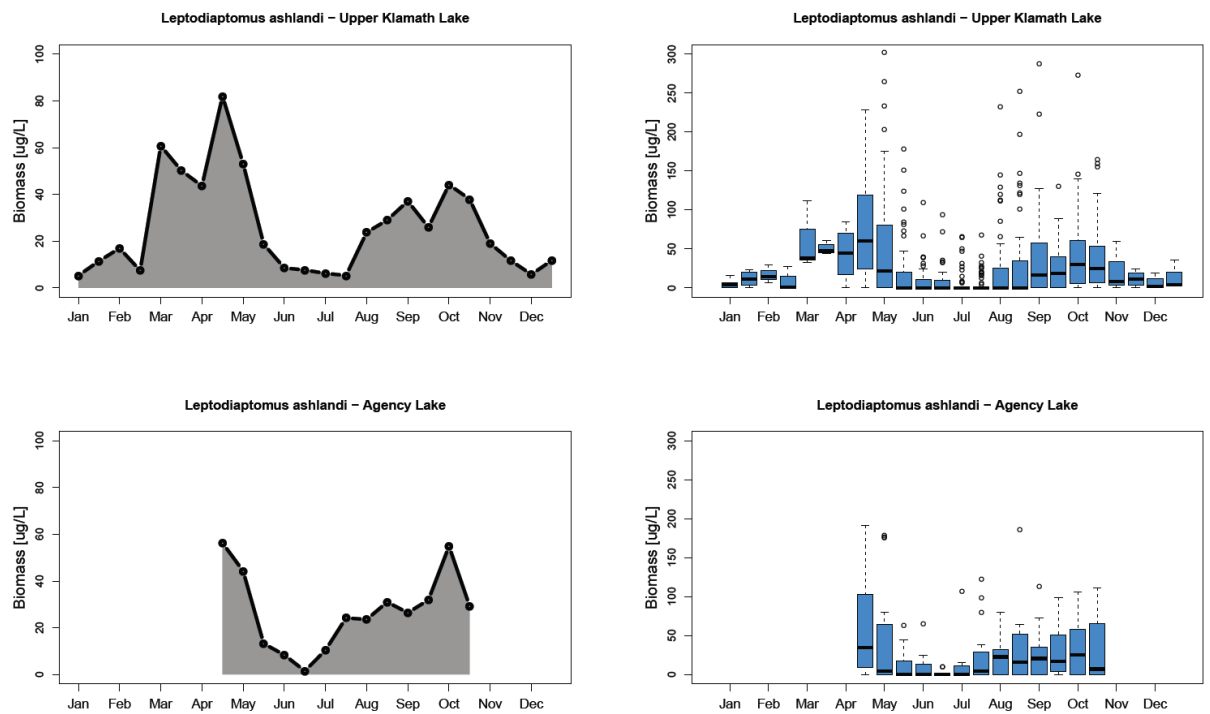


Figure 39: Seasonal dynamics of mean of *Leptodiaptomus ashlandi* biomass from (a,c) UKL and (b,d) AL. Note difference in scale of y-axis between line plots and boxplots.

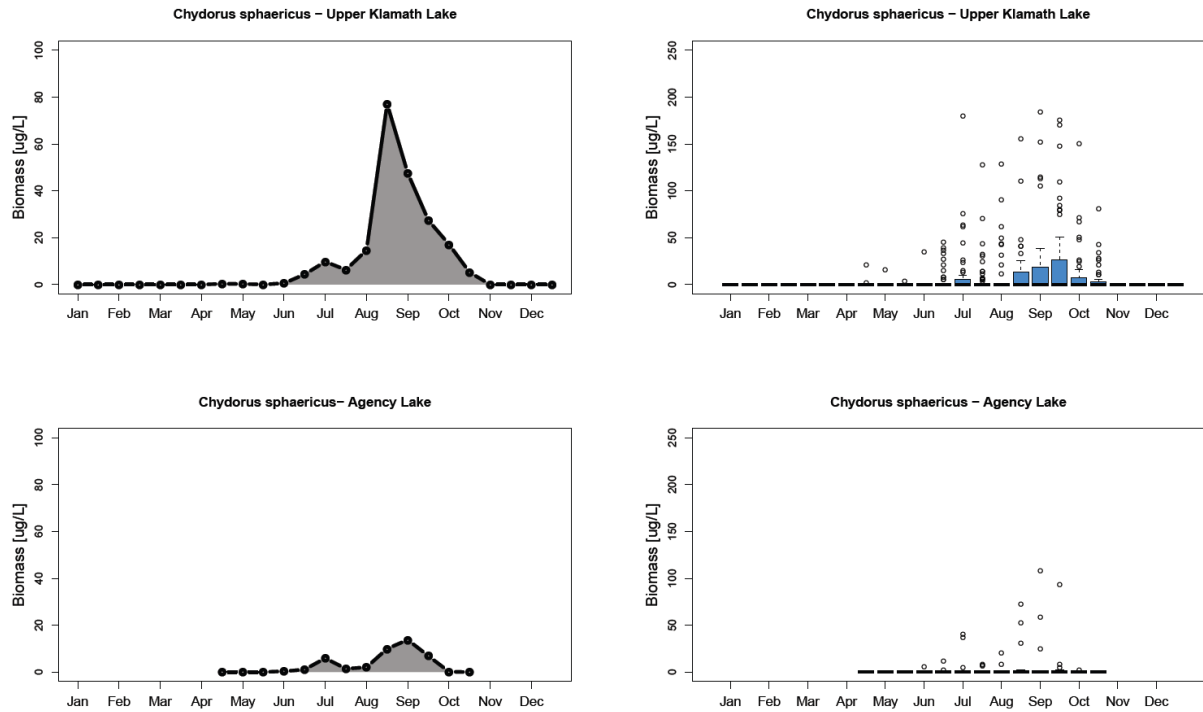


Figure 40: Seasonal dynamics of mean of *Chydorus sphaericus* biomass from (a,c) UKL and (b,d) AL. Note difference in scale of y-axis between line plots and boxplots.

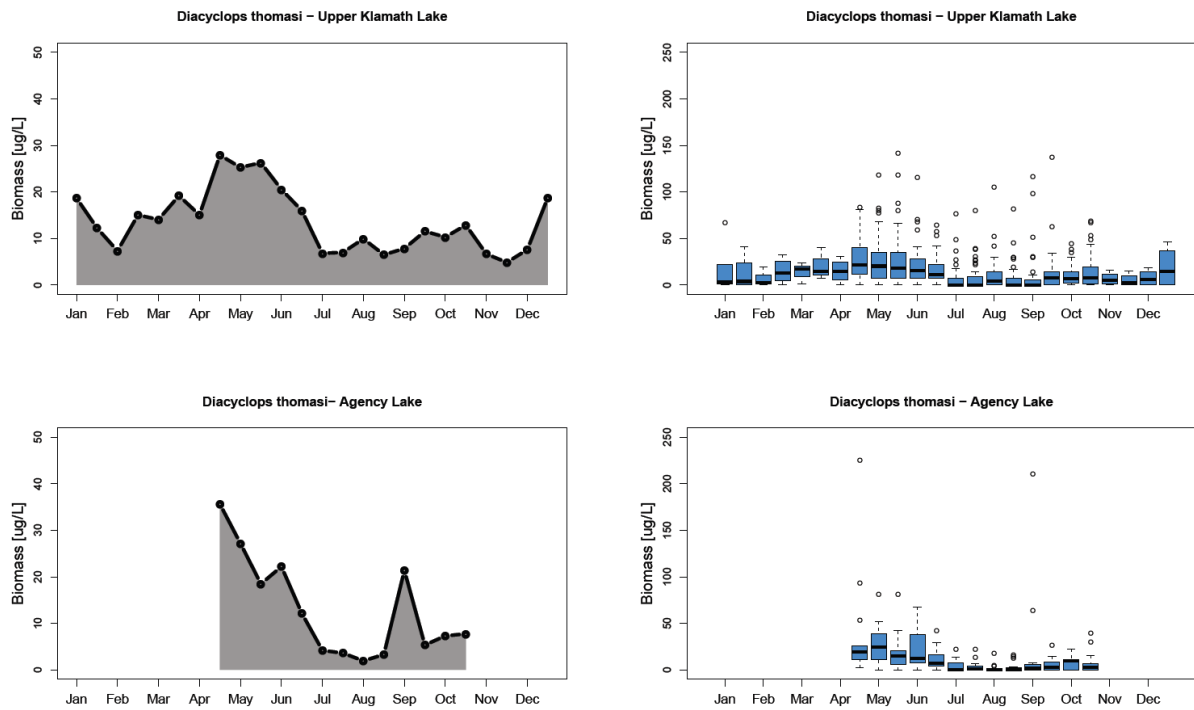


Figure 41: Seasonal dynamics of mean of *Diacyclops thomasi* biomass from (a,c) UKL and (b,d) AL. Note difference in scale of y-axis between line plots and boxplots.

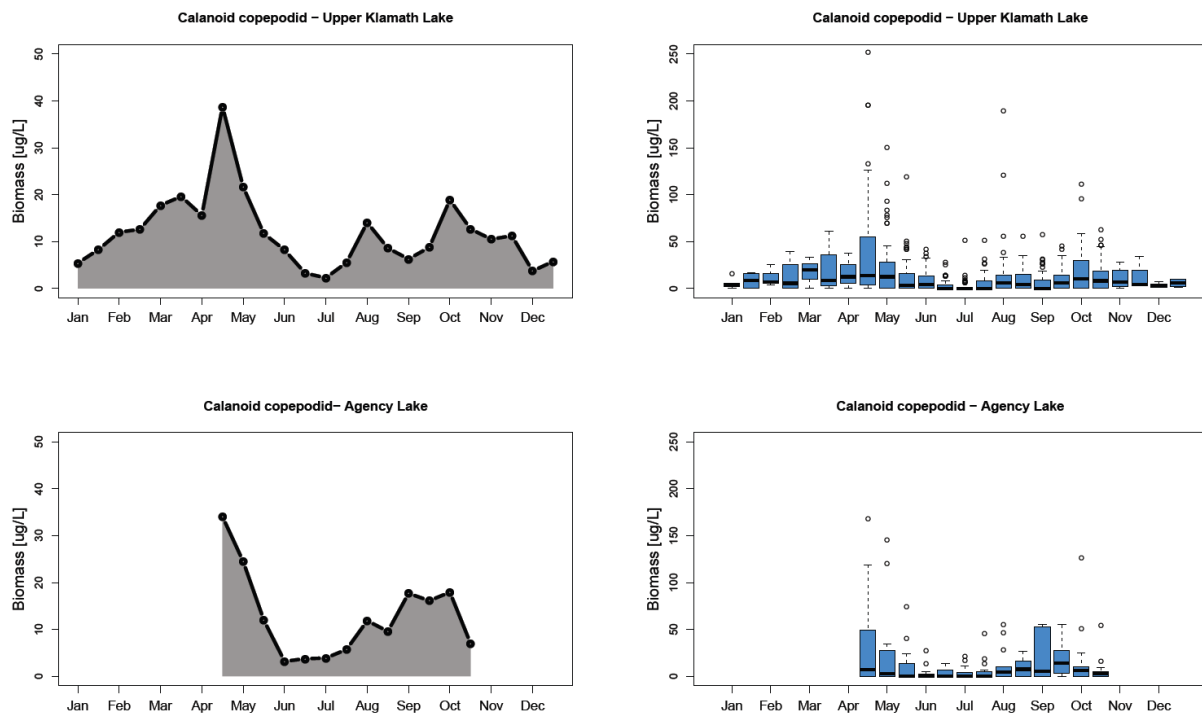


Figure 42: Seasonal dynamics of mean of Calanoid copepodid biomass from (a,c) UKL and (b,d) AL. Note difference in scale of y-axis between line plots and boxplots.

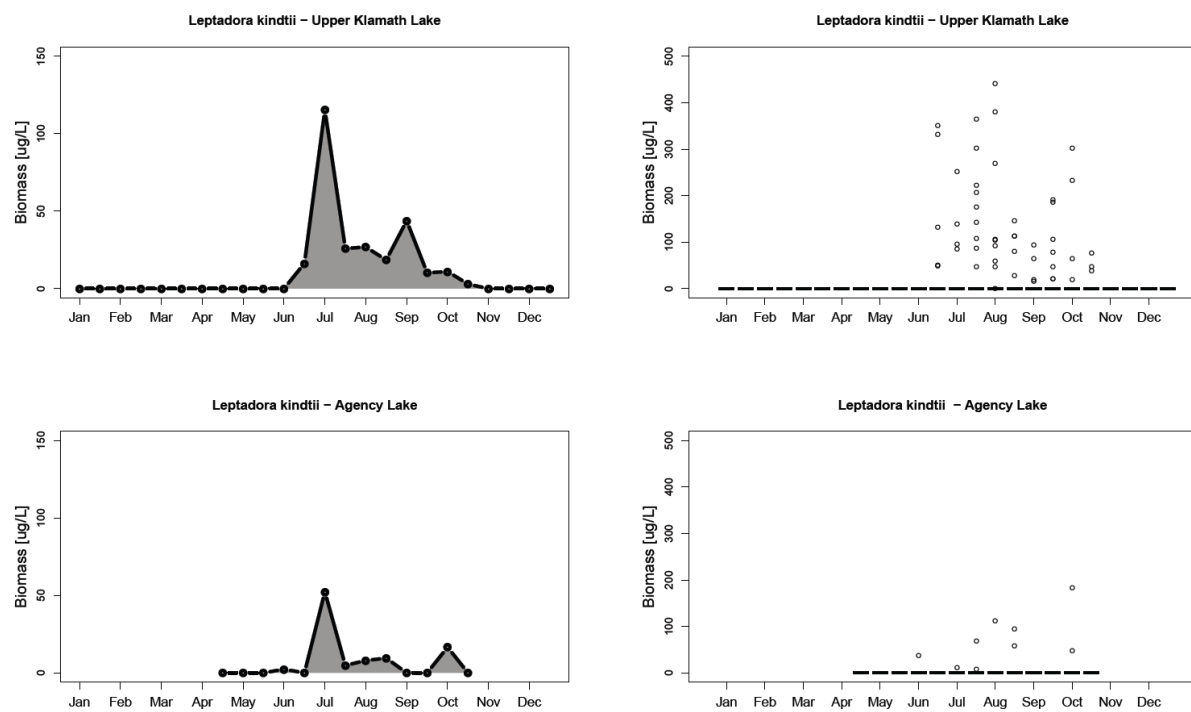


Figure 43: Seasonal dynamics of mean of *Leptodora kindtii* biomass from (a,c) UKL and (b,d) AL. Note difference in scale of y-axis between line plots and boxplots.

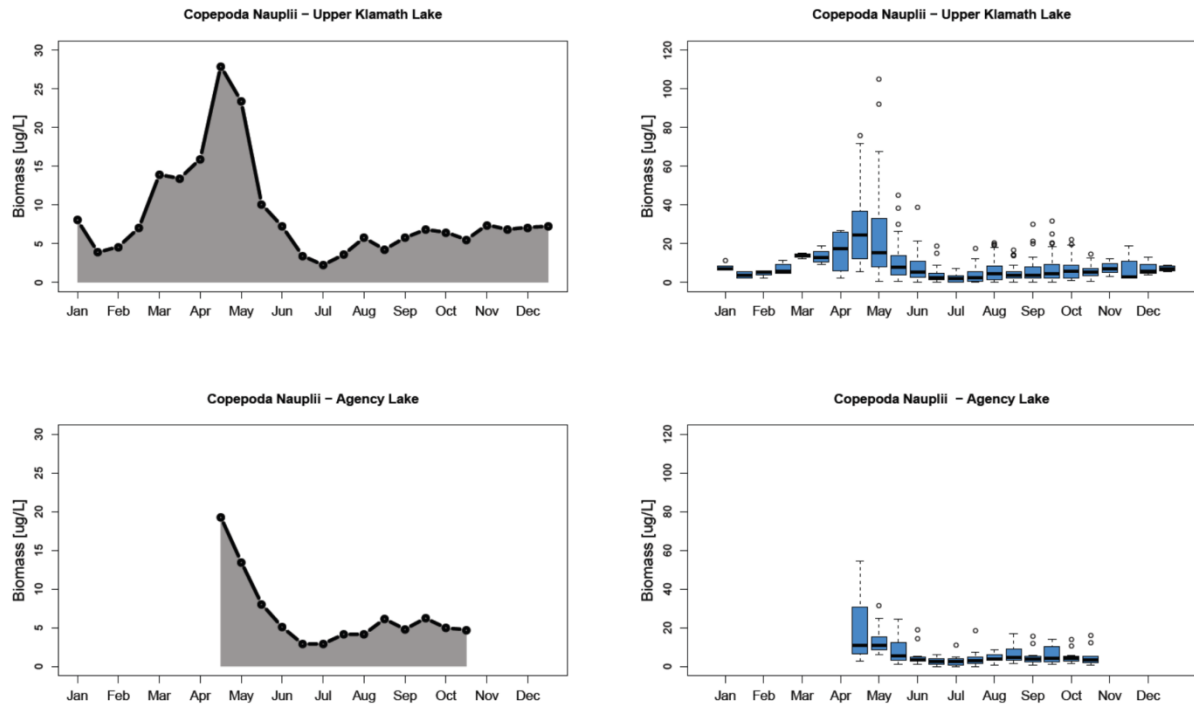


Figure 44: Seasonal dynamics of mean of Copepoda nauplii biomass from (a,c) UKL and (b,d) AL. Note difference in scale of y-axis between line plots and boxplots.

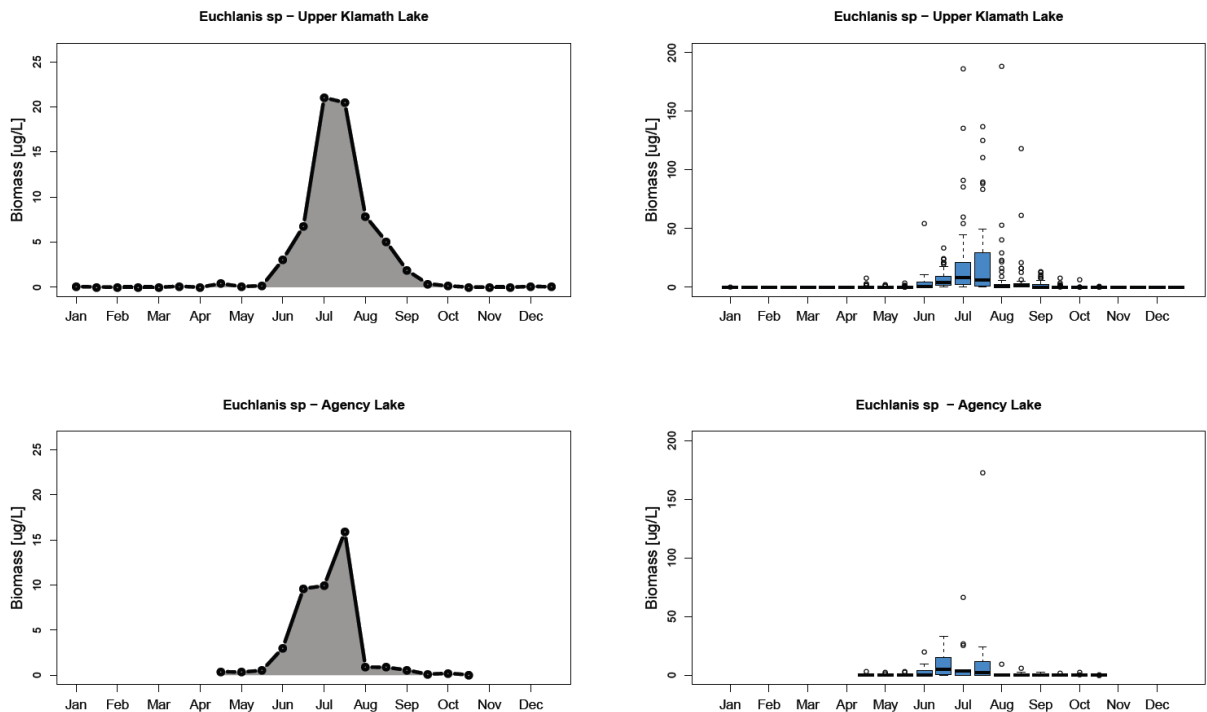


Figure 45: Seasonal dynamics of mean of *Euchlanis* sp. biomass from (a,c) UKL and (b,d) AL. Note difference in scale of y-axis between line plots and boxplots.

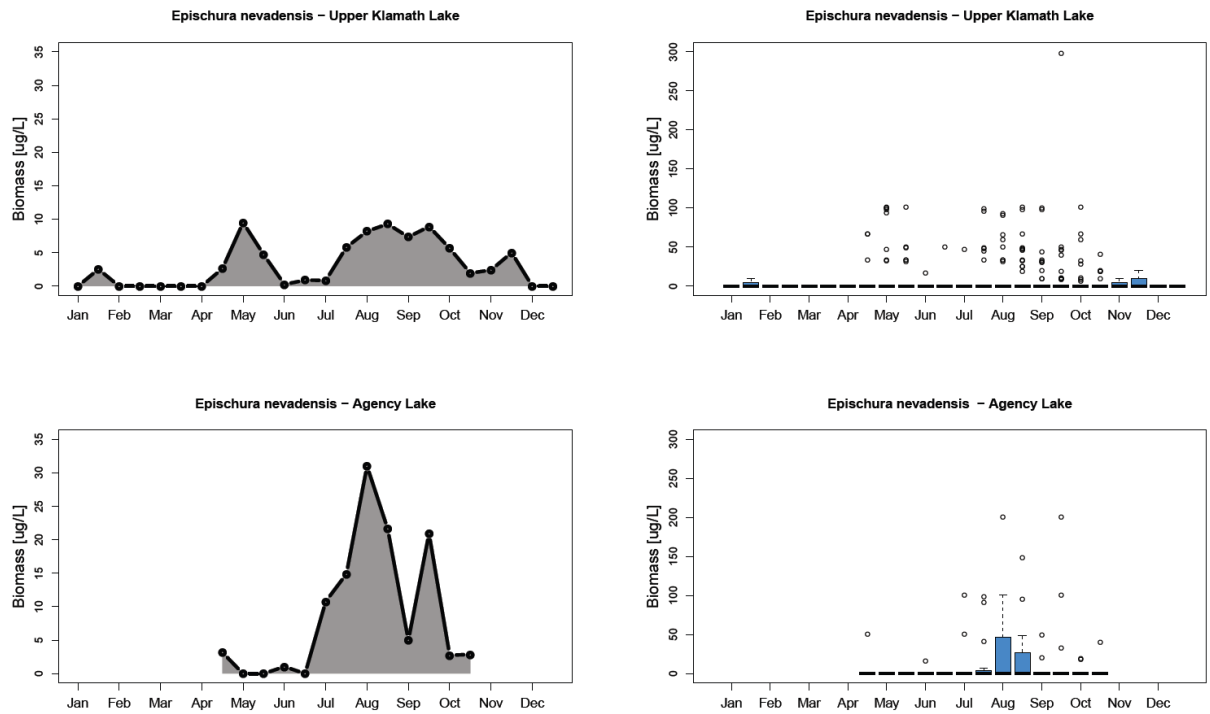


Figure 46: Seasonal dynamics of mean of *Epischura nevadensis* biomass from (a,c) UKL and (b,d) AL. Note difference in scale of y-axis between line plots and boxplots.

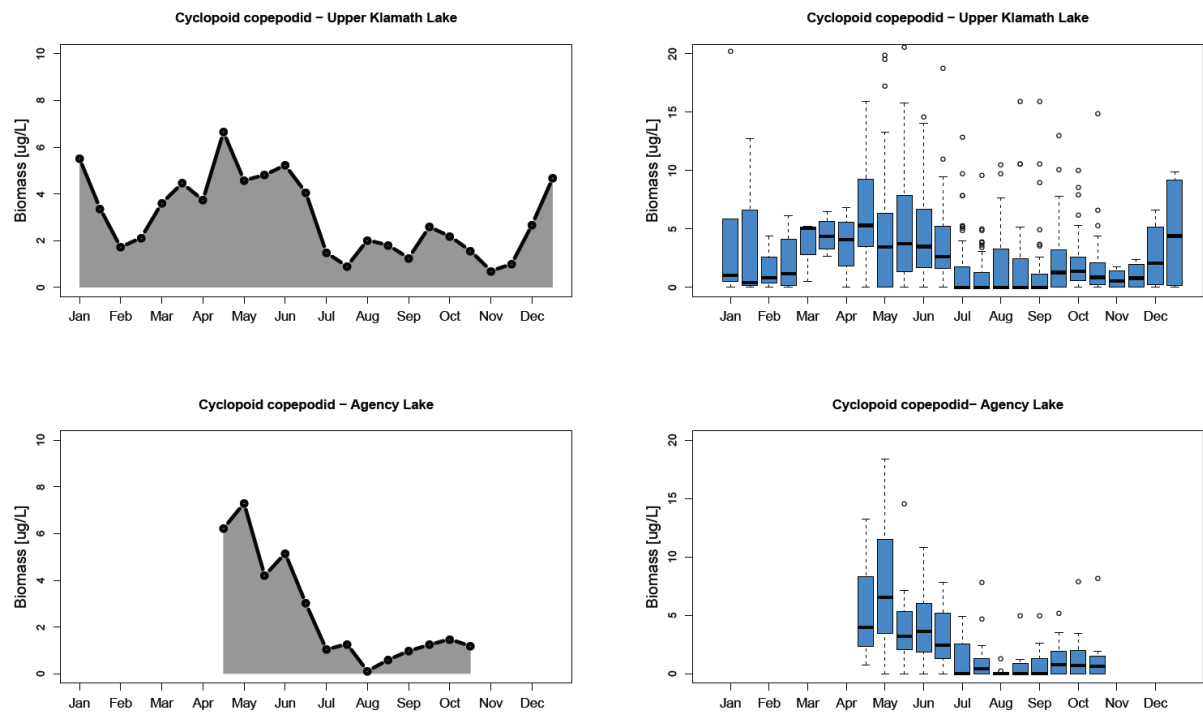


Figure 47: Seasonal dynamics of mean of Cyclopoid copepodid biomass from (a,c) UKL and (b,d) AL. Note difference in scale of y-axis between line plots and boxplots.

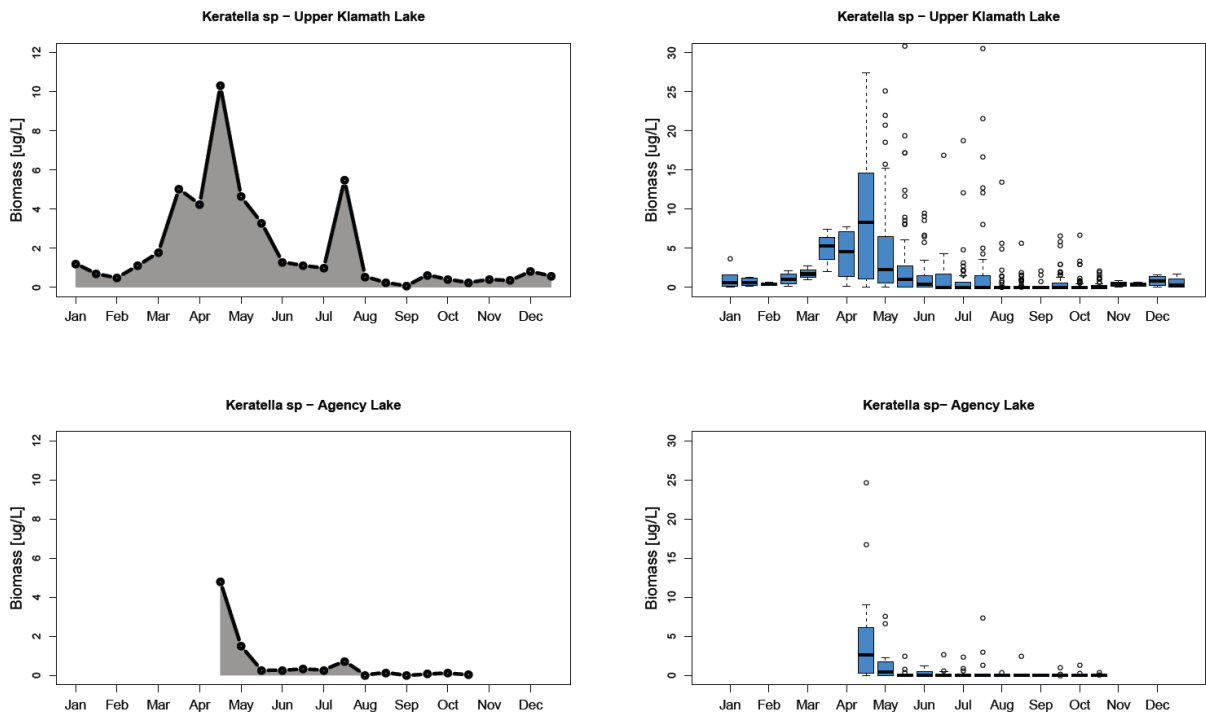


Figure 48: Seasonal dynamics of mean of *Keratella* sp. biomass from (a,c) UKL and (b,d) AL. Note difference in scale of y-axis between line plots and boxplots.

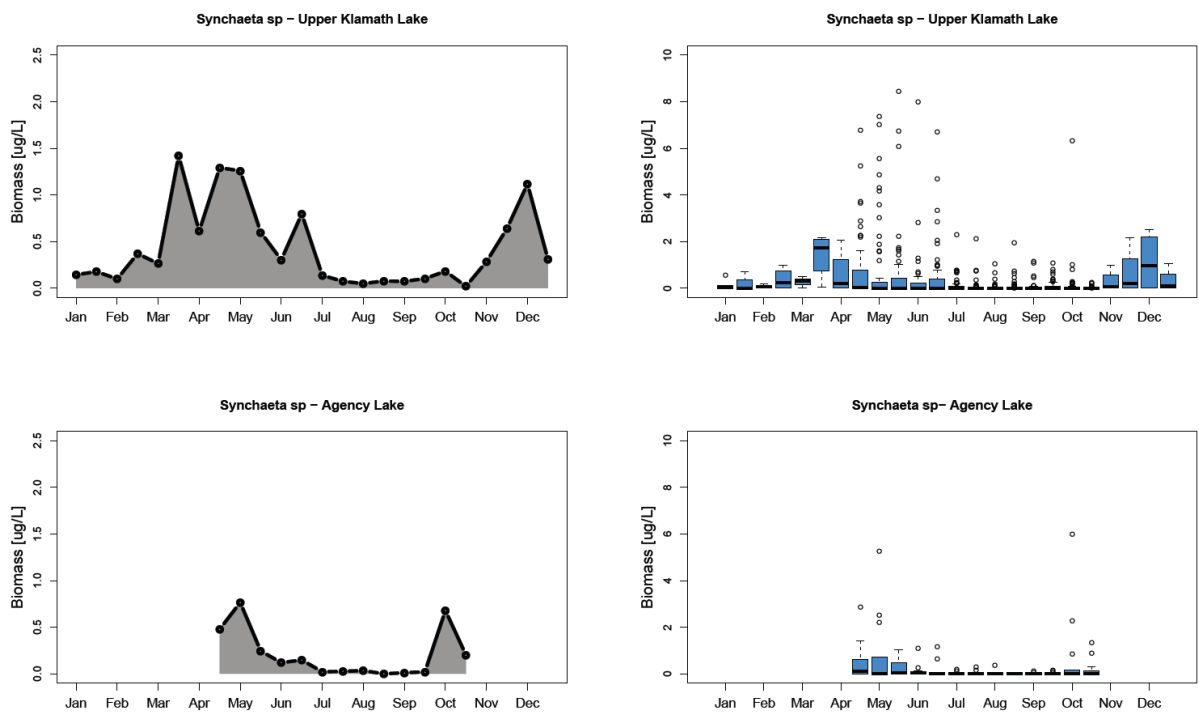


Figure 49: Seasonal dynamics of mean of *Synchaeta* sp. biomass from (a,c) UKL and (b,d) AL. Note difference in scale of y-axis between line plots and boxplots.

Combined seasonal cycles of plankton and major water quality parameters

Despite the relatively consistent seasonal patterns observed, the timing and succession of water quality parameters, phytoplankton and zooplankton vary from year to year. Therefore, to fully understand the ecological processes in UKL and AL further analyses are required to explain this inter-annual variability.

Looking at the combined data for the UKL stations showed a unimodal seasonal cycle with the peak phytoplankton biomass occurring during June-September, which also resulted in similar seasonally high levels of total phosphorus ($r^2=0.89$, $p<0.01$), soluble reactive phosphorus ($r^2=0.77$, $p<0.01$) and total nitrogen concentrations ($r^2=0.65$, $p<0.01$; Figure 50A-C). The main phytoplankton peak caused increased pH levels in June and July, and the decline caused decreasing DO generally in July and August. The seasonal cycle commonly started with a substantial diatom bloom in April-May, followed by the main summer cyanobacteria bloom in June-September, which constituted 99% of the phytoplankton biomass (Figure 50D). The initial diatom bloom in the spring caused a substantial decrease in available silica concentrations ($r^2=0.40$, $p<0.01$, Figure 50C) and is often followed by a sudden increase in *Daphnia* biomass and short clear-water phase (wherein water clarity on average increased from 0.5 to 1.1 m) prior to the onset of the main *Aphanizomenon* bloom (Figure 51).

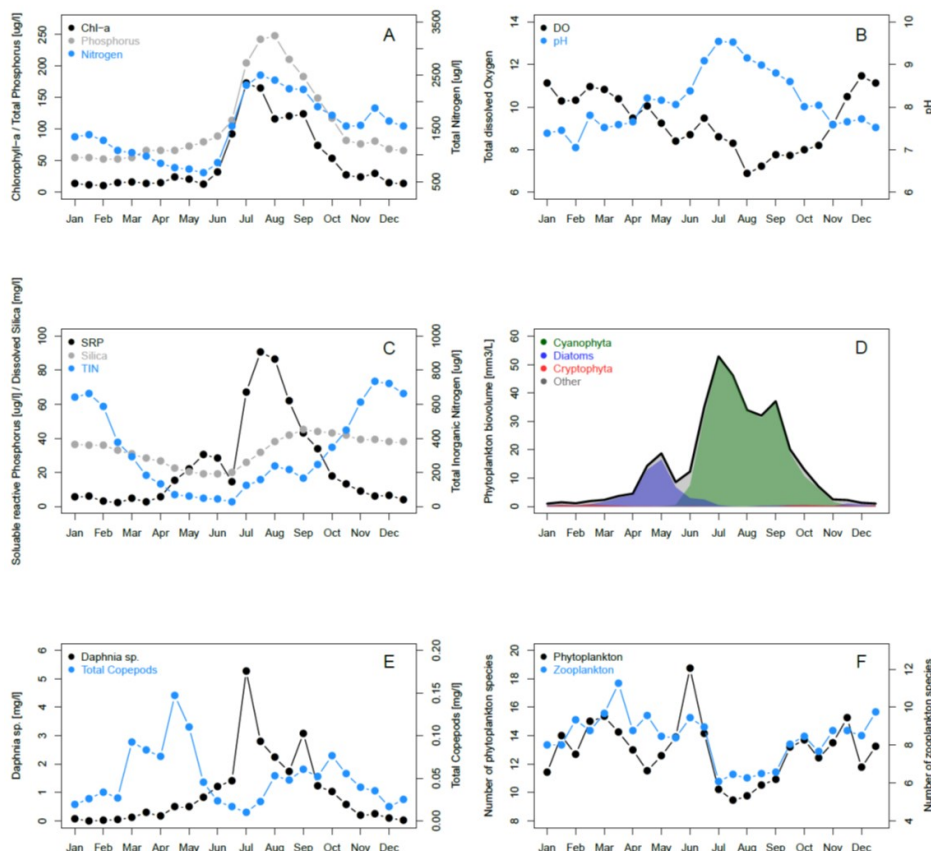


Figure 50: Upper Klamath Lake wide mean annual seasonal cycle of A) the biomass ($\mu\text{g/L}$) of chlorophyll-a (black), total phosphorus (grey) and total nitrogen (blue), B) total dissolved oxygen (black) and pH (blue), C) Soluble reactive phosphorus (black), Silica (grey) and Total inorganic nitrogen (blue), D) the biovolume (mm^3/L) of total phytoplankton (black line), Cyanophyta (green), diatoms (blue), Cryptophyta (red) and other phytoplankton taxa, E) Biomass (mg/L) of *Daphnia* sp. (black) and total copepods (blue), and F) species richness of phytoplankton (black) and zooplankton (blue).

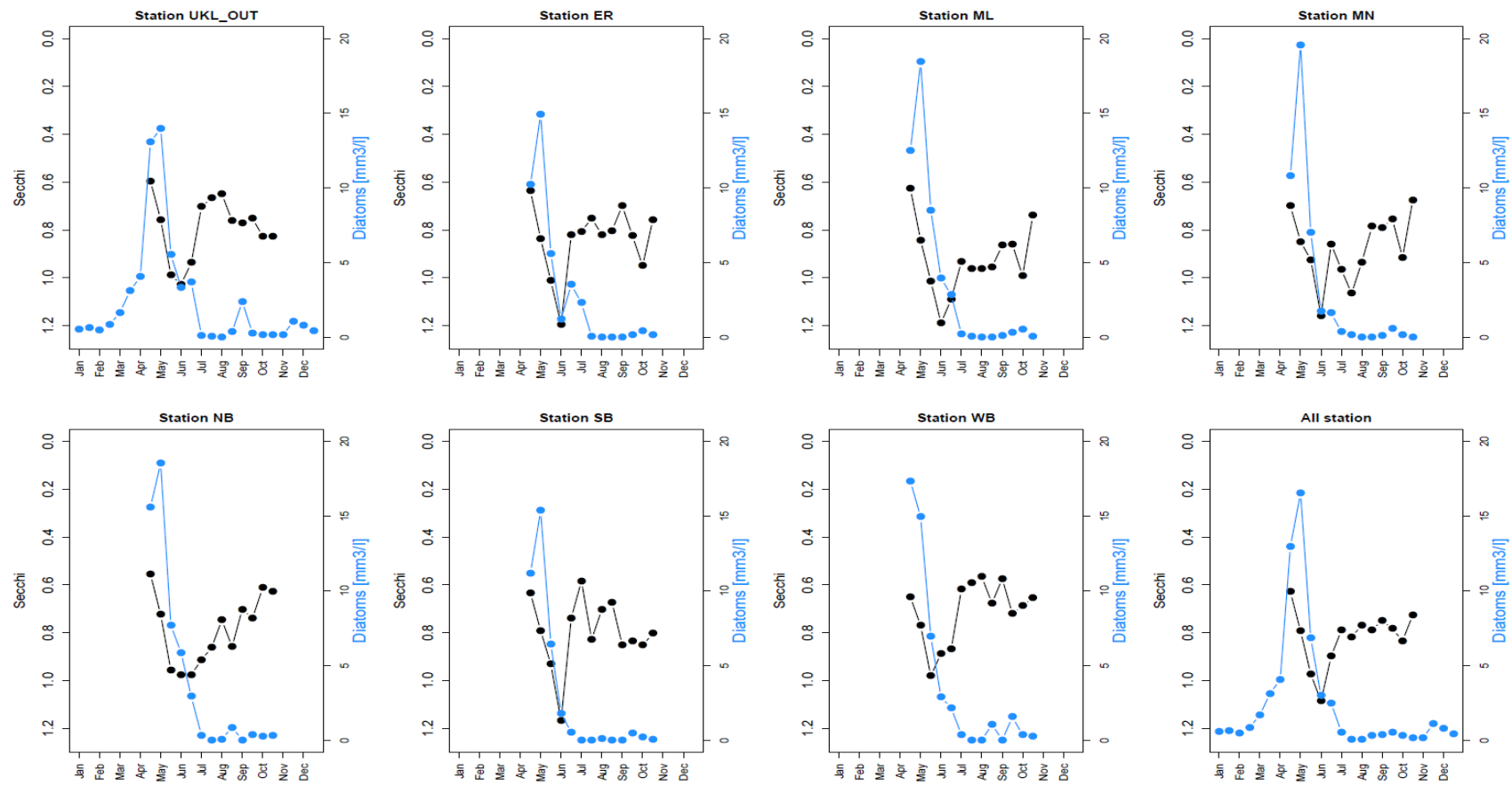


Figure 51. Seasonal dynamics of Secchi disk (black) and diatoms (blue) for individual stations and averaged for all stations. Note that Secchi y-axis is reverted

Daphnia, the main zooplankton group in the lake, becomes abundant in late May shortly after the diatom peak, and continues to increase in June, being abundant most of the summer, even during the main cyanobacteria bloom. There was a strong positive correlation between the biovolume of Cyanobacteria and the *Daphnia* biomass ($r^2=0.85$, $p<0.01$). Although *Daphnia* generally track the main phytoplankton bloom dynamics, a key observation is that *Daphnia* actually increase in early summer prior to the main cyanobacteria bloom in June. The initial increase prior to cyanobacteria growth could suggest that *Daphnia* are instead governed by the availability of other algae such as diatoms and cryptophytes which are abundant in the spring. Recent dietary analyses using fatty acids support this observation (M.T. Brett, unpublished data). Other zooplankton, such as calanoid copepods constitute only a minor component of the zooplankton biomass and are most abundant in the spring and fall, before and after the main *Daphnia* peak (Figure 50E).

Species richness

Phytoplankton and zooplankton species richness was highest in the spring and then declined rapidly after the onset of the summer *Aphanizomenon flos-aquae* bloom (Figure 50F). The high phytoplankton species richness in the spring was commonly due to the presence of different diatom species. The main chlorophyll-a peak was also statistically associated with reduced species richness for both phytoplankton ($r^2=0.33$, $p<0.01$) and zooplankton ($r^2=0.58$, $p<0.01$).

The change in species richness was also clearly visible when analyzing the data for the individual stations, as months of low species richness (Figure 52) occurred during high *Aphanizomenon flos-aquae* abundances (Figure 53). It is interesting to note that in AL a late summer secondary *Aphanizomenon flos-aquae* biovolume peak did not commonly occur, thus phytoplankton species richness was generally higher in AL in September and October compared to UKL. This suggests the suppressing role that *Aphanizomenon flos-aquae* had on other components of the phytoplankton community.

Phytoplankton richness [number of species]

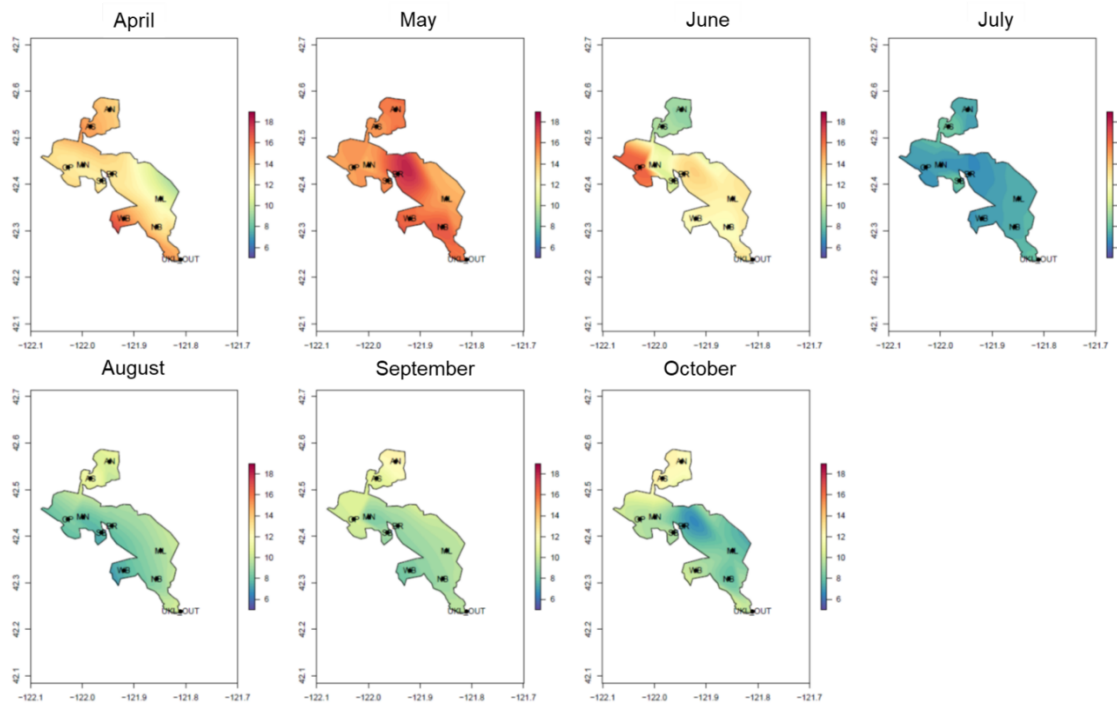


Figure 52: Spatial overview of phytoplankton richness based on mean number of phytoplankton species across all years. Data interpolated from all stations (denoted in black). Scale is the same for each month.

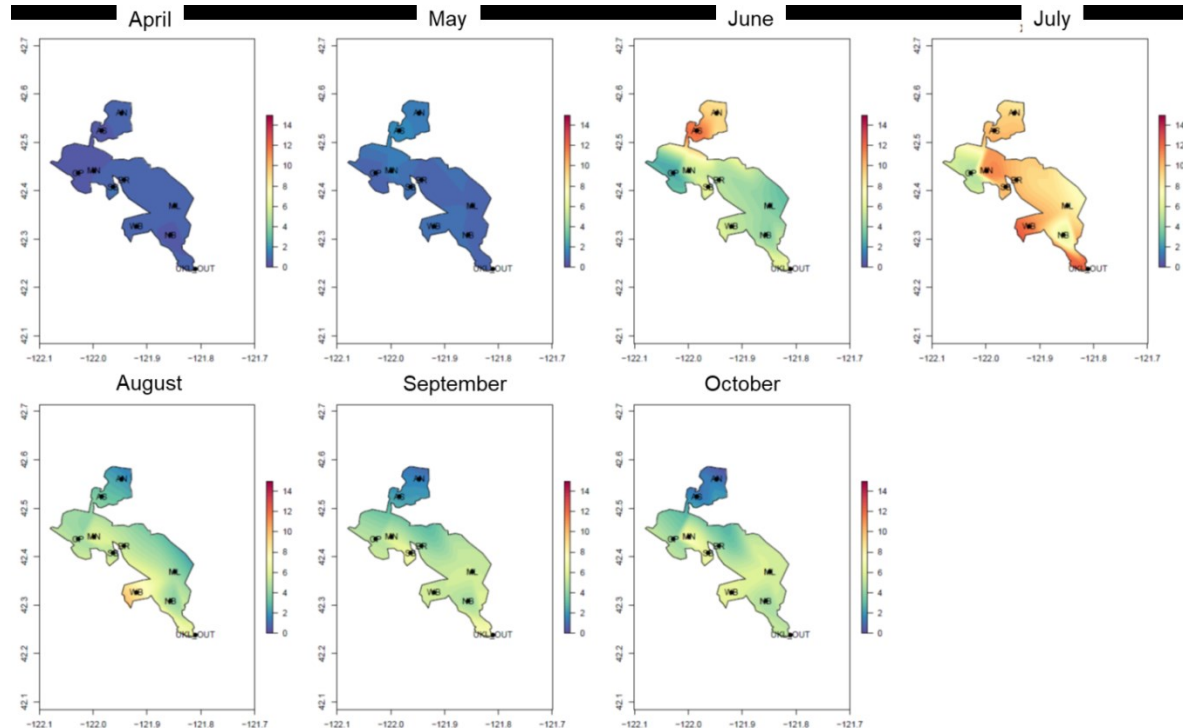


Figure 53: Spatial overview of *Aphanizomenon flos-aquae* biovolume [mm^3/L] across all years. Data extrapolated from all stations in UKL and AL (denoted in black). Scale is the same for each month.

Mann-Kendall analyses of long-term trends

In subsequent sections of this report, the year-to-year variability is explored using Mann-Kendall trend analyses to assess whether key water quality or plankton variables have decreased or increased during the 1990-2015 time period . We performed individual Mann-Kendall trend tests for key water quality parameters for each month during the range of April-September, a mean for the entire period (April-October) and for the main *Aphanizomenon flos-aquae* growing season (June-September). In AL there were relatively few significant trends for the water quality data, however the mean chlorophyll-a biomass did decline significantly from 1990 to 2015 (Table 3, **Error! Reference source not found.**).

The chlorophyll-a biomass decline was particularly visible in June. A similar decline was visible for total nitrogen concentrations in June, but not for phosphorus. The decline in nitrogen but not phosphorus also resulted in an overall decline in the TN:TP ratios in the lake. Interestingly, both light and wind levels also declined in the lake in the spring. The long-term changes in UKL were very similar to AL, which showed a noticeable overall (April-October) decline in chlorophyll-a and total nitrogen concentrations (Figure 54). Similarly, AL showed a trend towards lower wind speeds and lower light conditions.

Despite the overall lower chlorophyll-a levels, several phytoplankton species increased in both AL and UKL. In the spring total diatom biomass increased, including major species such as *Aulacoseira* sp. The increase in diatoms is also the likely reason for the increase in total phytoplankton in May, a pattern that was evident for both AL and UKL. Interestingly, there was also an increase in the toxic *Microcystis aeruginosa* in the months of August and September for AL, and for the combined July to October period in UKL. Both the increase in diatoms in the spring and the increase in the late blooming *Microcystis aeruginosa* were primarily driven by a few years with high abundances.

In AL there were few long-term changes in the respective biomass of the zooplankton taxa. In UKL there were some significant changes, including a decrease in fall calanoid copepods (August and September) and a decrease in *Daphnia* in May. However, overall there were generally few significant trends.

Table 3: P-values of Mann-Kendall trend analyses based on mean biomass or biovolume data for each month and for the period April to October, from 1990-2015 (2004-2015 for zooplankton) for Agency Lake. Red denotes statistically decreasing trends while blue denotes statistically increasing trends ($p < 0.05$).

<u>Agency Lake</u>	<u>Variable</u>	<u>April</u>	<u>May</u>	<u>June</u>	<u>July</u>	<u>August</u>	<u>September</u>	<u>October</u>	<u>April-October</u>
Water Quality:									
Water temperature		0.24	0.19	0.40	0.43	0.82	0.04	0.11	0.68
Total Phosphorus		0.98	0.61	0.12	1.00	0.71	0.68	0.21	0.26
Total Nitrogen		0.07	0.16	0.02	0.24	0.53	0.83	0.91	0.59
Dissolved Oxygen		0.41	0.48	0.77	0.05	0.39	0.59	0.19	0.40
Soluble reactive Phosphorus		0.63	0.12	0.71	0.83	0.36	0.29	0.00	0.18
Total Nitrogen to Phosphorus ratio		0.34	0.57	0.02	0.32	0.68	0.16	0.01	0.71
Mean windspeed		0.29	0.34	0.48	0.17	0.08	0.06	1.00	0.23
Mean 7 day average windspeed		0.09	0.47	0.02	0.03	0.00	0.38	0.57	0.00
Mean air temperature		0.14	0.27	0.60	0.57	0.76	0.06	0.79	0.25
mean 7 day average air temperature		0.41	1.00	0.48	0.13	0.96	0.13	0.74	0.86
pH		0.51	0.37	0.04	0.44	0.02	0.28	0.08	0.24
Light		0.04	0.01	0.50	0.39	0.02	0.48	0.31	0.00
Relative thermal resistance to mixing		0.33	0.31	0.97	0.74	0.87	0.08	0.78	0.87
Mean Chlorophyll-a		0.30	0.79	0.01	0.48	0.43	0.59	0.06	0.18
Phytoplankton									
Total Phytoplankton		0.10	0.83	0.54	0.26	0.14	0.16	0.76	0.96
Cyanophyta		0.01	0.02	0.43	0.24	0.16	0.24	0.70	1.00
Diatoms		0.11	0.01	0.01	0.66	0.03	0.34	0.73	0.26
Cryptophyta		0.45	0.65	0.03	0.93	0.34	0.91	0.65	0.78
Chlorophyta		0.50	0.02	0.02	0.64	0.87	0.46	0.11	0.65
Pyrrhophyta		0.40	0.56	0.94	0.08	0.33	0.42	0.87	0.67
Xanthophyta		0.85	0.06	0.57	0.07	0.27	1.00	0.00	0.13
Aphanizomenon sp.		0.01	0.03	0.46	0.26	0.19	0.26	0.68	1.00
Aphanizomenon sp. akinates		0.12	0.55	0.25	0.98	0.65	0.62	0.11	0.02
Asterionella formosa		0.60	0.34	0.71	0.25	0.03	0.73	0.58	0.30
Stephanodiscus niagarae		0.70	0.80	1.00	0.73	1.00	0.37	0.58	0.61
Fragilaria sp		0.54	0.01	0.01	0.04	0.82	0.05	0.17	0.00
Tribonema		0.85	0.06	0.57	0.07	0.27	1.00	0.00	0.13
Synedra sp		0.97	0.51	0.44	0.02	0.12	0.59	0.18	0.11
Aphanizomenon sp. heterocysts		0.12	0.10	0.40	0.26	0.27	0.28	0.59	0.54
Cryptomonas sp		0.49	0.74	0.03	0.91	0.22	0.12	0.94	0.82
Microcystis aeruginosa		1.00	1.00	1.00	0.08	0.00	0.01	0.10	0.01
Aulacoseira sp		0.86	0.00	0.03	0.42	0.11	0.10	0.03	0.00
miscellaneous microflagellate		0.30	0.01	0.00	0.00	0.00	0.00	0.00	0.00
Zooplankton									
Total Zooplankton		0.53	0.37	0.95	0.54	0.63	0.95	0.28	0.63
Total adult calanoid copepods		0.81	0.62	0.17	0.94	0.58	0.84	0.53	1.00
Total immature calanoid copepods copepodids		0.75	0.49	0.28	0.93	0.78	0.84	1.00	0.45
Total adult cladocerans		0.76	0.37	0.95	0.63	0.63	0.95	0.59	0.95
Total immature cladocerans		0.35	0.56	1.00	0.24	0.52	0.52	1.00	0.28
Total adult cyclopoid copepods		0.21	0.63	0.03	0.13	0.13	0.03	0.37	
Total immature cyclopoid copepods copepodids		1.00	0.84	0.84	0.17	0.01	0.17	0.11	0.30
Total naupliar copepods		0.76	0.73	0.30	0.95	1.00	0.63	0.72	0.73
Total ostracoda		1.00	1.00	1.00	1.00	0.38	1.00	1.00	0.38
Total rotifers		0.76	0.84	0.45	0.05	0.11	0.49	0.24	0.09
Daphnia.sp		0.76	0.37	0.95	0.73	0.63	0.73	0.59	0.95
Leptodiaptomus.ashlandi		0.70	0.62	0.14	0.36	1.00	0.63	0.41	0.63
Chydorus.sphaericus		1.00	1.00	0.36	0.07	0.04	0.14	0.06	0.10
Diacyclops.thomasi		0.21	0.63	0.54	0.03	0.13	0.13	0.03	0.37
Leptadora.kindtii		1.00	1.00	1.00	0.56	0.83	0.56	1.00	0.56
Euchlanis.sp		0.04	0.22	0.89	0.33	0.11	0.18	0.91	0.19
Epischura.nevadensis		0.64	1.00	0.39	0.76	0.94	0.65	0.76	0.89
keratella.sp		0.64	0.95	0.77	0.64	0.05	0.24	0.03	0.30
Acanthocyclops.vernalis		1.00	1.00	1.00	0.56	1.00	1.00	1.00	0.67
synchaeta.sp		0.65	0.89	0.72	0.12	0.28	0.46	1.00	0.84

Table 4. P values of Mann-Kendall long-term trend analyses based on mean biomass or biovolume data for each month and for the period April to October, from 1990-2015 (2004-2015 for zooplankton) for UKL, and combined for all months. Red denotes statistically decreasing trends while blue denotes statistically increasing trends ($p < 0.05$) with the value of the test statistics is also presented.

<u>Upper Klamath Lake</u>	<u>April</u>	<u>May</u>	<u>June</u>	<u>July</u>	<u>August</u>	<u>September</u>	<u>October</u>	<u>April-October</u>
Variable								
Water Quality:								
Water temperature	0.22	0.40	0.32	0.32	0.97	0.09	0.41	0.77
Total Phosphorus	0.68	0.19	0.74	0.62	0.31	0.17	0.01	0.45
Total Nitrogen	0.93	0.76	0.36	0.36	0.20	0.23	0.03	0.02
Dissolved Oxygen	0.20	0.33	0.45	0.45	0.32	0.53	0.05	0.56
Soluble reactive Phosphorus	0.84	0.25	0.49	0.04	0.23	0.11	0.07	0.56
Total Nitrogen to Phosphorus ratio	0.63	0.38	0.06	0.07	0.00	1.00	0.19	0.05
Mean windspeed	0.41	0.39	0.38	0.12	0.06	0.07	0.67	0.27
Mean 7 day average windspeed	0.05	0.44	0.02	0.05	0.00	0.25	0.29	0.00
Mean air temperature	0.27	0.27	0.86	0.45	0.83	0.05	0.83	0.29
mean 7 day average air temperature	0.91	0.94	0.43	0.45	0.86	0.13	0.40	0.69
pH	0.53	1.00	0.17	0.56	0.68	0.38	0.08	0.24
Light	0.11	0.00	0.60	0.31	0.00	0.91	0.22	0.03
Relative thermal resistance to mixing	0.92	0.43	0.68	0.23	0.34	0.03	0.33	0.02
Mean Chlorophyll-a	0.15	0.63	0.06	0.74	0.83	0.26	0.01	0.01
Phytoplankton								
Total Phytoplankton	0.13	0.02	0.91	0.24	0.82	0.74	0.21	0.57
Cyanophyta	0.00	0.06	0.65	0.13	0.57	0.91	0.26	0.37
Diatoms	0.16	0.05	0.03	0.37	0.76	0.76	0.12	0.69
Cryptophyta	0.97	0.29	0.34	0.74	0.54	0.46	0.18	0.96
Chlorophyta	1.00	0.16	0.06	0.35	0.96	0.57	0.12	0.40
Pyrrophyta	0.87	0.06	0.24	0.77	0.76	0.31	0.13	0.59
Xanthophyta	0.36	0.76	0.50	0.61	0.43	0.66	0.01	0.50
Aphanizomenon sp.	0.00	0.08	0.74	0.16	0.57	0.91	0.29	0.31
Aphanizomenon sp. akinates	0.08	0.27	0.19	0.37	0.36	0.27	0.12	0.01
Asterionella formosa	0.54	0.24	0.22	0.61	0.97	0.28	0.27	0.16
Stephanodiscus niagarae	0.29	0.64	1.00	0.39	0.66	0.79	0.85	0.23
Fragilaria sp	0.52	0.72	0.05	0.13	0.26	0.93	0.01	0.19
Tribonema								
Synedra sp	0.12	0.65	0.13	0.77	0.07	0.19	0.87	0.14
Aphanizomenon sp. heterocysts	0.00	0.04	0.78	0.37	0.91	0.69	0.34	0.14
Cryptomonas sp	0.85	0.88	0.24	0.80	0.18	0.23	0.12	0.78
Microcystis aeruginosa	0.49	0.65	0.22	0.00	0.01	0.00	0.01	0.00
Aulacoseira sp	0.11	0.00	0.01	0.04	0.72	0.03	0.01	0.00
miscellaneous microflagellate	0.06	0.01	0.00	0.01	0.03	0.00	0.01	0.00
Zooplankton								
Total Zooplankton	0.19	0.03	0.11	0.95	0.54	0.54	0.03	0.30
Total adult calanoid copepods	0.45	0.11	0.15	1.00	0.54	0.02	0.02	0.19
Total immature calanoid copepods copepodids	0.63	0.05	0.63	0.34	0.03	0.04	0.01	0.45
Total adult cladocerans	0.19	0.37	0.05	0.95	0.54	0.63	0.03	0.30
Total immature cladocerans	0.65	0.72	0.62	0.33	0.52	0.43	0.06	0.37
Total adult cyclopoid copepods	0.37	0.30	0.15	0.95	0.24	0.09	0.15	0.09
Total immature cyclopoid copepods copepodids	0.84	0.45	0.84	0.37	0.24	0.02	0.47	0.45
Total naupliar copepods	0.45	0.24	0.95	0.03	0.24	0.11	1.00	0.73
Total ostracoda	1.00	0.52	0.25	1.00	1.00	0.77	0.30	0.44
Total rotifers	0.84	0.19	0.24	0.63	0.06	0.11	0.59	0.01
Daphnia.sp	0.19	0.37	0.05	1.00	0.54	0.63	0.02	0.37
Leptodiaptomus.ashlandi	0.45	0.09	0.15	0.89	0.45	0.15	0.02	0.30
Chydorus.sphaericus	0.78	0.14	0.01	0.05	0.18	0.18	0.21	0.11
Diacyclops.thomasi	0.19	0.30	0.19	0.95	0.24	0.11	0.15	0.06
Leptadora.kindtii	1.00	1.00	0.80	0.72	0.62	0.44	0.79	0.30
Euchlanis.sp	0.17	0.01	0.73	0.37	0.09	0.05	0.00	0.00
Epischura.nevadensis	0.78	0.43	0.41	0.62	0.34	0.29	0.35	0.19
keratella.sp	0.95	0.15	0.05	0.95	0.49	0.89	0.37	0.95
Acanthocyclops.vernalis	0.83	0.56	0.38	1.00	0.41	0.52	0.44	0.30
synchaeta.sp	0.01	1.00	0.19	0.68	0.94	0.89	0.59	0.84

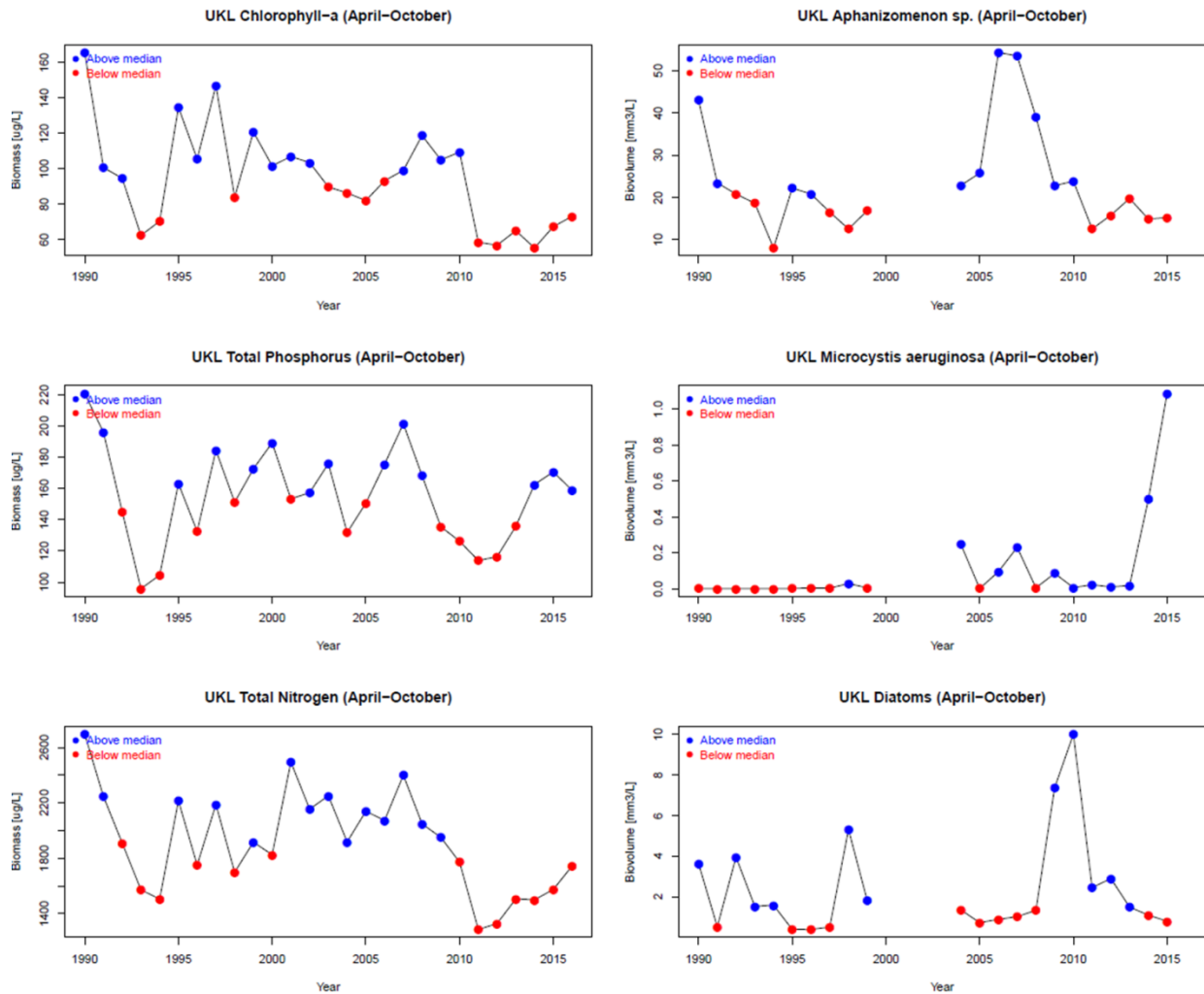


Figure 54: UKL long-term annual plot of mean chlorophyll-a, total phosphorus, total nitrogen, *Aphanizomenon flos-aquae*, *Microcystis aeruginosa* and diatoms averaged for the April to October time period. Red denotes below the overall long-term median biomass or biovolume for a specific time-series, and blue denotes above the long-term median. Trend statistics are presented in **Error! Reference source not found.**

Long-term changes of specific key variables

Mann-Kendall estimates of multiple time-series

Using Mann-Kendall regional tests we estimated the long-term trend using data from the individual stations. These analyses were restricted to the most common variables which were consistently measured at all stations and performed on the combined data for the months of the main growing season (June-September). Similar to the individual trend tests, the regional Mann-Kendall test showed a decline in total chlorophyll-a ($Z=-2.30$, $S=549$, $p<0.05$) and nitrogen concentrations ($Z=-2.15$, $S=565$, $p<0.05$) across all stations. However, there were no trends for phosphorus or for dissolved oxygen. The Regional Mann-Kendall for dissolved oxygen was calculated for the combined data of July-September when concentration in the lake are normally the lowest.

Long-term relationships between water quality, chlorophyll-a, and *Aphanizomenon flos-aquae*

The long-term dynamics for several key variables were significantly correlated during the years 1990-2016 in UKL. For example, the yearly chlorophyll-a and total phosphorus concentrations, based on mean data for April-October correlated significantly (Figure 55). A similar pattern was present for chlorophyll-a and the total nitrogen concentration (Figure 56). *Aphanizomenon flos-aquae* showed a similar pattern and was also significantly positively correlated with total nitrogen and phosphorus concentrations (Figure 57, Figure 58).

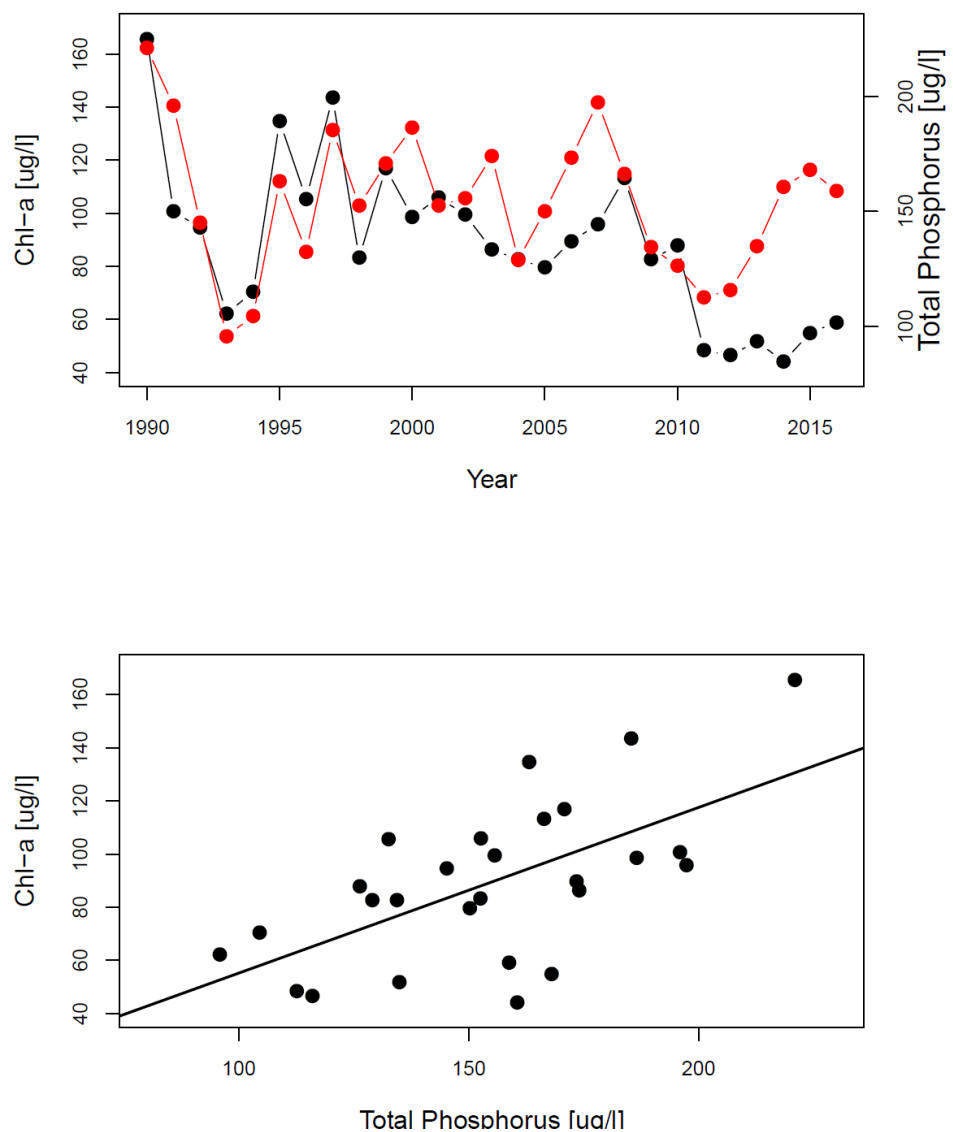


Figure 55: A) Temporal dynamics of chlorophyll-a (black) and total phosphorus (red) in UKL and B) the correlation of yearly mean values (April-October) of chlorophyll-a and total phosphorus concentration ($r^2 = 0.36$, $p < 0.01$).

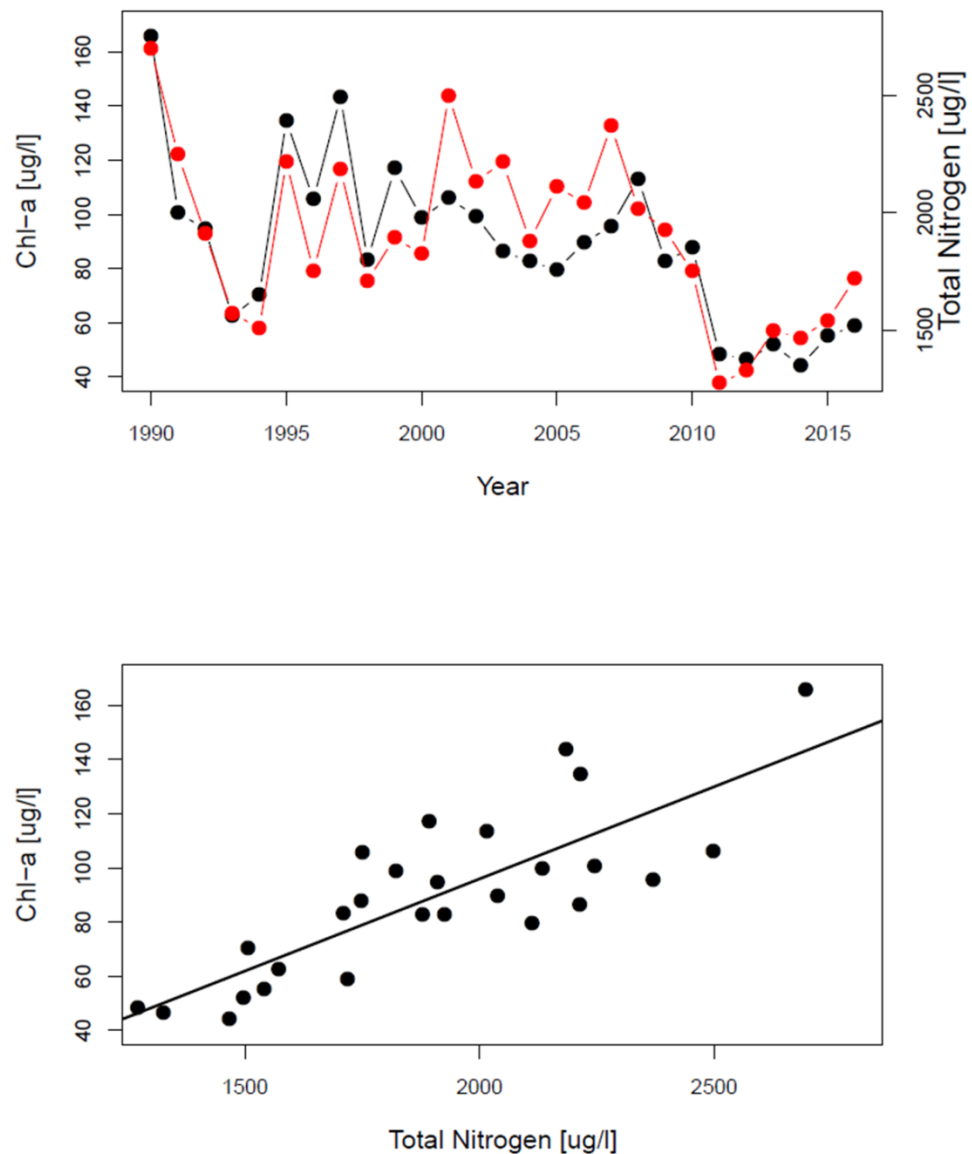


Figure 56: A) Temporal dynamics of chlorophyll-a (black) and total nitrogen (red) in UKL and B) the correlation of yearly mean values (April–October) of chlorophyll-a and total nitrogen concentration ($r^2 = 0.64$, $p < 0.01$).

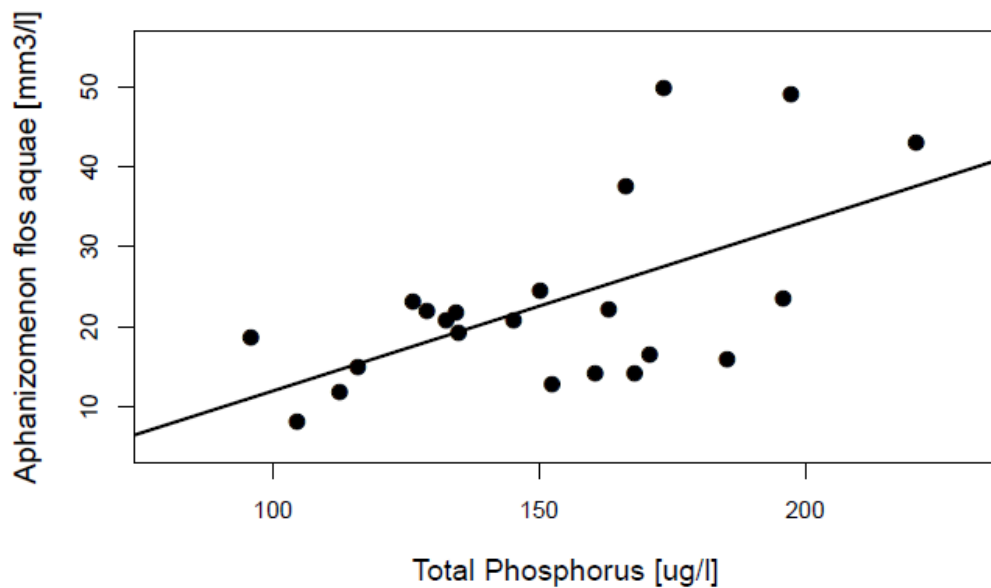
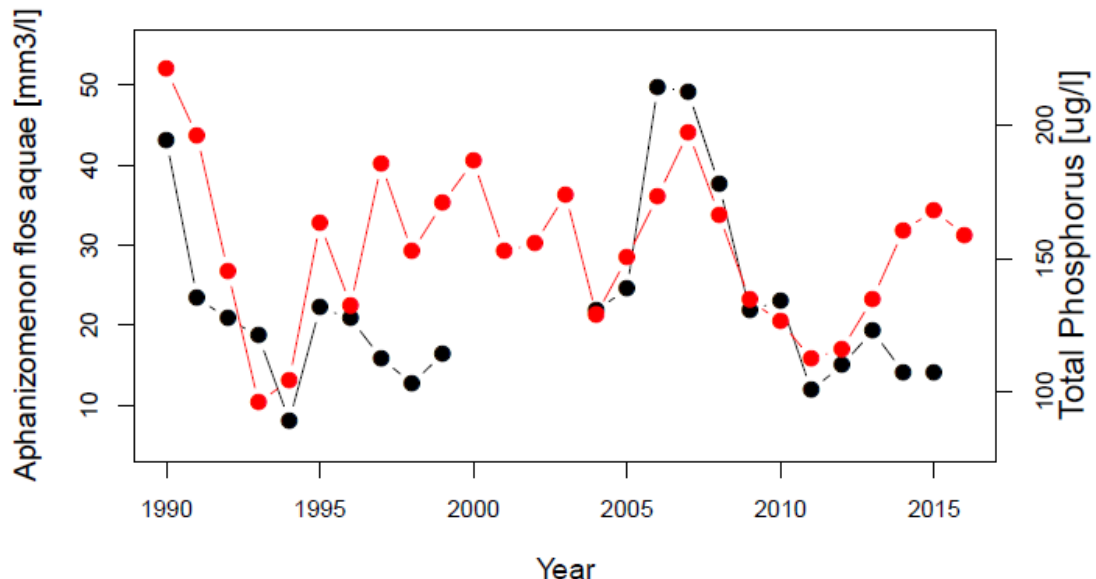


Figure 57: A) Temporal dynamics of *Aphanizomenon flos-aquae* (black) and total phosphorus (red) in UKL and B) the correlation of yearly mean values (April-October) of *Aphanizomenon flos-aquae* and total phosphorus concentration ($r^2 = 0.31$, $p < 0.01$).

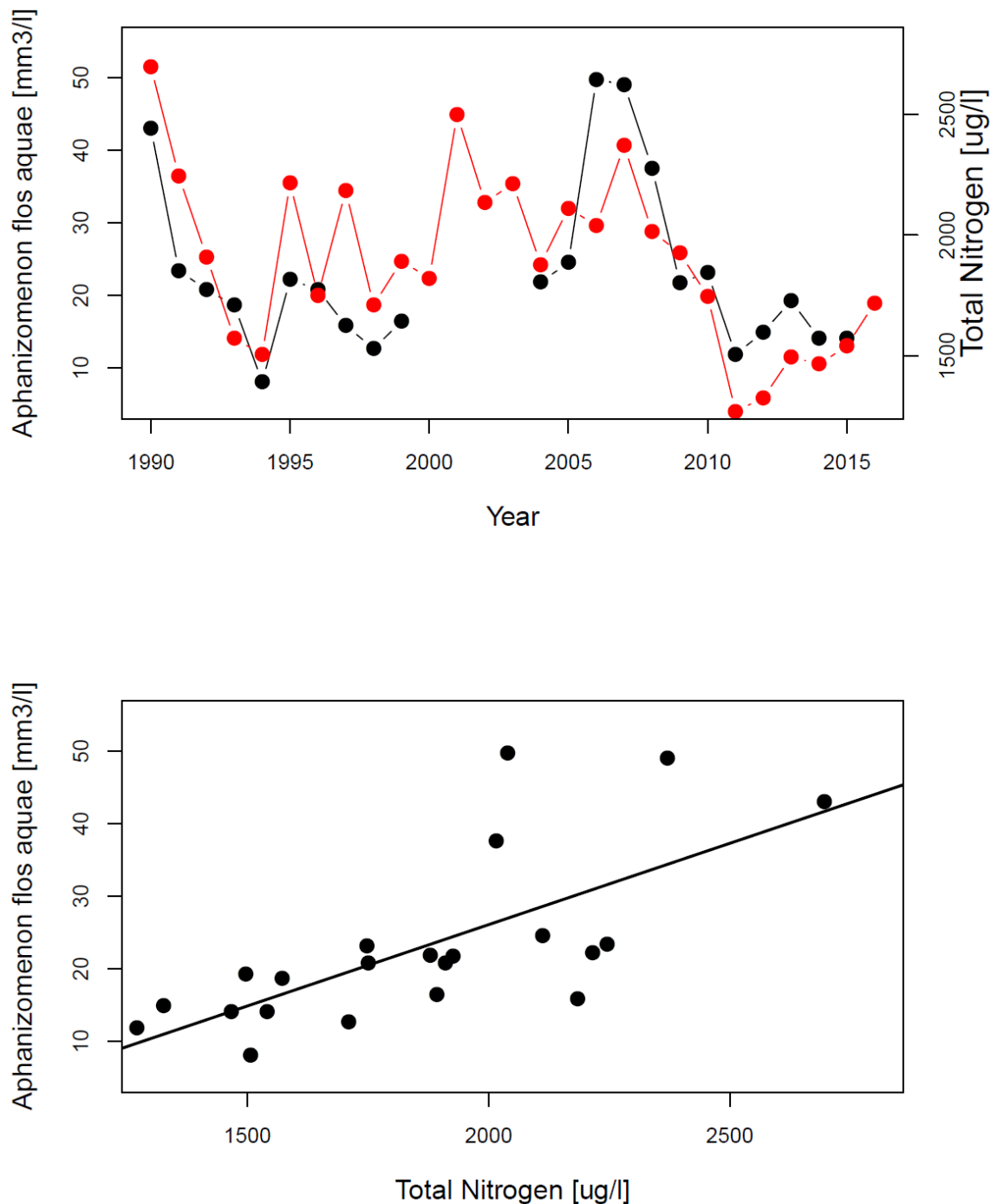


Figure 58: A) Temporal dynamics of *Aphanizomenon flos-aquae* (black) and total nitrogen (red) in UKL and B) the correlation of yearly mean values (April-October) of *Aphanizomenon flos-aquae* and total nitrogen concentration ($r^2 = 0.46$, $p < 0.01$).

Variability in dissolved oxygen occurs mainly in late summer during the collapse of the chlorophyll-a bloom. Thus, to assess the relationship between chlorophyll-a bloom phenology and potential changes in dissolved oxygen levels, we assessed data from August and September. A clear positive correlation was apparent between the mean values for August-September chlorophyll-a and the corresponding dissolved oxygen concentrations (Figure 59).

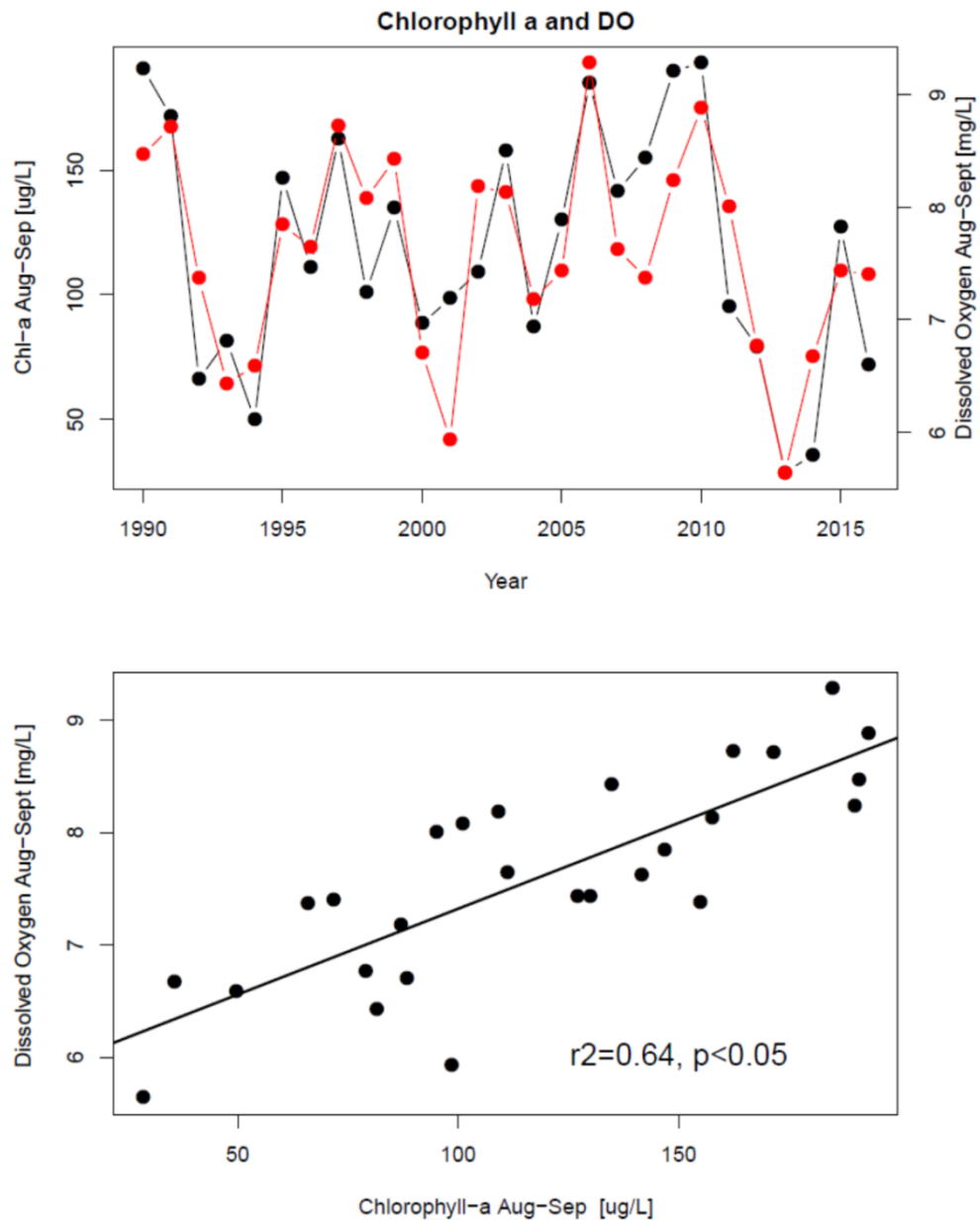


Figure 59: A) Temporal dynamics of chlorophyll-a (black) and dissolved oxygen (red) in UKL and B) the correlation of the mean values (August-September) of chlorophyll-a and dissolved oxygen.

A similar positive relationship was apparent between dissolved oxygen and pH for the August-September period (Figure 60A). There was a negative correlation between pH and dissolved oxygen, when comparing pH in July with the dissolved oxygen in August (Figure 60B). This likely reflects a higher July biomass magnitude which translates to a more severe August biomass decline. Combined with the positive correlation between chlorophyll-a, pH and dissolved oxygen in Aug.-Sept. this suggests that when phytoplankton photosynthesis is high dissolved oxygen and pH are also high. However, during the summer phytoplankton bloom collapse and subsequent decay, organic matter decomposition eventually lowers oxygen levels in the lake.

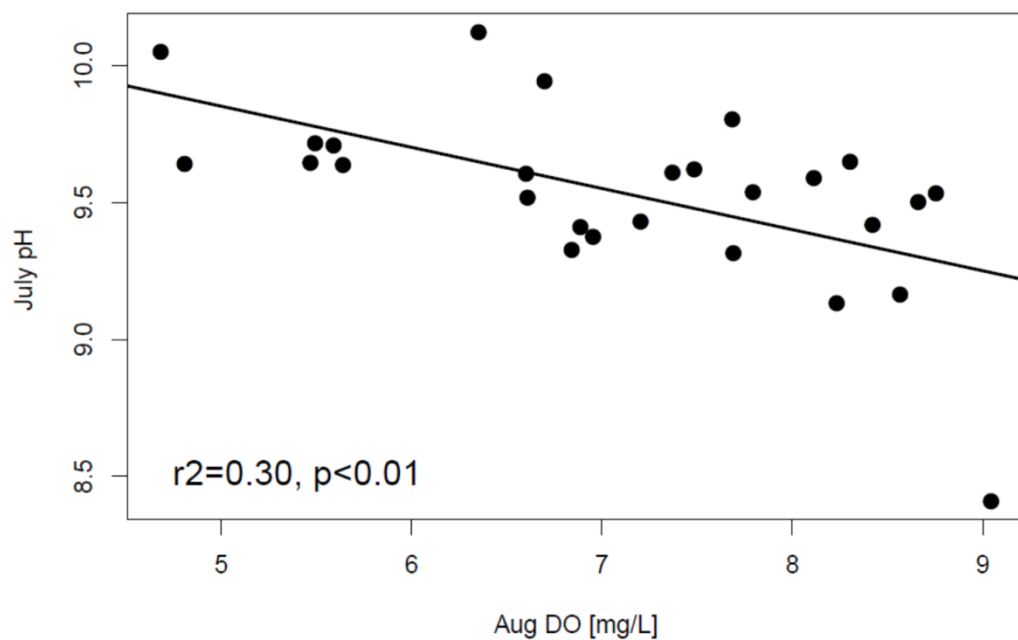
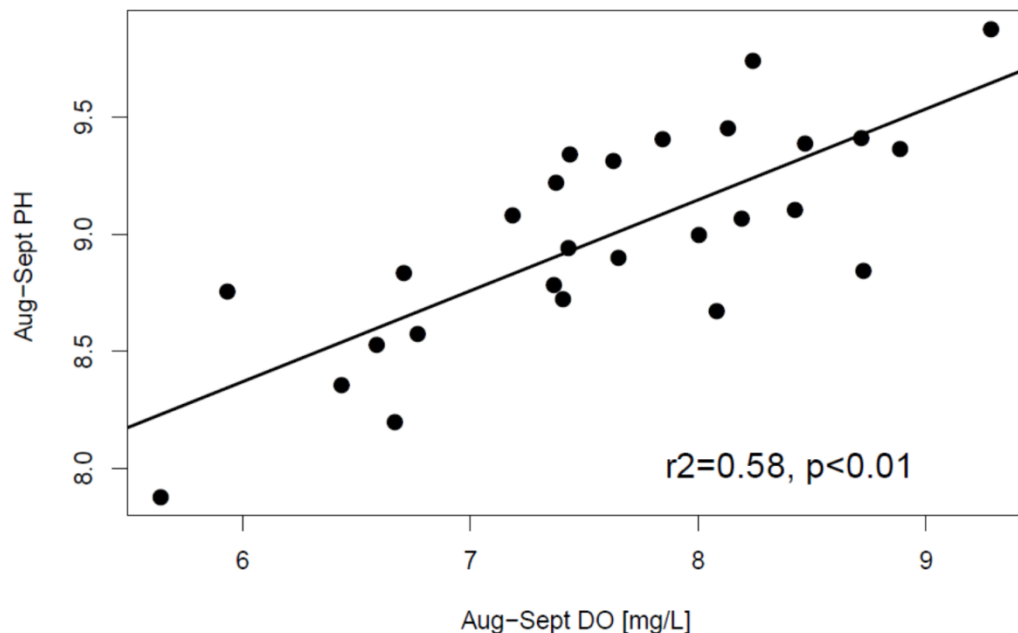


Figure 60: Relationship between DO and pH for a) August-September data and b) a monthly lag between DO (Aug) and pH (July).

As shown previously there was a good correlation between the phytoplankton biovolume in the summer and the total nitrogen and phosphorus concentration in the lake, which is primarily caused by the phytoplankton biomass producing inorganic nitrogen via nitrogen fixation and sequestering total phosphorus from the water column and sediments in its tissues.

Monthly correlations among key variables

Previously we showed correlations among key variables in the lake for the entire growing season. However, several of these significant relationships can be further pinpointed to particular months, which implies that processes in certain months are particularly important for regulating the summer bloom. The positive relationship between chlorophyll-a and total phosphorus concentrations was particularly strong in the months of June, September and October (Figure 61). Correlations between data in the months of July and August, though still significant, were relatively weak, while there were no significant trends in the months of April and May. A similar pattern was evident for the positive relationship between chlorophyll-a and total nitrogen. Again, the months of June, September and October were particularly strong (Figure 62), while there were no trends for the April and May data. Trends between total phosphorus and total nitrogen concentrations were positive and significant for all months, except April and May (Figure 63).

Aside from June and October when the total nitrogen to total phosphorus ratio was significantly correlated to chlorophyll-a concentrations, the TN:TP ratio for other months did not show significant trends with chlorophyll (Figure 64). Although in June the relationship was positive and in October it was negative, the relationships showed high variability. The relationship between chlorophyll-a and soluble reactive phosphorus was only significant in September and October, while there were no trends between these variables in any of the other months (Figure 65).

The relationship between the dominant phytoplankton *Aphanizomenon flos-aquae* and phosphorus concentrations was strongly positive in June, September and October, weakly significant in August, with no significant trends for the other months (Figure 66). This pattern, with the months of June, September and October showing the strongest correlations, was similar for the relationship between *Aphanizomenon flos-aquae* and the nitrogen concentration (Figure 67). Chlorophyll-a and *Aphanizomenon flos-aquae* correlated in all summer months except for July. However, the poor July relationship was primarily driven by one outlier for *Aphanizomenon flos-aquae* (Figure 68). Not surprisingly, there was no trend in April and May before the *Aphanizomenon flos-aquae* bloom initiated. The fact that particular relationships in particular months regulate bloom dynamics also suggests that multivariate analyses of the bloom dynamics should cover both analyses for the entire growing season as well as for data from months which are of the greatest importance.

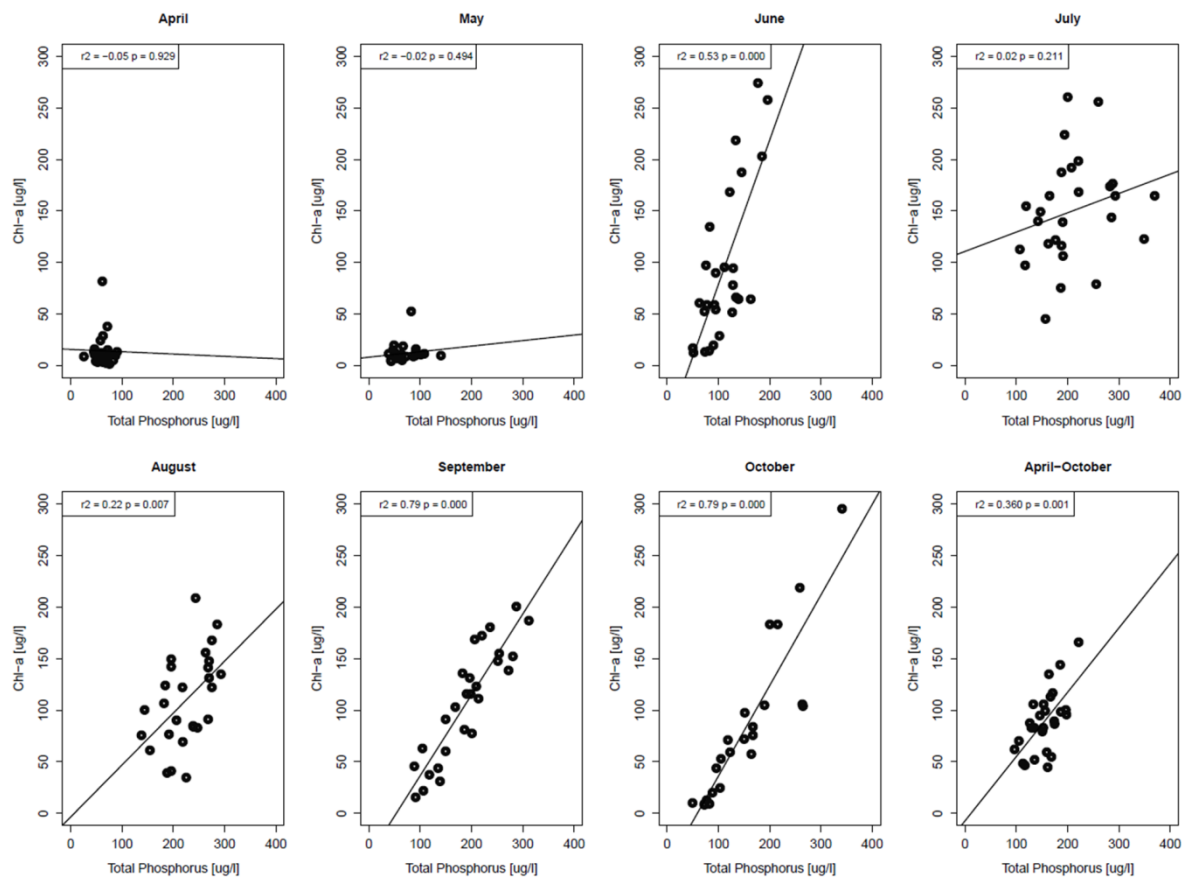


Figure 61: Correlation between total phosphorus and chlorophyll-a for each month.

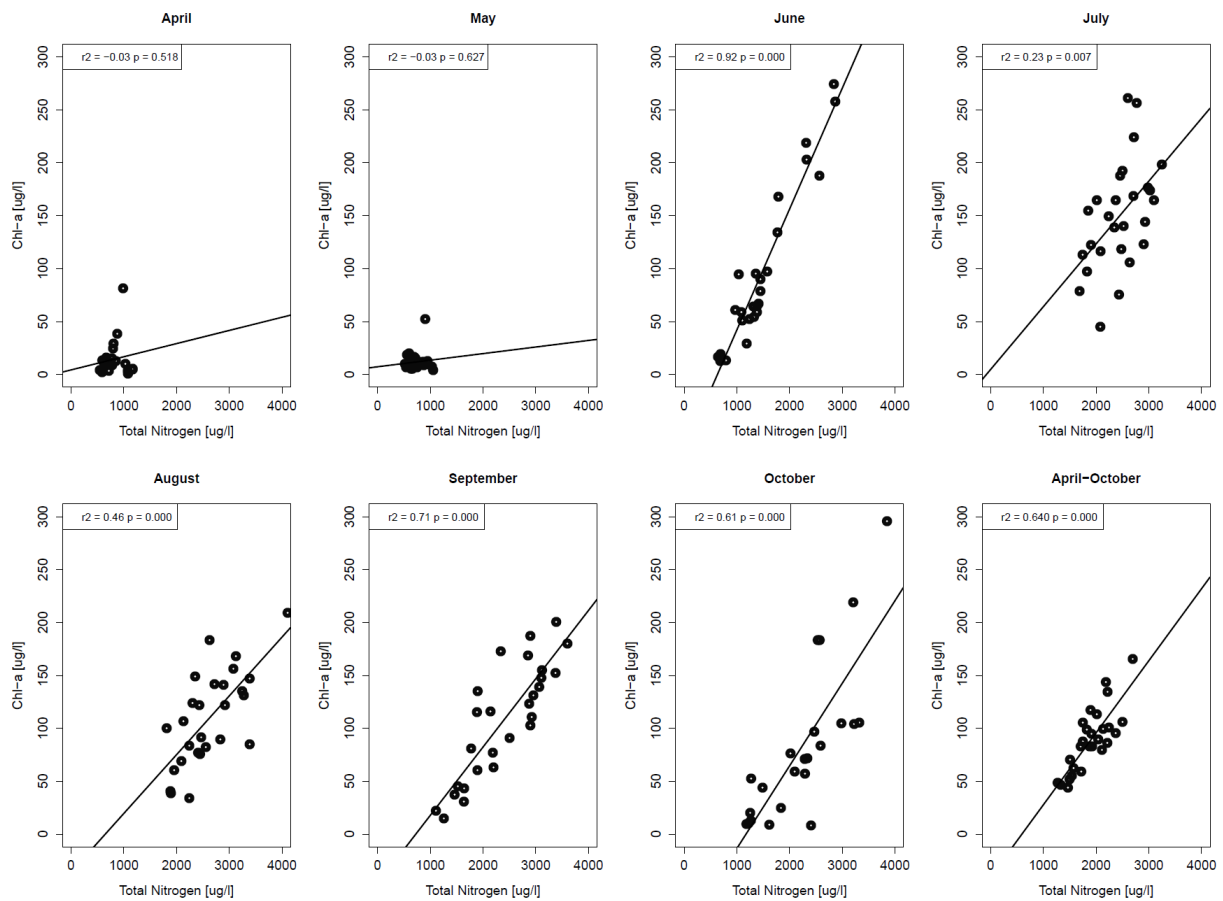


Figure 62: Correlation between total nitrogen and chlorophyll-a for each month.

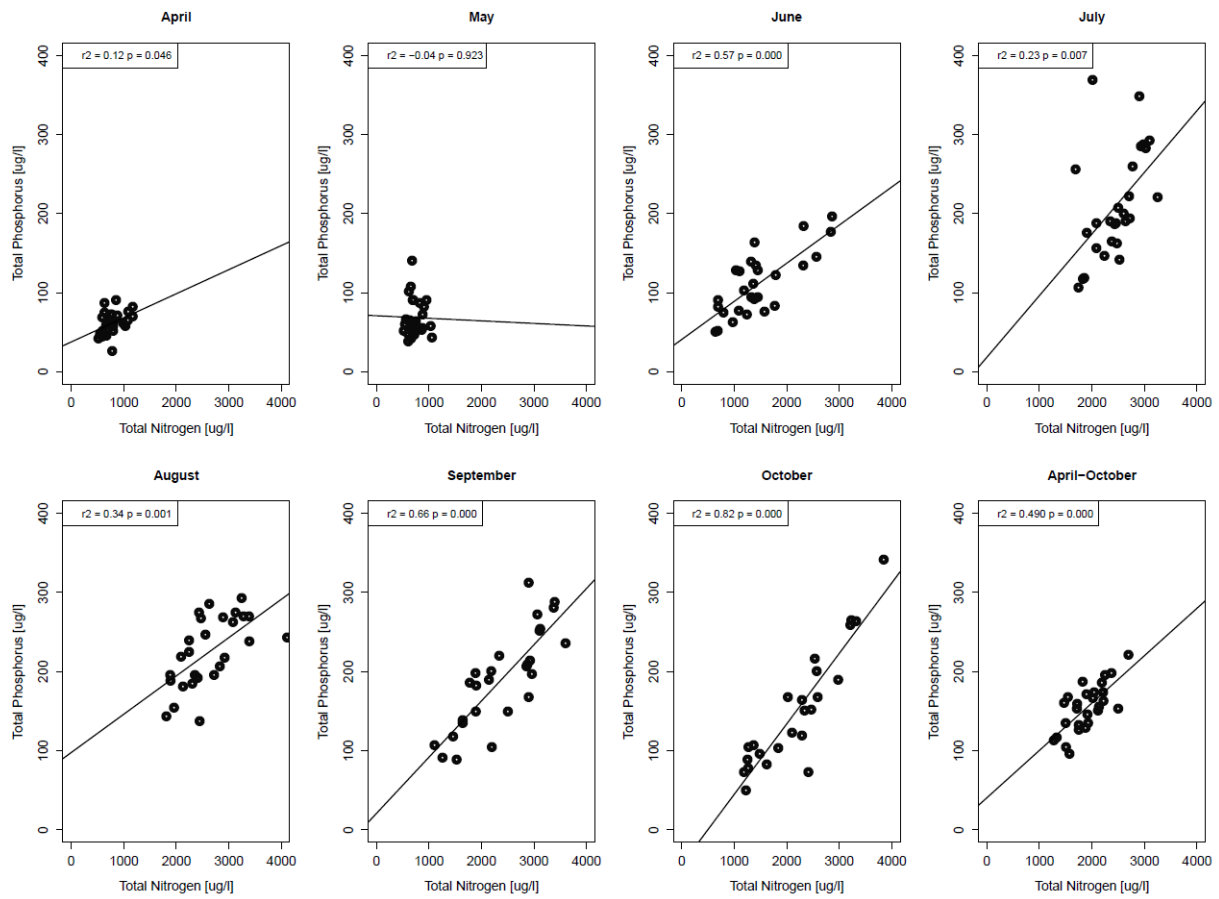


Figure 63: Correlation between total nitrogen and total-phosphorus for each month.

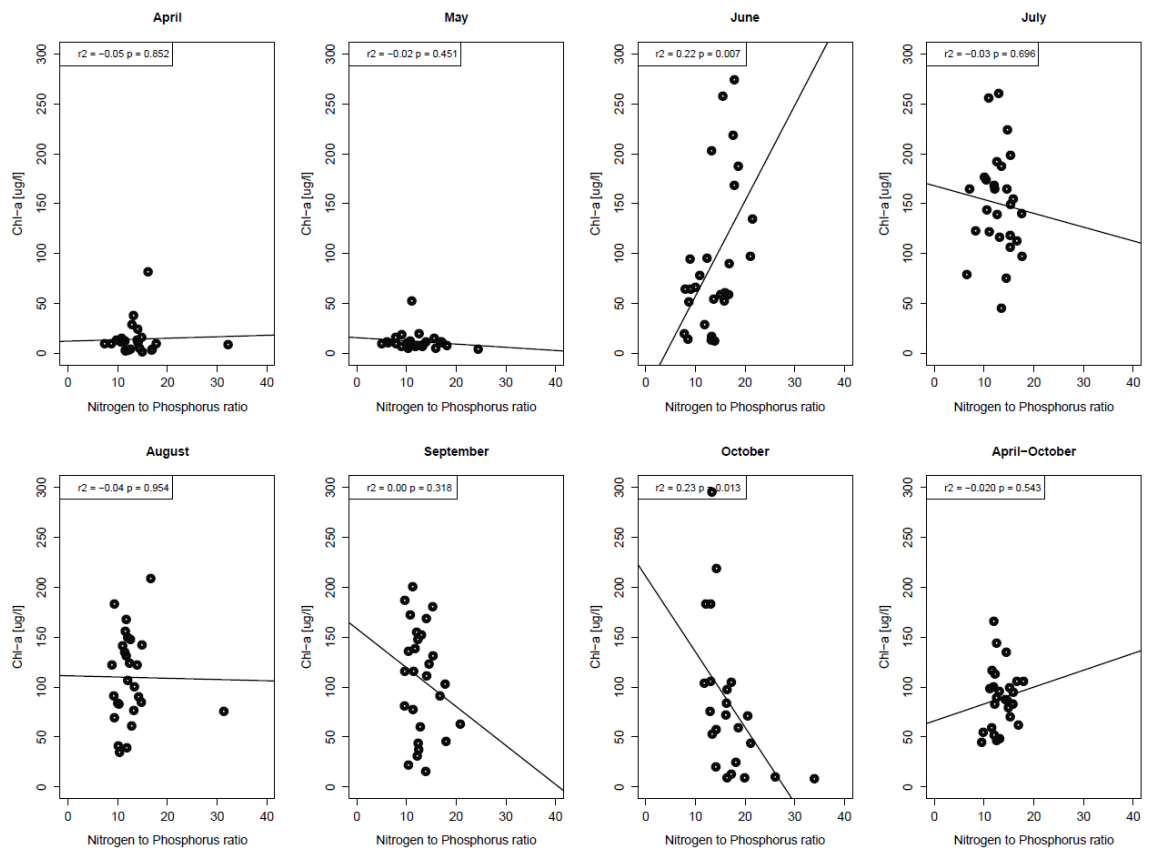


Figure 64: Correlation between the nitrogen to phosphorus ratio and total-chlorophyll-a for each month.

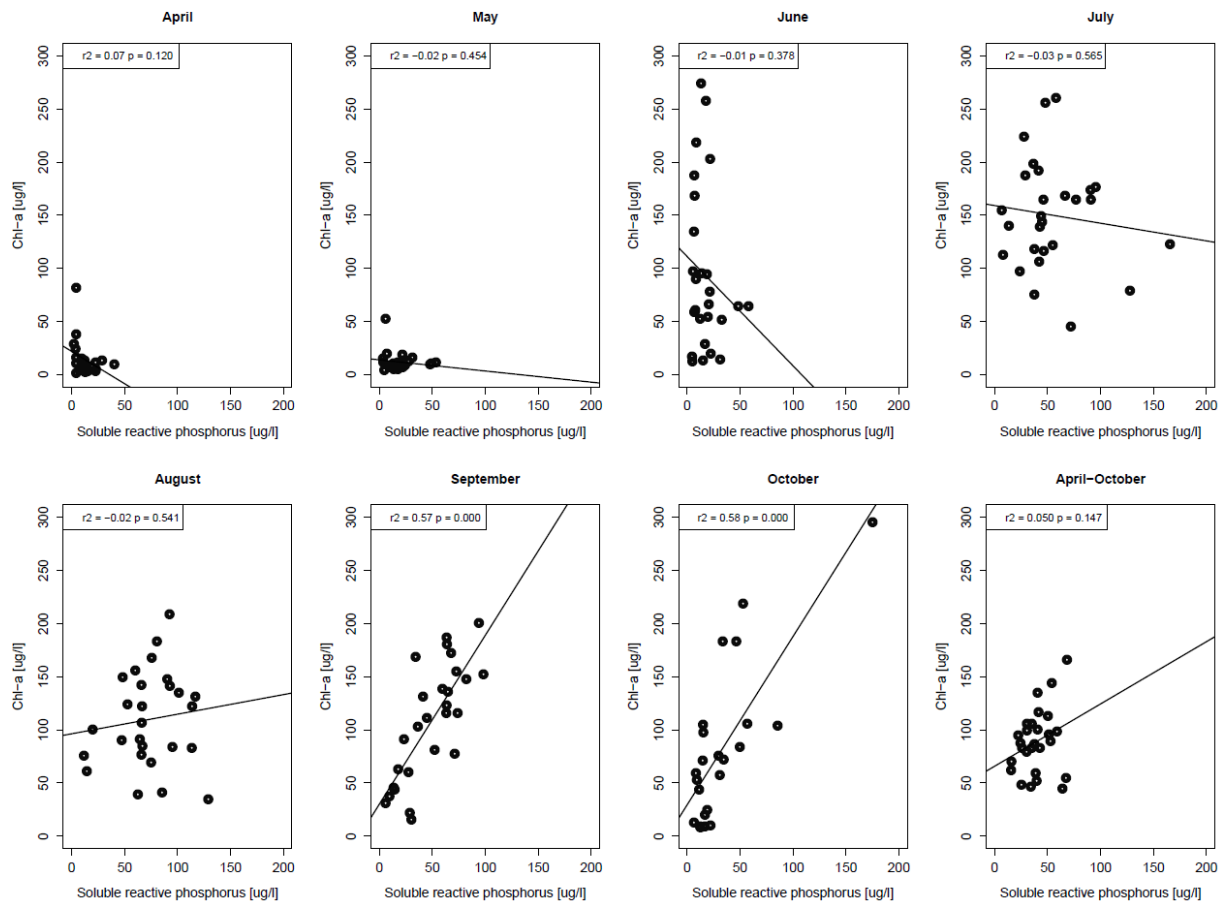


Figure 65: Correlation between soluble reactive phosphorus and chlorophyll-a for each month.

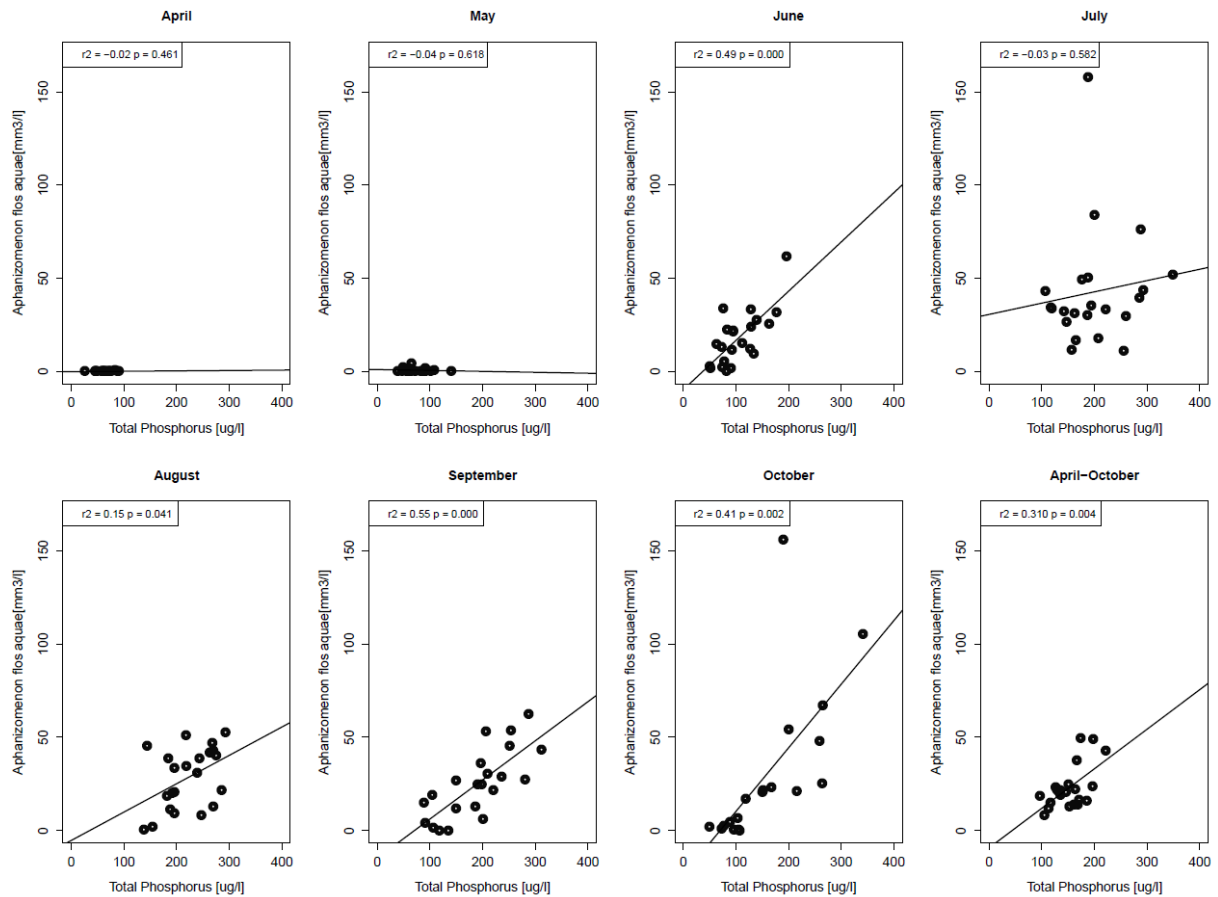


Figure 66: Correlation between total phosphorus and *Aphanizomenon flos-aquae* for each month.

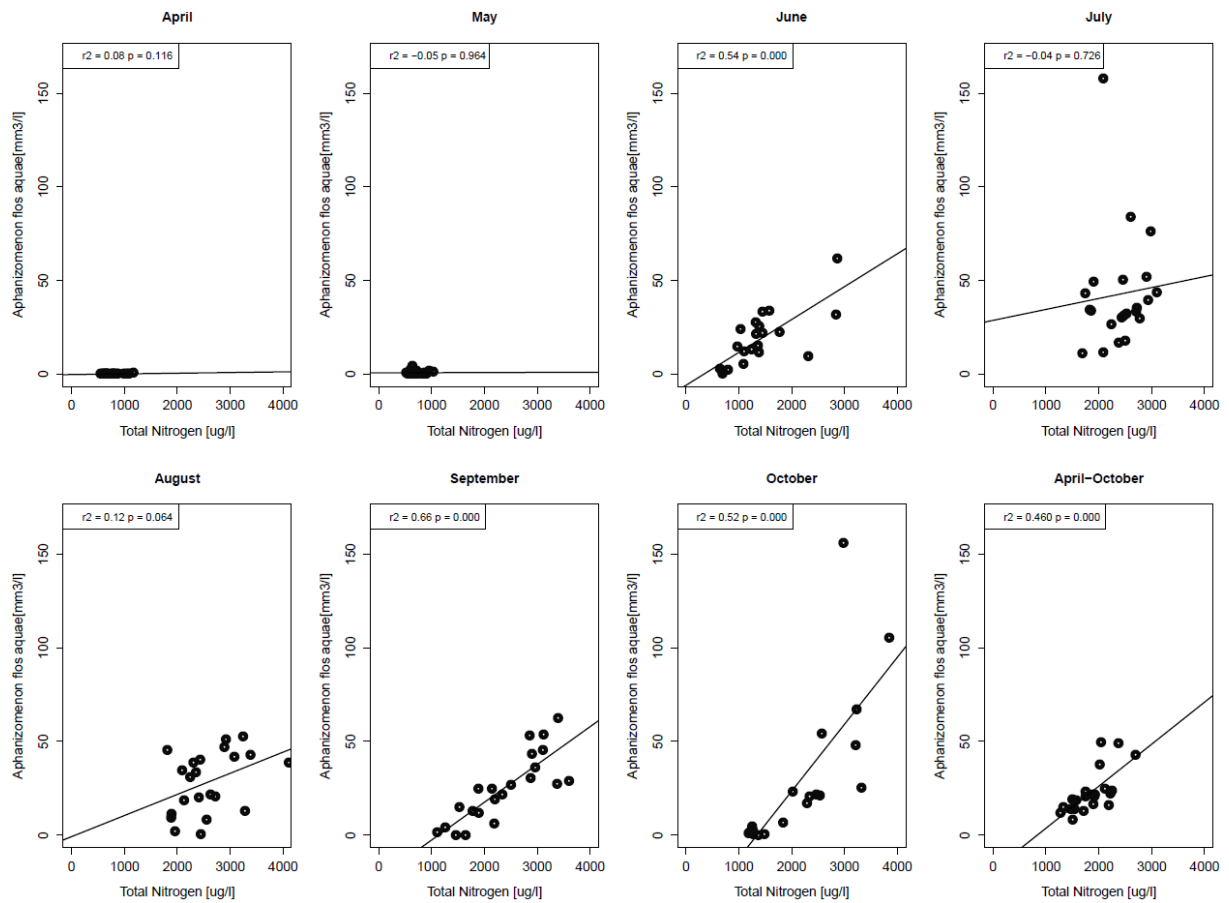


Figure 67: Correlation between total nitrogen and *Aphanizomenon flos-aquae* for each month.

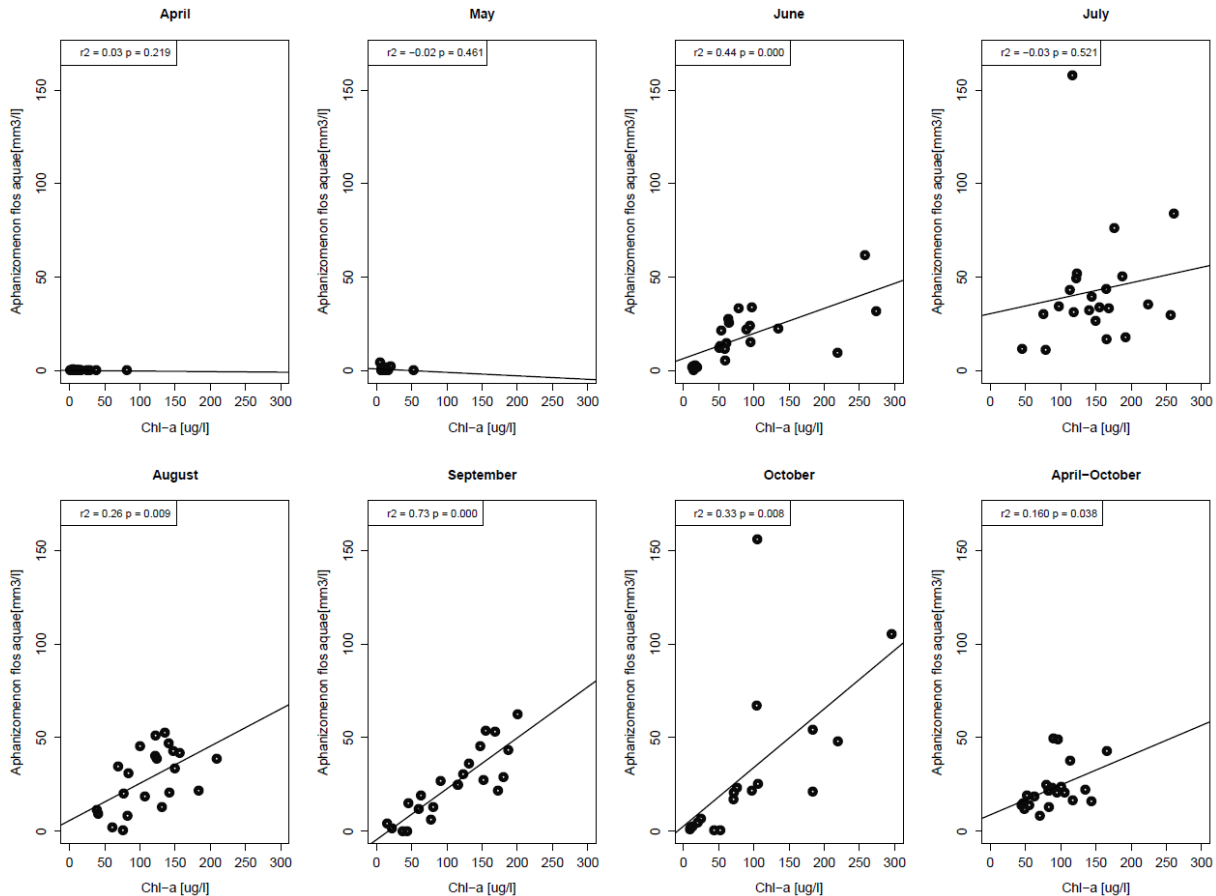


Figure 68: Correlation between chlorophyll-a and *Aphanizomenon flos-aquae* for each month.

Phenology models to assess factors influencing the bloom onset, peak and collapse.

A changing climate can alter ecosystems through shifts in species phenology (Walters et al. 2013). A common outcome of increased lake temperatures is a prolonged growing season and an earlier occurrence of blooms (Winder & Schindler 2004), though particular species may shift and bloom later in the season (Walters et al. 2013). Here we assessed the extent to which climatic variability or other abiotic factors influenced plankton phenologies in UKL and AL using the spline phenology model calculations described previously. We limited our analyses to major parameters such as chlorophyll-a, *Aphanizomenon flos-aquae* (and thus also total Cyanobacteria), as well as TP and TN which showed consistent seasonal cycles across years. As mentioned earlier, for chlorophyll-a we limited the input data to the June-October period to exclude the influence of diatoms which in some years have high abundance in April-May. All phenology calculations were performed on the 7 stations consistently measured in the main part of the lake (thus AS and AN were not included).

There was considerable variability in the timing and magnitude of the cyanobacteria bloom. Estimates of chlorophyll-a phenology showed substantial variation in the onset of the bloom (Julian day: 125-191), timing of the main peak period (Julian Day:180-243) and the timing of the bloom decline (Julian Day: 237-311) during the 1990-2016 time period (Figure 69A).

Similar variation was also found in model estimates of the length of the chlorophyll-a bloom (91-148 days; Figure 70). There was a strong positive correlation between the chlorophyll-a timing of the peak period and both the onset ($r^2=0.83$, $p<0.01$) and decline ($r^2=0.69$, $p<0.01$). The length of the bloom was weakly but positively correlated with the decline of the bloom ($r^2=0.23$, $p<0.01$) but not correlated with either the onset or main peak timing ($r^2=0.01$, $p=n.s.$).

Using the spline approximation method, we also calculated phenology estimates for the onset, peak timing, decline, and length of the *Aphanizomenon flos-aquae* bloom, total phosphorus, concentration, total nitrogen concentration, *Daphnia* biomass, and the soluble reactive phosphorus concentration (Figure 69B-F). Generally, the timing of the onset, main peak and decline varied similar to the chlorophyll-a phenology. With the exception of correlations between *Daphnia* and chlorophyll-a, total phosphorus, or soluble reactive phosphorus which showed no significant trends, pairwise correlation among all variables showed positive correlations for most combinations (Table 5). A similar pattern was observed for pairwise correlations between variables for the timing of the main peak where only the associations between *Daphnia* and total phosphorus or soluble reactive phosphorus showed non-significant trends. This pattern was also evident in estimates of the declines, where again *Daphnia* showed no trend with all variables except total phosphorus. All other pairwise correlations were positive and significant. Estimates of the length of the main bloom showed correlations among chlorophyll-a, total phosphorus, total nitrogen and *Aphanizomenon flos-aquae*, respectively (Table 5).

It would be expected that chlorophyll-a (measured from June-October) and *Aphanizomenon flos-aquae* are highly correlated as AFA is by far the dominant phytoplankton species during this time frame. Similarly, *Aphanizomenon flos-aquae* should correlate highly with the dynamics of phosphorus and nitrogen in the lake. Nonetheless, the generally coupled relationship between phenology estimates suggests that the phenology estimates provide a robust description of the changes in bloom timing in the lake. Interestingly, *Daphnia* phenology was not tightly coupled to the timing of the main bloom suggesting that other factors also influence the timing of *Daphnia* bloom. This might indicate that the abundance and bloom timing of other algae species is important in initiating the *Daphnia* bloom however our phenology analyses were not able to capture the phenology of the diatoms which bloom earlier in the spring, oftentimes before the main lake sampling program has been initiated. Similarly, it was not possible to obtain robust estimates of Cryptophyta which generally peak in the spring before the main cyanobacteria peak because cryptophytes comprise a much smaller portion of the phytoplankton community.

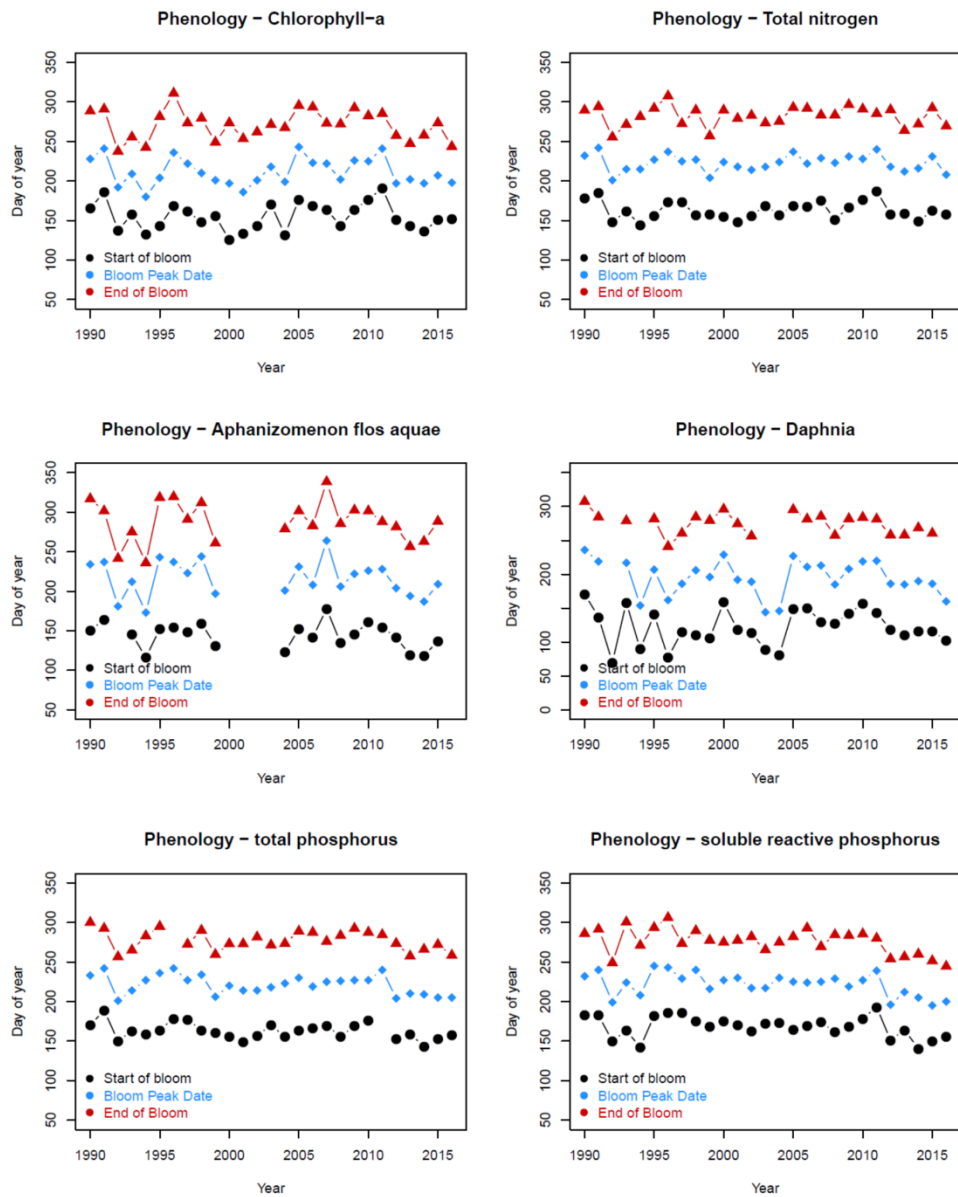


Figure 69: Phenology estimates onset, peak timing and decline, of A) chlorophyll-a, B) *Aphanizomenon flos aquae*, C) total nitrogen concentration, D) *Daphnia*, E) total phosphorus concentration and F) soluble reactive phosphorus concentration in Upper Klamath Lake (Data from 7 stations in the main part of the lake).

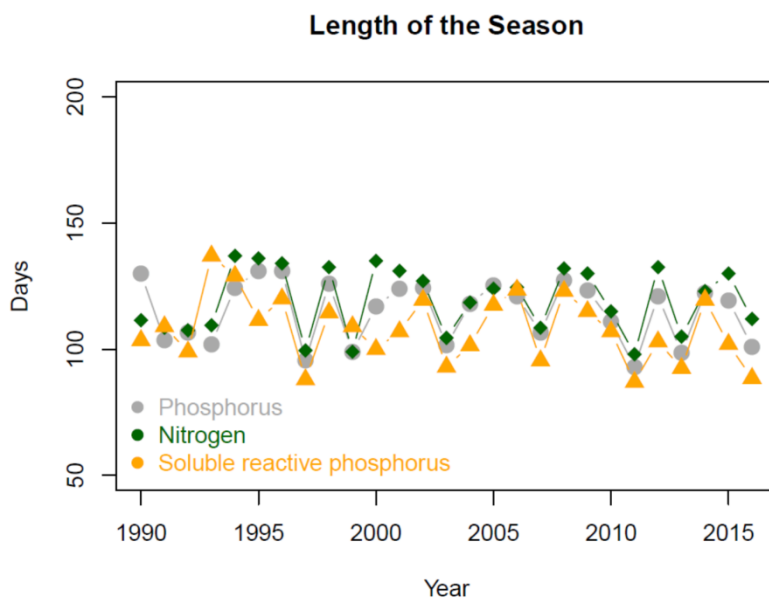
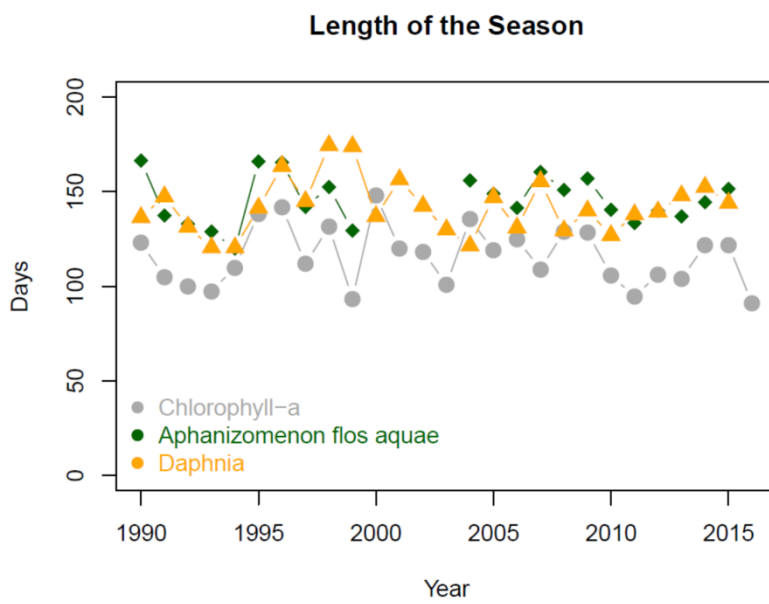


Figure 70: Estimates of the length of the season (number of days between onset and decline phenology estimates), of **A**) chlorophyll-a (grey), *Aphanizomenon flos-aquae* (green) and *Daphnia* (orange) and **B**) total phosphorus concentration (grey), total nitrogen concentration (green) and soluble reactive phosphorus concentration (orange) in Upper Klamath Lake (Data from 7 stations in the main part of the lake).

Table 5: Phenology correlations between the major variables in the main part of Upper Klamath Lake. Pairwise correlations were done for the onset measurements of all variables, the peak timing decline and length of season, respectively. Data show the r^2 for all pairwise correlations, with blue denoting all significant positive correlations ($p<0.05$).

Onset	Chlorophyll-a	<i>Aphanizomenon flos aquae</i>	Total phosphorus	Total nitrogen	Daphnia
Chlorophyll-a	X				
<i>Aphanizomenon flos aquae</i>		0.48 X			
Total phosphorus		0.65	0.47 X		
Total nitrogen		0.83	0.51	0.76 X	
Daphnia		0.10	0.17	0.03	0.14 X
Soluble reactive phosphorus		0.27	0.40	0.55	0.49
					0.08
Peak timing	Chlorophyll-a	<i>Aphanizomenon flos aquae</i>	Total phosphorus	Total nitrogen	Daphnia
Chlorophyll-a	X				
<i>Aphanizomenon flos aquae</i>		0.49 X			
Total phosphorus		0.41	0.43 X		
Total nitrogen		0.60	0.52	0.65 X	
Daphnia		0.17	0.27	0.05	0.15 X
Soluble reactive phosphorus		0.25	0.48	0.73	0.37
					0.10
Decline	Chlorophyll-a	<i>Aphanizomenon flos aquae</i>	Total phosphorus	Total nitrogen	Daphnia
Chlorophyll-a	X				
<i>Aphanizomenon flos aquae</i>		0.61 X			
Total phosphorus		0.65	0.41 X		
Total nitrogen		0.68	0.46	0.71 X	
Daphnia		0.01	0.05	0.23	0.01 X
Soluble reactive phosphorus		0.42	0.23	0.44	0.26
					0.02
Length of season	Chlorophyll-a	<i>Aphanizomenon flos aquae</i>	Total phosphorus	Total nitrogen	Daphnia
Chlorophyll-a	X				
<i>Aphanizomenon flos aquae</i>		0.60 X			
Total phosphorus		0.58	0.32 X		
Total nitrogen		0.52	0.09	0.75 X	
Daphnia		0.01	0.01	0.01	0.01 X
Soluble reactive phosphorus		0.05	0.01	0.29	0.26
					0.01

Mann-Kendall trend analyses of phenology estimates

Mann-Kendall trend analyses were computed for the phenology of all major variables in the lake. Overall there were very few significant changes in the phenology of UKL, and the Mann-Kendall trend tests showed few long-term changes to the phenology in UKL (Table 6). Only soluble reactive phosphorus had a negative trend for the onset, main peak and decline at $p\leq 0.05$. Total phosphorus also showed a negative trend for both onset and peak timing, but at $p\leq 0.10$. The negative trends suggests that the phenology of the soluble reactive and total phosphorus concentrations occurred earlier in the latter part of the time series compared to the early part of the time series in the 1990s. While not significant it is interesting that the trend analyses for the phenology estimates generally show negative trends. Multivariate regional Mann-Kendall trends test for each station also showed no long-term changes in the timing of the chlorophyll-a bloom onset, peak and decline (Regional Mann-Kendall, $p = \text{n.s.}$, Table 7).

Table 6: Mann-Kendall trend analyses of phenology estimates of onset, peak timing, decline and length of season for all major variables measured at stations in the main part of Upper Klamath Lake. Significant p-values are denoted in red for $p < 0.05$, and light red for $p < 0.10$, and in this case all negative as shown by the negative Tau value.

Onset	Z	N	p value	S	varS	Tau
Chlorophyll-a	0.17	27	0.87	9	2297.0	0.03
<i>Aphanizomenon flos aquae</i>	-1.18	21	0.24	-40	1094.6	-0.19
Total phosphorus	-1.68	26	0.09	-77	2054.3	-0.24
Total nitrogen	0.10	27	0.92	6	2296.0	0.02
Daphnia	-0.06	27	0.95	-4	2300.0	-0.01
Soluble reactive phosphorus	-2.07	27	0.04	-100	2298.0	-0.29
Peak timing						
Chlorophyll-a	-0.27	27	0.79	-14	2293.3	-0.04
<i>Aphanizomenon flos aquae</i>	-0.99	22	0.32	-36	1256.7	-0.16
Total phosphorus	-1.78	27	0.08	-86	2286.7	-0.25
Total nitrogen	-0.25	27	0.80	-13	2292.3	-0.04
Daphnia	-1.21	26	0.22	-56	2052.7	-0.17
Soluble reactive phosphorus	-2.36	27	0.02	-114	2294.0	-0.33
Decline						
Chlorophyll-a	-0.44	27	0.66	-22	2297.3	-0.06
<i>Aphanizomenon flos aquae</i>	-0.59	22	0.55	-22	1254.0	-0.10
Total phosphorus	-1.06	26	0.29	-49	2054.0	-0.15
Total nitrogen	0.10	27	0.92	6	2295.3	0.02
Daphnia	-1.38	22	0.17	-50	1252.6	-0.22
Soluble reactive phosphorus	-2.40	27	0.02	-116	2298.0	-0.33
Length of season						
Chlorophyll-a	-0.69	27	0.49	-34	2300.0	-0.10
<i>Aphanizomenon flos aquae</i>	-0.23	22	0.82	-9	1257.7	-0.04
Total phosphorus	-1.13	27	0.26	-55	2297.0	-0.16
Total nitrogen	-0.52	27	0.60	-26	2298.0	-0.07
Daphnia	0.29	26	0.77	14	2057.3	0.04
Soluble reactive phosphorus	-1.40	27	0.16	-68	2298.0	-0.19

Table 7. Regional Mann-Kendall trend test for chlorophyll-a estimated for all individual stations.

Upper Klamath Regional Mann-Kendall trend tests 1990-2015

Chlorophyll - a phenology	Z	S	varS	p
Timing of peak	0.03	7	66054	0.98
Onset of bloom	0.43	114	69892	0.67
Decline of bloom	-0.11	-29	65066	0.91
Length of season	-0.62	-148	57561	0.54

Temperature and phytoplankton phenology

The effect of temperature on the phytoplankton phenology could be pinpointed specifically to the air temperature in the spring (April-May), which was significantly and negatively correlated with both the bloom onset and the peak timing for both chlorophyll-a and *Aphanizomenon flos-aquae* (Figure 71). These findings were also supported by previous plankton analyses in UKL (Kann 1998; Jassby & Kann 2010).

The negative correlation with spring air temperature suggests that the main phytoplankton bloom occurs earlier when the spring is warm and later when it is cold. However, the total peak bloom biomass was not different in years with warmer springs. Also there was no significant relationship between the total length of the growing season (as estimated by the phenology models) and the temperature (data not shown, $p=n.s.$).

The phenology of the bloom also resulted in changes in the dissolved oxygen concentrations and pH later in the season (August-September). Years with an earlier bloom onset and earlier peak timing were associated with lower dissolved oxygen concentrations in August-September (Figure 72, Figure 73). A similar pattern was evident when comparing the phenology for chlorophyll-a for both the bloom onset and peak timing, with the lowest observed DO value for a given year (Figure 74, Figure 75). A potential explanation for this pattern is that during an earlier bloom onset the decline also happens earlier which results in a decline of overall photosynthesis while temperature mediated bacterial respiration of decayed phytoplankton results in greater oxygen depletion. For example, the highest summer water temperatures occur in late-July to mid-August in UKL which would be expected to cause higher rates of microbial decomposition of phytoplankton organic material relative to cooler temperatures in the fall. Lower dissolved oxygen concentrations and consequent poorer water quality is suggested to be one of the main causes of increased summer kills of adult suckers (Perkins et al. 2000; Kann and Welch 2005; Banish et al. 2009).

Due to the similarity between the phenology estimates for chlorophyll-a, total cyanobacteria and *Aphanizomenon flos-aquae*, the phenology of the latter two showed a similar statistically significant relationship with dissolved oxygen concentrations. Interestingly, there was no clear relationship between the onset and peak timing of the bloom and the total magnitude of the bloom (Figure 76).

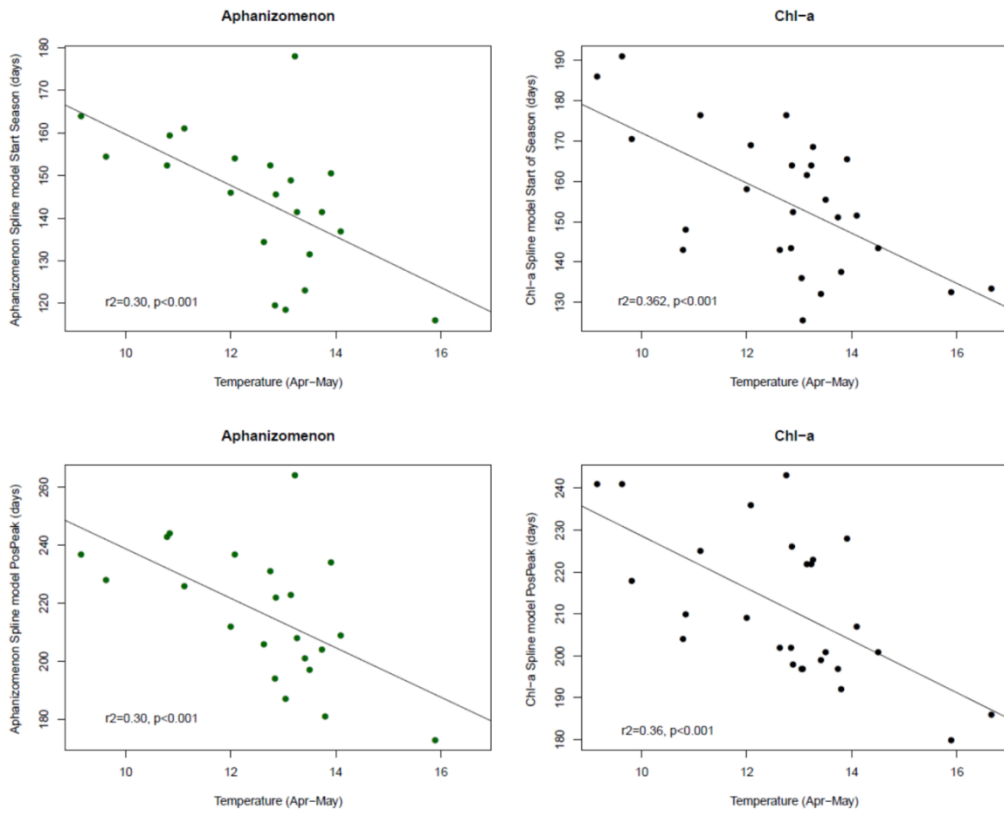


Figure 71: Air temperature in April–May showed a clear negative relationship with both the timing of the maximum peak and the start of the bloom in UKL, a pattern visible both in the chlorophyll-a and *Aphanizomenon flos-aquae* data.

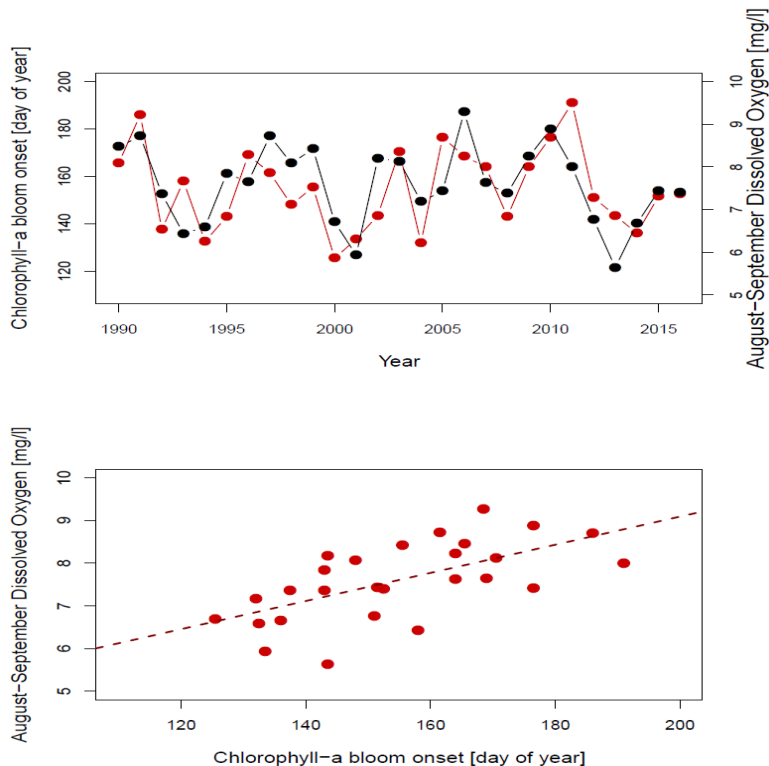


Figure 72: a) showing the long-term trend and b) correlation ($r^2 = 0.37$, $p < 0.01$) of the August–September mean of dissolved oxygen (black) and the estimated onset of the chlorophyll-a bloom (red) for UKL.

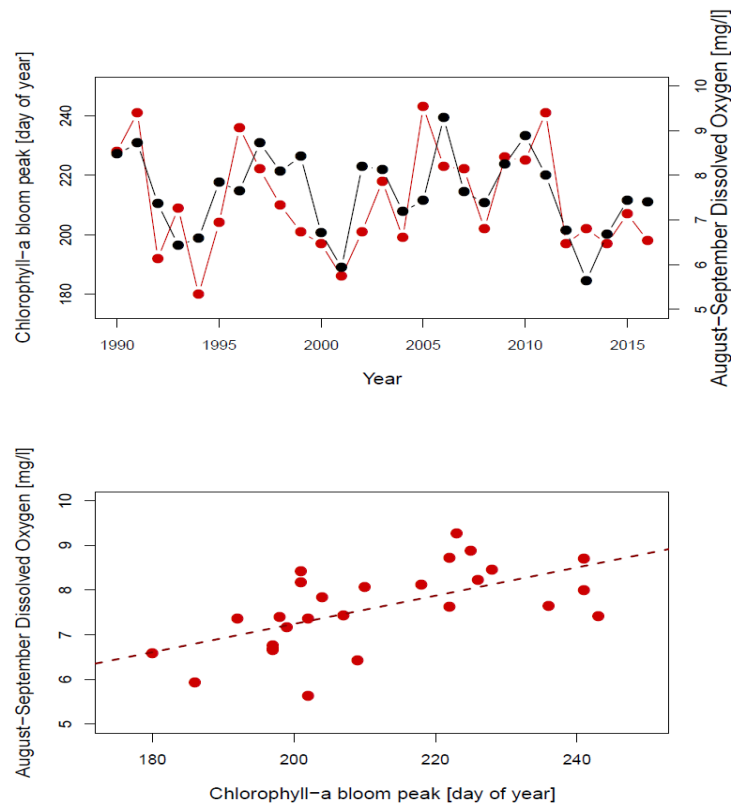


Figure 73: a) showing the long-term trend and b) correlation ($r^2 = 0.37$, $p < 0.01$) of the August-September mean of DO (black) and the timing of the chlorophyll-a bloom peak, (red) for UKL.

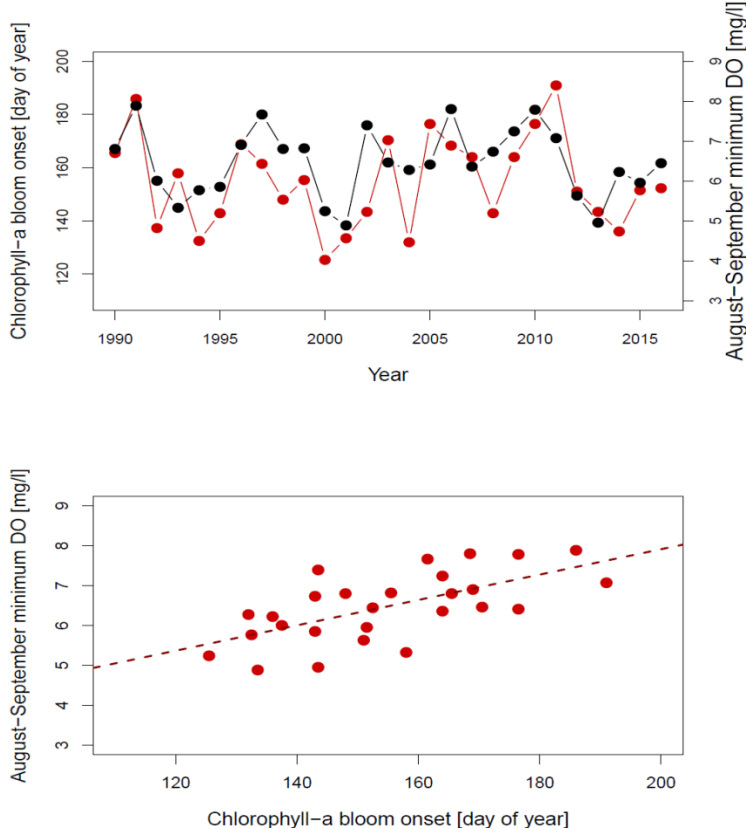


Figure 74: a) showing the long-term trend and b) correlation ($r^2 = 0.39$, $p < 0.01$) of the minimum dissolved oxygen (black) from the period (April-October) and onset of the chlorophyll-a bloom (red) for UKL.

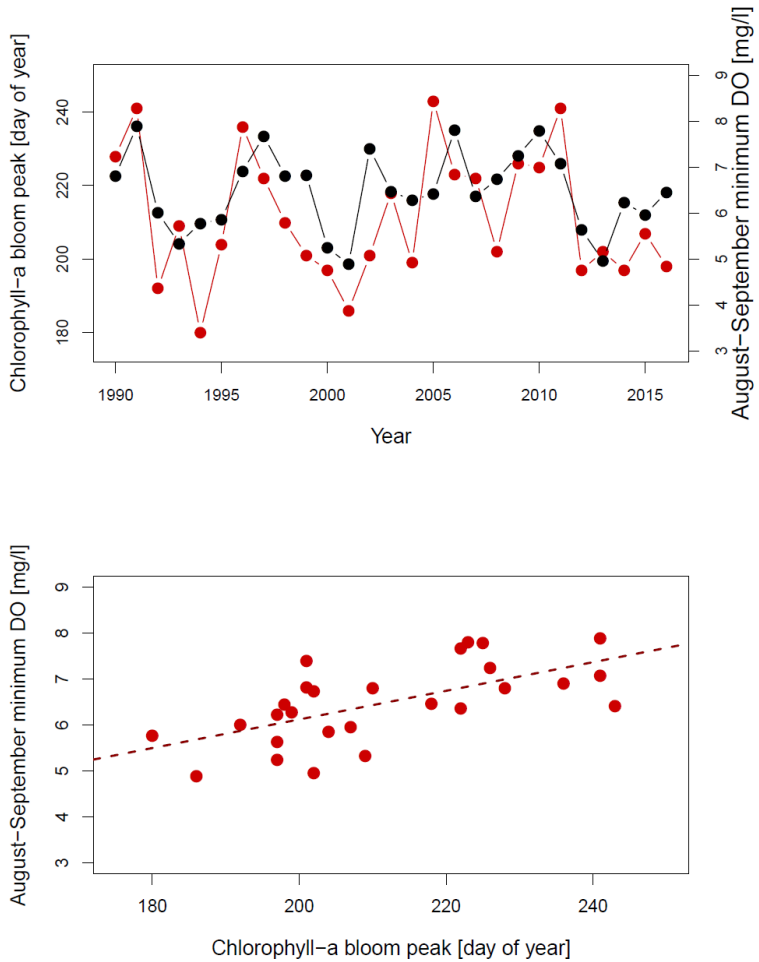


Figure 75: a) showing the long-term trend and b) correlation ($r^2 = 0.38, p < 0.01$) of the minimum dissolved oxygen (black) from the period (April-October) and peak timing of the chlorophyll-a bloom (red) for UKL

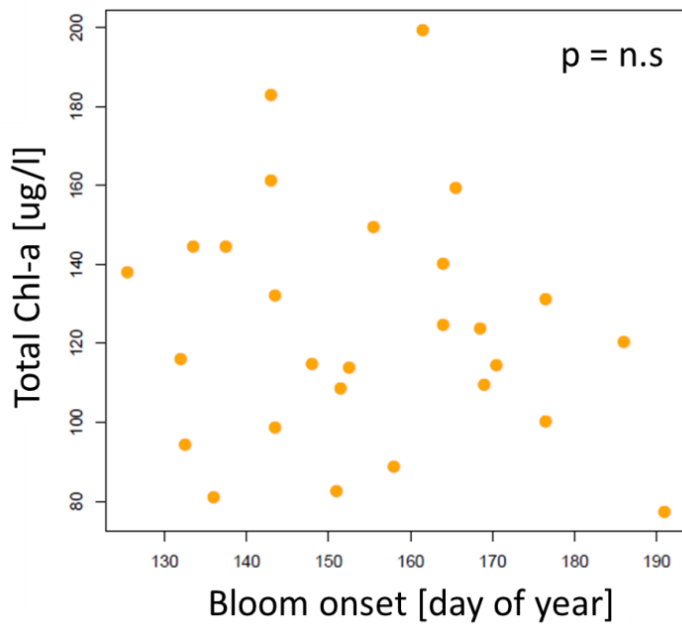


Figure 76: Relationship between the timing of the chlorophyll-a onset and the total chlorophyll-a summer biomass (June-September).

Plankton trophic interactions—*Daphnia* and phytoplankton

Two plankton species dominate in UKL during the summer, with *Aphanizomenon flos-aquae* comprising 99% of the phytoplankton abundance and *Daphnia* the primary zooplankton species in the Lake. Interestingly, these species show a very high level of co-occurrence. For example, variation in annual summer *Daphnia* abundance was influenced by both the amount of *Aphanizomenon flos-aquae* and the general phytoplankton community composition. Annual summer *Daphnia* biomass was correlated positively with summer *Aphanizomenon flos-aquae* biovolume ($r^2 = 0.36$, $p < 0.01$, Figure 77A). Similarly, the annual timing of the *Aphanizomenon flos-aquae* peak and the *Daphnia* biomass peak was positive and significant ($r^2 = 0.27$, $p < 0.01$, Figure 77B). Since *Aphanizomenon flos-aquae* constitutes 99% of the total phytoplankton biomass, similar positive correlations were visible between chlorophyll and *Daphnia* biomass ($r^2 = 0.27$, $p < 0.01$, data not shown) and peak timing ($r^2 = 0.28$, $p < 0.01$, data not shown). Interestingly, the peak timing of *Daphnia* usually occurred several weeks earlier than the peak timing of *Aphanizomenon flos-aquae* (Figure 77B). There was a significant negative relationship between the log biovolume of Cryptophyta and *Daphnia* biomass in summer ($r^2 = 0.34$, $p < 0.01$, Figure 77C), which suggests higher grazing of cryptophytes in years when *Daphnia* are more abundant.

Similarly, we found a negative relationship between the phytoplankton community dissimilarity and *Daphnia* biomass ($r^2 = 0.38$, $p < 0.01$, Figure 77D). Low phytoplankton community dissimilarity, indicative of lower abundance of algae other than *Aphanizomenon flos-aquae*, occurred in years with higher than average summer *Daphnia* biomass. That may be a result of substantial *Daphnia* grazing on these other algae groups. These results agree with Kann (1998) who showed that *Daphnia* biomass was positively correlated with *Aphanizomenon*, and negatively correlated with cryptophytes, chlorophytes, and chrysophytes.

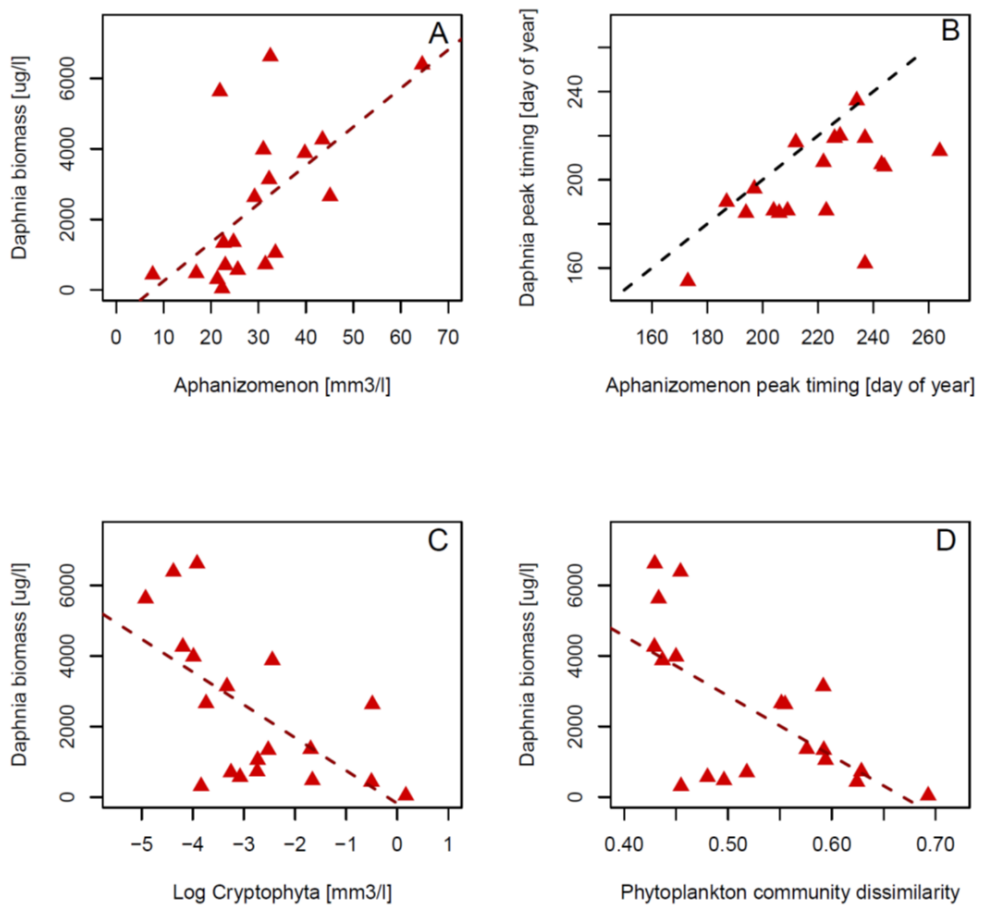


Figure 77 : Change *Daphnia* biomass in relation to A) *Aphanizomenon flos-aquae* biovolume ($r^2 = 0.36, p < 0.01$) in summer, B) relationship between *Aphanizomenon flos-aquae* and *Daphnia* peak timing ($r^2 = 0.27, p < 0.05$), relationship between summer *Daphnia* biomass and C) summer Cryptophyta biovolume ($r^2 = 0.34, p < 0.01$) and D) phytoplankton community dissimilarity ($r^2 = 0.38, p < 0.01$). Note that in B the black line denotes a 1:1 relationship to show the apparent offset in peak timing between *Daphnia* and *Aphanizomenon flos-aquae*.

The summer *Daphnia* biomass was also positively correlated with the timing of the chlorophyll-a decline (Figure 78A, $r^2 = 0.27, p < 0.05$), and the timing of the *Daphnia* biomass peak was positively correlated with the timing of the chlorophyll-a peak (Figure 78B, $r^2 = 0.28, p < 0.05$). These results confirm not only co-existence but also co-variation between these two main components of the planktonic food web in UKL, although *Daphnia* tended to peak slightly earlier than the chlorophyll-a bloom (black line, Figure 78B)

Interestingly, the phytoplankton community turnover measured using the Bray-Curtis dissimilarity index, as a measure of the change of phytoplankton composition during the growing season was negatively correlated with the main cyanobacteria bloom decline, as evident in both the chlorophyll-a decline estimates (Figure 78C, $r^2 = 0.47, p < 0.05$) and in the phenology estimates of the decline of *Aphanizomenon flos-aquae* (Figure 78D, $r^2 = 0.40, p < 0.05$).

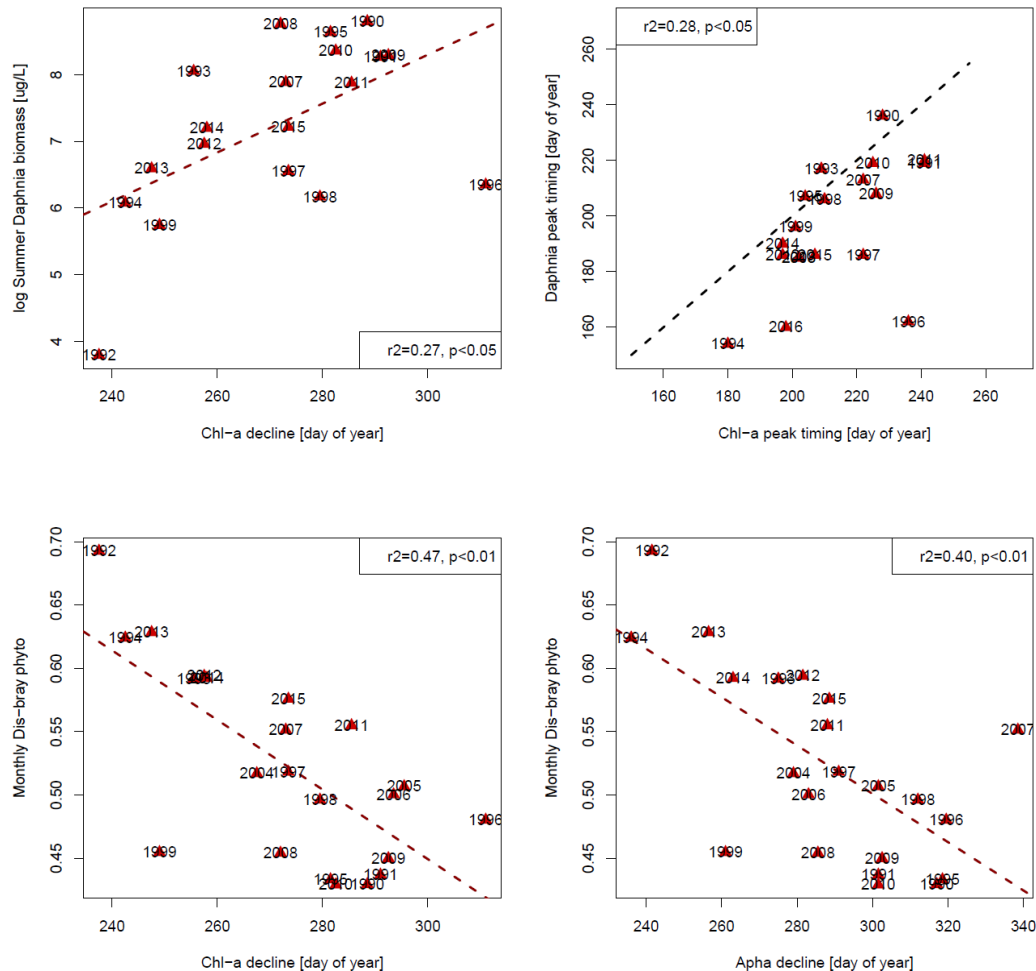


Figure 78: Relationship between A) the decline of the bloom and the summer *Daphnia* biomass, B) the chlorophyll-a and *Daphnia* peak timings, C) the chlorophyll-a decline and the Bray-Curtis dissimilarity index and D) the decline of the *Aphanizomenon flos-aquae* bloom and the phytoplankton Bray-Curtis dissimilarity index. Note that in B the black line is the 1:1 line and thus denotes if *Daphnia* peak before or after the chlorophyll-a bloom.

Multivariate Analyses

Multiple linear regression models

A multiple linear regression model was constructed to help determine which factors cause inter-annual variation in UKL. Initially three models were considered that either included dissolved nutrients (soluble reactive phosphorus and total inorganic nitrogen), total nutrients (TN, TP) or nutrient ratios (TIN:SRP or TN:TP). Because these groups of variables were highly collinear it was necessary to assess their importance in separate models.

Diatom models:

For the diatom models we specifically focused on data collected in the spring months of April and May because limnological sampling was less consistent in the months preceding this time.

The results for the three separate models for the diatom data suggested similar mechanisms, so we will focus our discussion on the dissolved nutrient model.

The diatom dissolved nutrient model included log transformed chemical (SRP and TIN) and physical (water temperature, light attenuation, relative thermal resistance to mixing, the mean 7-day air temperature, and the mean 7-day wind speed) data as explanatory variables. Relative thermal resistance to mixing is used as a predictor of water column stability, with higher relative thermal resistance to mixing values indicating a more strongly stratified water column. The most parsimonious model for diatoms included soluble reactive phosphorus, relative thermal resistance to mixing, and the light extinction coefficient as explanatory variables ($r^2=0.51$, $F=7.164$, $DF=3, 15$, $p<0.01$, Table 8). The April/May diatom biomass showed a negative relationship with soluble reactive phosphorus, which most likely indicates high diatom biomass leads to increased SRP uptake and lower lake water SRP concentrations. The most parsimonious total nutrient and nutrient ratio models were similar to each other and included temperature, light extinction coefficient and relative thermal resistance to mixing as explanatory variables (SRP was not included in these models), although the overall model fits were slightly weaker ($r^2=0.40$, $F=5.002$, $DF=3, 15$, $p<0.05$) than the dissolved model. In this case the sign for temperature was negative indicating cooler temperature was associated with higher diatom biomass. Because the light extinction coefficient and relative thermal resistance to mixing can be correlated (though collinearity was not a problem in the model, as indicated by a low variance inflation factor value), we further tested for the dissolved nutrient diatom model to determine whether the overall model changed substantially by *a priori* excluding either relative thermal resistance to mixing or the light extinction coefficient. These modifications did not change the overall model fits substantially and SRP was still the most important explanatory variable.

Table 8. Model summary of the diatom model using dissolved nutrient and physical data.

Diatoms - dissolved nutrients model	Coefficients	Standard Error	t	p-value
Intercept	1.647	1.025	1.607	0.129
Soluble reactive phosphorus	-0.861	0.251	-3.425	0.004
Extinction coefficient	1.660	0.604	2.750	0.015
Relative thermal resistance to mixing	0.419	0.223	1.881	0.080
Adjusted R ² = 0.51				

Chlorophyll-a bloom onset models:

To better understand the factors that are the most important for regulating the timing of the *Aphanizomenon flos-aquae* bloom initiation, we constructed multiple linear regression models for data sampled during the period of 15 May to 10 June (Figure 79). This period was chosen to capture the best and most consistent temporal coverage for field sampling across years. Because of the close relationship between Chl-a and *Aphanizomenon flos-aquae* during the

bloom, Chl-a was used for all models as this variable was sampled in all years while phytoplankton species composition data was missing for the 2000-2003 time period.

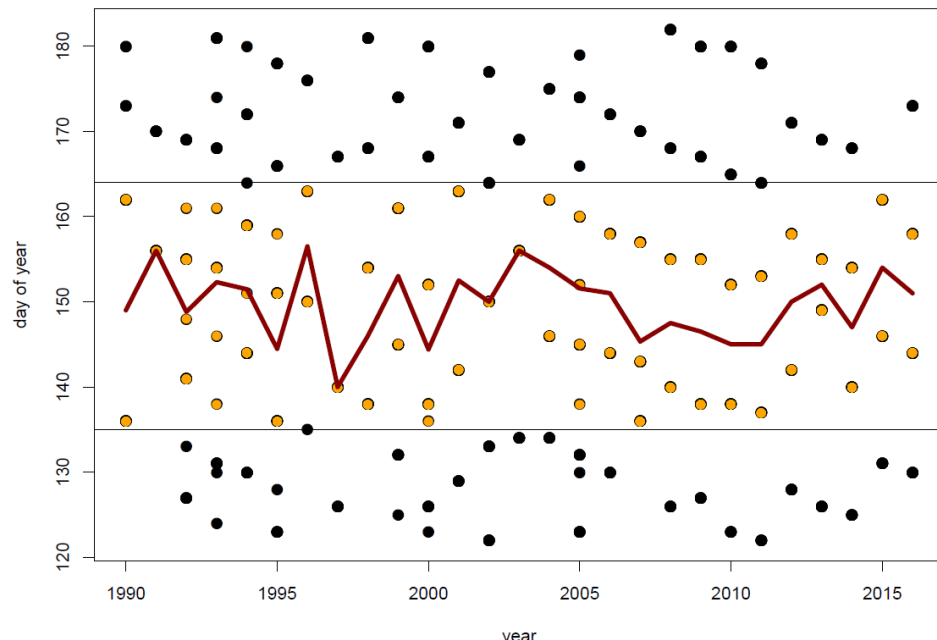


Figure 79. Overview of the time period for which chlorophyll-a data was used for the multiple linear regression models to assess the *Aphanizomenon flos-aquae* bloom onset.

The dissolved nutrient model for bloom initiation (with Chl-a as the response variable) included log transformed data for dissolved nutrients (TIN and SRP) and the major physical variables (water temperature, relative thermal resistance to mixing, the mean 7-day air temperature, the mean 7-day wind speed, and the light extinction coefficient). The most parsimonious model resulted in SRP, relative thermal resistance to mixing, and the light extinction coefficient being significant factors ($r^2=0.59$, $F=9.03$, $DF=3, 19$, $p<0.01$). Again, SRP was negatively correlated with Chl-a, while relative thermal resistance to mixing and the light extinction coefficient were positively correlated with Chl-a (Table 9). Because of the potential covariation of relative thermal resistance to mixing and the light extinction coefficient we again tested if excluding either one influenced the model fits. Excluding relative thermal resistance to mixing did not significantly change the final bloom initiation model, while exclusion of the light extinction coefficient did result in a lower overall fit.

Table 9. Model summary of the bloom onset model using dissolved nutrients and physical data:

Bloom onset - nutrient dissolved model	Coefficients	Standard Error	t	p-value
Intercept	1.338	0.627	2.134	0.046
Soluble reactive phosphorus	-0.351	0.163	-2.154	0.044
Relative thermal resistance to mixing	0.560	0.152	3.693	0.002
Extinction coefficient	2.007	0.524	3.830	0.001
Adjusted R ² = 0.59				

The nutrient ratio model for bloom initiation (with Chl-a as the response variable) included TN:TP ratio as well as the same physical parameters as the dissolved model. The most parsimonious ratio model used to explain the bloom onset showed a good fit ($r^2=0.50$, $F=8.31$, $DF=3, 19$, $p<0.01$, (Table 10), and also included the relative thermal resistance to mixing, the light extinction coefficient and the TN:TP ratio (although the later variable was not significant at $p<0.05$ but was at $p<0.10$). A model that used the TIN:SRP ratio instead of the TN:TP ratio resulted in a similar final outcome.

Table 10. Model summary of the Chl-a bloom onset model using ratio and physical data:

Bloom onset - nutrient ratio model	Coefficients	Standard Error	t	p-value
Intercept	-0.958	0.990	-0.968	0.345
Nitrogen to Phosphorus ratio	0.605	0.322	1.880	0.076
Relative thermal resistance to mixing	0.513	0.155	3.311	0.004
Extinction coefficient	1.916	0.529	3.622	0.002
Adjusted R ² = 0.50				

Both models suggest the importance of the physical conditions, in the form of water column mixing and light availability for bloom initiation. The spring increase in *Aphanizomenon flos-aquae* biomass often occurs very rapidly, so even a high sampling frequency (week - biweekly) may not fully cover the relationship between these variables.

Bloom peak models:

The dissolved nutrient model for bloom peak (with Chl-a as the response variable) included log transformed data for dissolved nutrients (TIN and SRP) and the major physical variables (water temperature, relative thermal resistance to mixing, the mean 7-day air temperature, the mean 7-day wind speed, and the light extinction coefficient). The most parsimonious model was significant ($r^2=0.65$, $F=14.99$, $DF=3, 19$, $p<0.01$, (Table 11), although only the light extinction coefficient had a significance value of $p<0.05$.

Table 11. Model summary of the bloom peak model using dissolved nutrients and physical data:

Bloom peak - nutrient dissolved model	Coefficients	Standard Error	t	p-value
Intercept	7.002	2.774	2.524	0.021
Extinction coefficient	1.457	0.237	6.141	0.001
Total inorganic nitrogen	0.072	0.046	1.558	0.136
Temperature	-1.339	0.893	-1.499	0.150
Adjusted R ² = 0.65				

The nutrient ratio model resulted in a similar outcome in terms of r^2 ($r^2=0.66$, $F=22.6$, $DF=2$, 20 , $p<0.01$), although the TIN:SRP ratio ($p=0.066$) was included in the model instead of TIN and temperature (Table 12).

Table 12. Model summary of the bloom peak model using nutrient ratio and physical data:

Bloom peak - nutrient ratio model	Coefficients	Standard Error	t	p-value
Intercept	3.144	0.278	11.318	0.001
Extinction coefficient	1.494	0.232	6.448	0.001
Total inorganic nitrogen : soluble reactive phosphorus	0.067	0.034	1.945	0.066
Adjusted $R^2 = 0.66$				

Exploring a model with different temporal data for explanatory and response variables.

The difficulty in differentiating between cause and effect for the primary explanatory factor the light extinction coefficient led us to further explore a model using data of the explanatory variables from the time period immediately before the Chl-a data was measured. In other words, a model was constructed using explanatory data from the time period June 1-June 20 was used to explain the Chl-a data sampled in the subsequent time period 20 June to 10 July. However, the model using dissolved nutrients, although significant, did not produce a better fit ($r^2=0.19$, $F=6.3$, $DF=1$, 21 , $p<0.05$) than the non-lagged model shown above, and the light extinction coefficient was still the only variable included in the model ($p= 0.0203$). A similar result was obtained for the nutrient ratio model when response variables were lagged in the same way relative to explanatory variables.

This initial analysis using multiple linear regression illustrates the difficulty in applying a predictive model to an apparent sequence of physical, chemical, and biological events that may control diatom and cyanobacterial bloom development in Upper Klamath Lake. For example, the positive association with light extinction for most models likely illustrates the effect of biomass accrual on water column light rather than the effect of light on bloom development, even though graphical analysis indicates a consistent year-to-year clear-water phase prior to *Aphanizomenon* onset (e.g., Figure 51C). In addition, the annual pattern of declining TIN and increasing SRP occurring in May and early-June (e.g., Figure 50) as *Aphanizomenon* develops is also not captured by the above models, or in monthly correlations of nitrogen to phosphorus ratios vs. algal biomass (Figure 64). The fact that these variables are not retained in the models (or were retained but not in the expected direction) despite that both increasing light and low nitrogen to phosphorus ratios are expected to foster growth and onset of diazotrophic algal species such as *Aphanizomenon*, likely reflect limitations of the modelling approach, and not necessarily that these variables may not exert control over the inter-annual variability in bloom dynamics. Limitations include relatively small sample size ($n=25$ for chlorophyll and $n=21$ for phytoplankton inter-annual models), and inability to capture both appropriate temporal lags and potential non-linear relationships among variables. Further predictive modelling efforts that account for these limitations are recommended.

Hierachal clustering analyses

The hierachal clustering analyses using Ward's minimum variance separated the annual phytoplankton composition data, based on the major groups in UKL (Chrysophyta, Cryptophyta, *Aphanizomenon flos-aquae*, diatoms, *Microcystis aeruginosa*), into three significant clusters (PERMANOVA, model F: 4.79, p<0.01, df =20). The first cluster included the annual data from the years: 1990, 1991, 1993, 1995, 1996, 1997, 1999, 2005, 2006, 2007, 2008, 2009, 2012 (green, Figure 80), the second cluster comprised the years: 1992, 1994, 1998, 2010, 2011, 2013 (red, Figure 80), and the third cluster comprised the years 2004, 2014 and 2015 (black Figure 80). The first cluster generally had the years with the highest relative abundances of *Aphanizomenon flos-aquae*. The second cluster was driven by years with higher relative abundance of diatoms, Chlorophyta, Cryptophyta, while the third cluster was associated with years with above average *Microcystis aeruginosa* abundance.

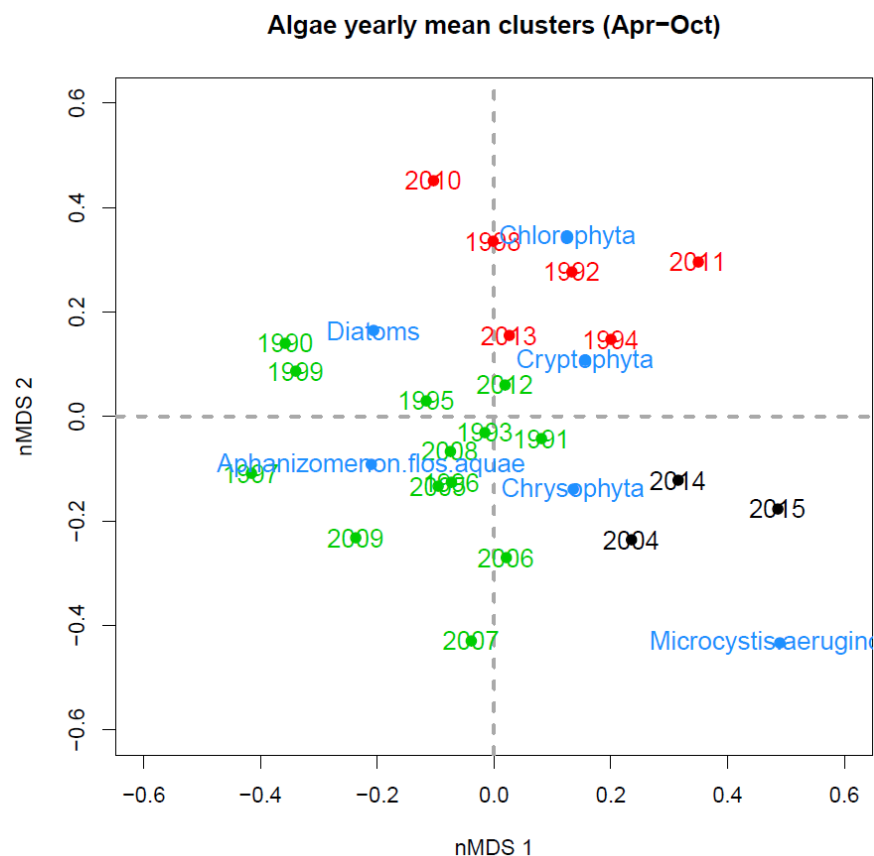


Figure 80: nMDS of the major phytoplankton composition for each year, with cluster 1 (green), 2 (red) and 3 (black) as partitioned by the hierachal clustering analysis (PERMANOVA, p<0.01)

Redundancy analyses

A combined RDA model was computed to characterize the combined influence of the physical and nutrient parameters on the phytoplankton composition. The most parsimonious model used to associate variation in the phytoplankton composition with the physical and

chemical variables explained 55.2% of the total variance (adj. $r^2= 0.403$, $F_{(5,15)} = 3.7$, $p<0.01$, Figure 81). The first and second RDA axes significantly explained 31.3% and 18.6% of the constrained variance, respectively ($p<0.01$). The final model included SRP which explained 16.0% of the constrained variance ($p<0.01$), while 8.6% of the variance was explained by RTRM ($p<0.01$), 8.4% by the TN:TP ratio ($p<0.01$), 6.0% by water temperature ($p=0.051$) and 5.1% by total nitrogen ($p=0.079$). The RDA model suggest that data on soluble reactive phosphorus, total nitrogen, the ratio of nitrogen to phosphorus, temperature and relative thermal resistance to mixing were all factors that explain the annual phytoplankton composition. Years with higher than normal temperatures were 2004, 2014, 2015 (black dots) also had higher levels of *Microcystis*. Whereas higher relative thermal resistance to mixing were also associated with years of higher than average *Aphanizomenon flos-aquae* biomass (years denoted with green dots). In contrast, years that had higher spring abundances of diatoms, Cryptophyta and Chlorophyta generally occurred during colder and also more mixed years (red dots). The unconstrained component of the model (i.e., variation not explained by the physical and chemical data) accounted for 44.8% of the total variance, suggesting that other parameters not include in our dataset also influence the annual phytoplankton community composition, something that should be explored in the future.

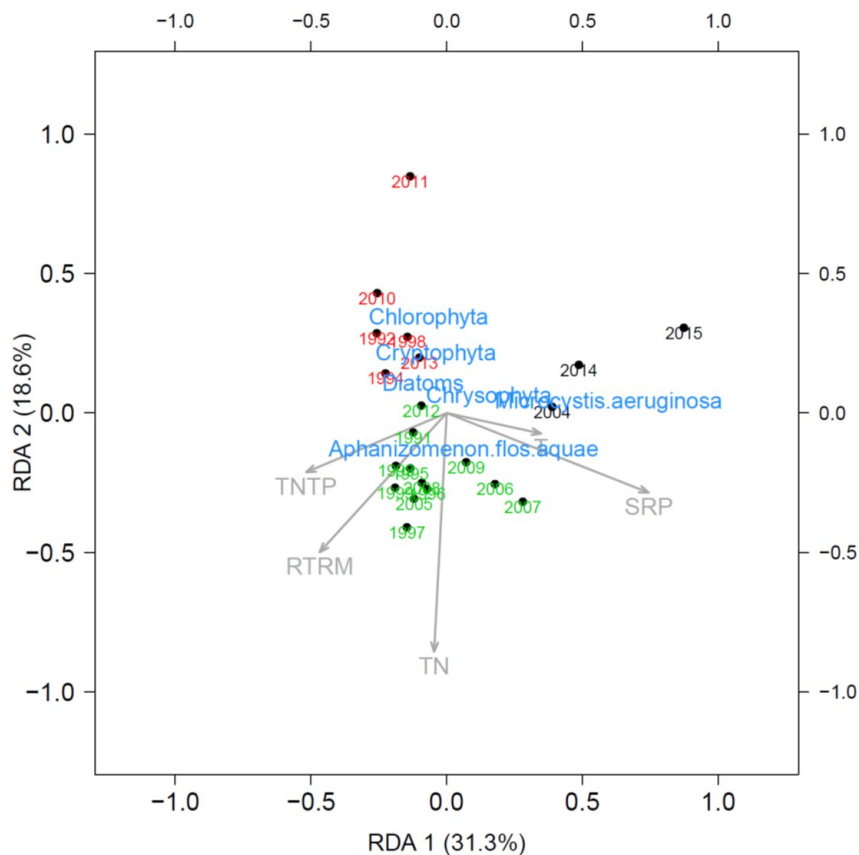


Figure 81: Redundancy analyses showing the relationship between major phytoplankton groups and the primary physical and chemical parameters in the main part of UKL. Data based on annual specific means values (see method for full details). Yearly phytoplankton clusters based on the hierachal clustering analyses are denoted in red, green and black, respectively.

Two-way cluster analyses

To better visualize concurrent patterns in the multivariate data we used a two-way cluster analysis of the data, based on the April to October mean values. The principle of the two-way cluster analysis is to identify the variables and/or years that tend to co-vary. First, we constructed a two-way cluster analysis using all the major variables (Figure 82). Yearly clusters (vertical dendograms), separated into five clusters. Similar to the one-way phytoplankton cluster analysis, the years 2014 and 2015 separated out, showing especially high biomass of *Microcystis aeruginosa* and high temperature and SRP concentrations. A separate cluster which included the years 1993, 1996, 1997 and 1998 was also separated from other years. These years showed higher than normal concentrations of total inorganic nitrogen and total ammonia, as well as higher total inorganic nitrogen to soluble reactive phosphorus and total inorganic nitrogen to total phosphorus ratios. These years also showed generally low levels of phytoplankton such as Cryptophytes, Chlorophytes and Chrysophytes.

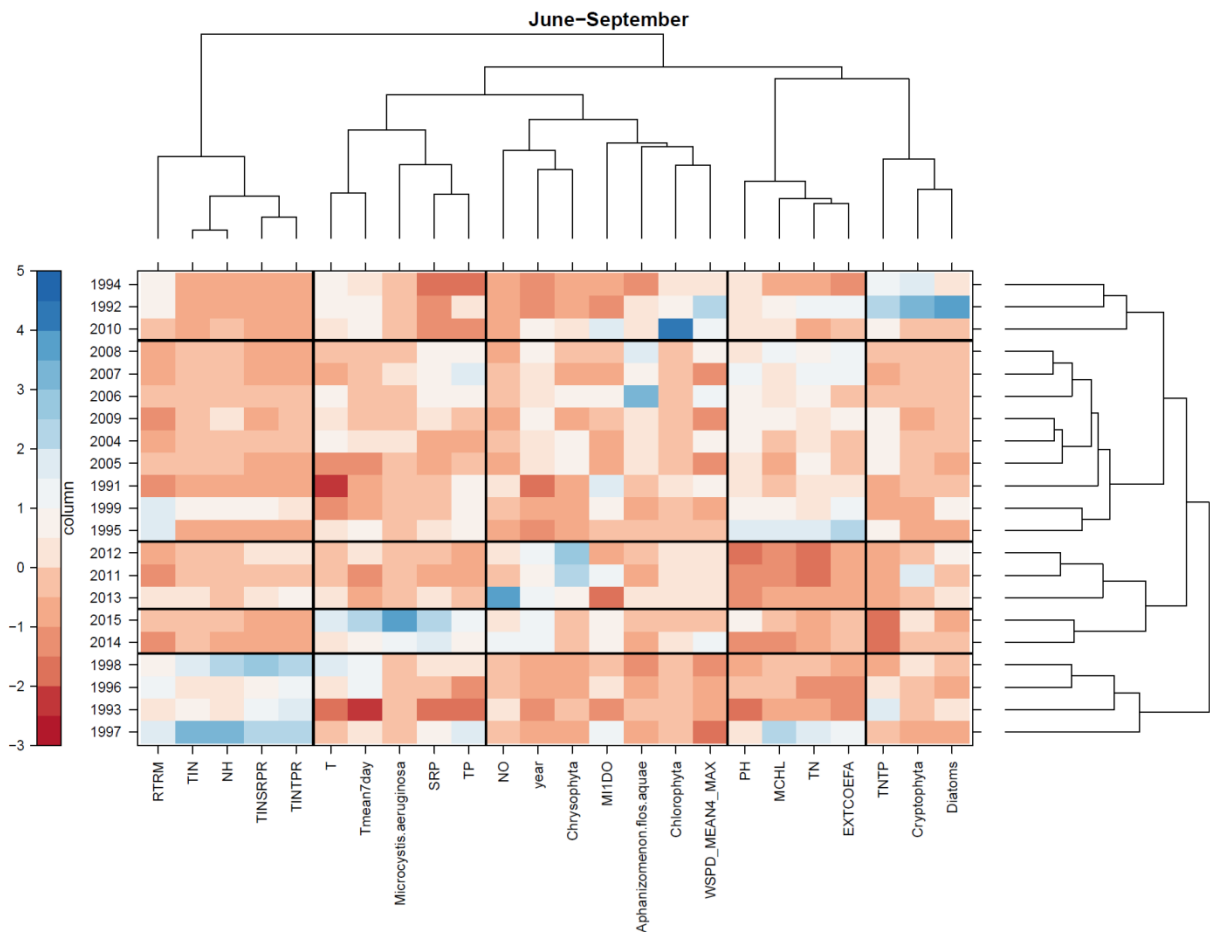


Figure 82: Two-way cluster analysis of the data for the major variables (dendrogram on top, label on x-axis) for each year (y-axis, dendrogram on right). Black lines show major cluster separations

However, different processes and relationships between major variables occur in early summer as compared to later in the year, thus a seasonal two-way cluster analyses was performed. For these analyses we only included variables that were in these distinct time periods. For example, diatoms, which bloom in April and May were included as a spring variable, while minimum dissolved oxygen was included as a late summer to fall parameter,

as this is usually the time period when dissolved oxygen concentrations are lowest. Similarly, *Aphanizomenon flos-aquae* was included as a summer variable, while *Microcystis aeruginosa* is most abundant in the fall. Spring temperature and wind conditions were also included as these variables commonly influence the summer bloom dynamics. Finally, we included phenology estimates for chlorophyll-a to assess how variation in these variables influences key water quality parameters.

In the seasonal two-way cluster analysis, similar to the general cluster analyses, the years 2014 and 2015 showed high fall *Microcystis aeruginosa* biomass, high summer soluble reactive phosphorus, and high summer total phosphorus concentrations (Figure 82; Figure 83). It is interesting to note the high similarity between summer values of soluble reactive phosphorus and total phosphorus and the average *Microcystis aeruginosa* biomass in the fall, which indicates that in above average years phosphorus plays a role in promoting *Microcystis aeruginosa* bloom formation. Variation in the *Aphanizomenon* bloom onset, peak timing and decline all aligned closely with the fall minimum dissolved oxygen concentrations, similar to our previous analyses suggesting that years with an earlier than normal bloom development also resulted in lower dissolved oxygen concentrations later in the summer.

Higher than normal diatom abundance seemed to occur in years with relatively high wind speeds and thus a higher water column mixing, which likely promotes both nutrient and diatom resuspension in the spring. Although in contrast to the positive association of diatoms with water column stability in the multiple linear regression models, the association of diatoms with wind speed observed in this approach is expected given the non-buoyant nature of diatoms relative to cyanobacteria (e.g., Reynolds 1994). Since RTRM is based on surface to bottom density differences due to temperature, the positive relationship between diatoms and RTRM in the spring based on the multiple linear regression models maybe more a reflection of lake warming during the diatom development period in April and May as opposed to water column mixing. For example, in Lake Washington, Washington State, the annual spring diatom bloom often starts during warm high-pressure weather events in March prior to the onset of thermal stratification (Arhonditsis et al. 2004). Similarly, calm high-pressure weather systems in April and May probably promote diatom blooms in UKL because temperatures are higher and light is more available for the diatoms during these conditions. However, during the middle of the summer when temperatures of UKL are much higher, and hence the viscosity of water is much lower, we still expect that calm weather is disadvantageous for diatoms.

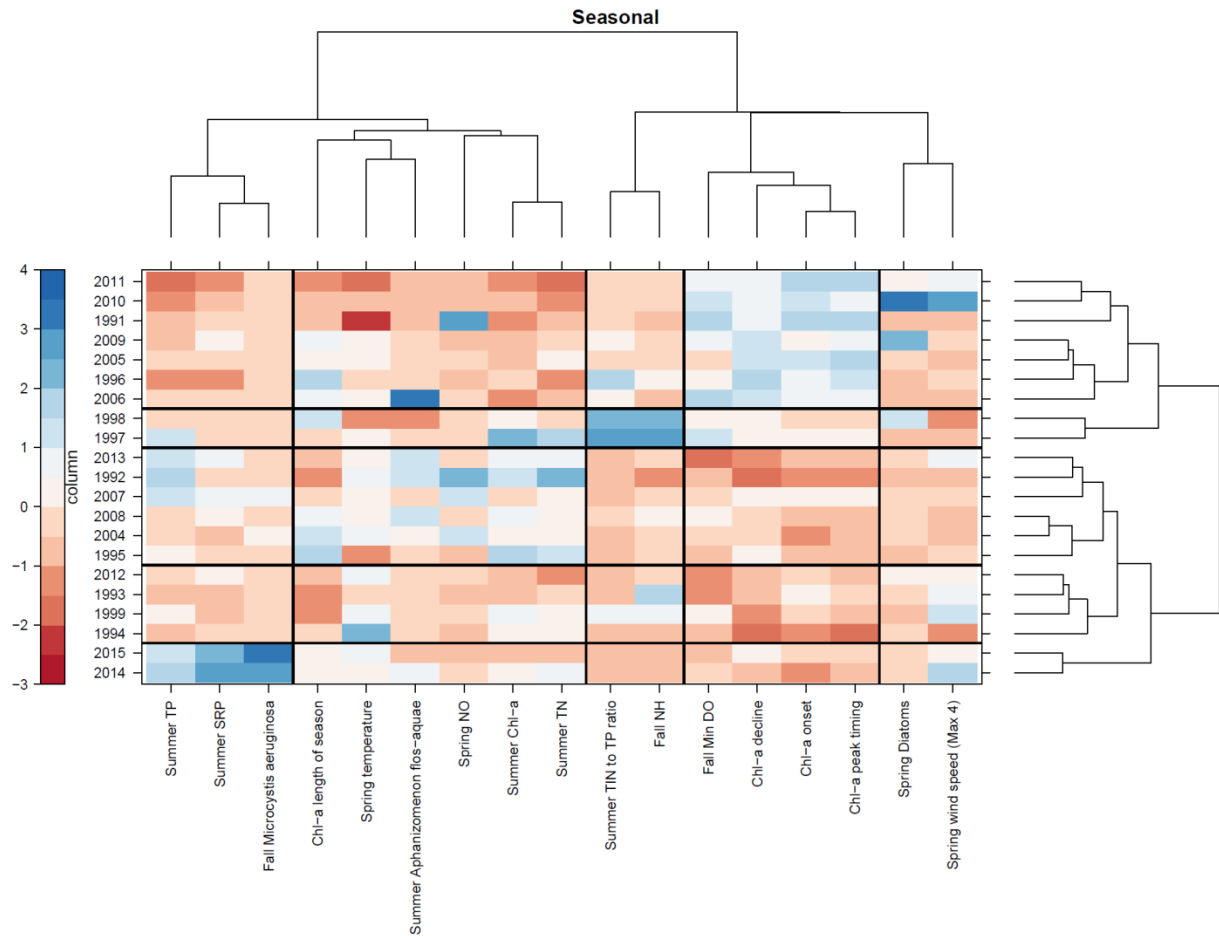


Figure 83: Two-way cluster analysis, based on season specific average values for the major variables in UKL (dendrogram on top, label on x-axis) for each year (y-axis, dendrogram on right). Black lines show major cluster separations.

SUMMARY

Spring temperature regulates summer bloom phenology

The combined analyses of the plankton dynamics revealed that spring water temperature is an important regulator of the bloom phenology in UKL. Above average temperatures initiate an earlier cyanobacteria bloom. Furthermore, an earlier bloom onset also commonly results in an earlier collapse of the main bloom later in summer. The tight coupling between the intense summer cyanobacteria bloom and the amount of nitrogen and phosphorus, due to nutrient release and re-suspension means spring temperatures also have a substantial impact on the timing of the nutrient recycling. Interestingly, the magnitude of the cyanobacteria bloom in the summer was not controlled directly by the phenology, although the magnitude of the bloom did influence the total length of the growing season. The significant relationship between bloom length and decline may be partly explained by the occasional occurrence of a distinct second bloom *Aphanizomenon flos-aquae* in Aug-Sep. Overall, the phenology analyses indicated that the primary change in phenology is due to an overall shift in bloom timing.

The influence of phenology on oxygen levels in Upper Klamath Lake

The change in phenology had substantial impacts on the chemical properties of the lake as an earlier bloom onset resulted in years with lower than average water column dissolved oxygen concentrations in the late summer. The amount of dissolved oxygen in the lake is of critical importance since low oxygen concentrations are detrimental to both juvenile and adult suckers. Our results showed that an earlier bloom onset and thus also an earlier bloom decline was associated with low minimum DO values in the lake. A plausible reason that years with an early bloom collapse were particularly susceptible to low dissolved oxygen levels is that enhanced microbial respiration of decaying cyanobacteria occurs when late summer temperatures are still high and thus respiration and oxygen consumption remains high. Further, during warmer periods in the late summer, the lake's saturation capacity for oxygen is lower, which additionally exacerbates the potential for hypoxic conditions to occur.

The consequences of changing phenology on the plankton food web

On a seasonal scale, there was a clear decrease in both phyto- and zooplankton species richness after the onset of the summer cyanobacteria bloom. This pattern was generally consistent across years, and especially in years when the main cyanobacteria bloom maintained a high biomass in the late summer. Years with a later than normal bloom decline resulted in low community turnover, which is likely indicative of continued *Aphanizomenon* dominance and suppression of other phytoplankton species and thus also lower species richness. The negative linkage between species richness and the timing of the cyanobacteria bloom suggests that other plankton species remain low or absent either due to direct effects of competition or due to the light limitation in the form of shading by *Aphanizomenon*. However, we also found a negative relationship between *Daphnia* biomass and phytoplankton community turnover, which also suggests that phytoplankton richness may also be depressed by intense zooplankton grazing.

***Daphnia* and cyanobacteria co-existence.**

There is clear evidence of co-existence between Cyanobacteria and *Daphnia* as both plankton species dominate in the summer. It is remarkable that in a highly productive system such as UKL, only two species, *Aphanizomenon* and *Daphnia*, constitute more than 95% of the respective phyto- and zooplankton biomass. Cyanobacteria are considered a poor dietary resource (Wilson et al 2006, Tillmanns et al. 2008) lacking most essential organic molecules crucial for organismal growth (Brett et al. 1997, Martin-Creuzburg et al. 2008). Long filamentous cyanobacteria, such as *Aphanizomenon flos-aquae*, can also obstruct the feeding apparatus of *Daphnia* resulting in poorer growth (DeMott 2001), thus it is quite interesting that a large *Daphnia* population thrives during the summer when *Aphanizomenon* comprise ~99% of the total phytoplankton biomass, although they un-surprisingly seem unable to control *Aphanizomenon* through grazing. *Daphnia*, which are the most abundant zooplankton in UKL, are thought to be an important dietary resource for larval and juvenile fish, such as the endangered sucker species in UKL. Does *Daphnia* feed on *Aphanizomenon* or are they

capable of selective filter feeding on the small fraction (< 1%) of the “understory” microalgae? Recent work studying the dietary uptake of *Daphnia* using fatty acid analyses in UKL suggests that *Daphnia* are capable of a high degree of selective feeding. Despite being low in abundance but potentially having a relatively high production, diatoms and cryptophyta comprised approximately 60% of the diet contribution in *Daphnia* (M.T. Brett, unpublished data). Our data support substantial grazing by *Daphnia* on cryptophyta. The field data also show that the *Daphnia* population usually begins to peak in late May and early June at the same time that the diatom bloom usually collapses. Nonetheless, cyanobacteria still constituted about 35-40% of the diet (M.T. Brett, unpublished data) suggesting that *Daphnia* manage to survive and grow during the cyanobacteria bloom as long as feeding is complimented by high quality diets such as cryptophytes and diatoms. While the large filaments of *Aphanizomenon* are too big for *Daphnia* to readily ingest there are likely smaller filaments which are within the appropriate size spectrum for *Daphnia* grazing (Holm et al. 1983). Cyanobacteria have relatively high levels of nitrogen and thus these phytoplankton may be good sources of dietary protein while important fatty acids are assimilated from other diet resources such as cryptophytes and diatoms. Such complimentary feeding is supported in controlled empirical studies where *Daphnia* seem to grow well as long as a smaller contribution of a high quality dietary resource is available (DeMott & Muller-Navarra 1997).

The importance of long-term temperature regimes in Upper Lake Klamath

We observed decreasing trends in total summer chlorophyll-a and total nitrogen concentrations from 1990-2016. Recent wetland restoration efforts and cessation of associated agricultural pumping to the lake should reduce nutrient loading to the lake, and several such wetlands are no longer grazed or farmed, and are in varying stages of restoration (e.g. Wong et al., 2011; USBLM, 2005; Carpenter et al., 2009; Duff et al., 2011). Thus, the declining chlorophyll-a and nitrogen concentrations could be due to the enhanced management of human mediated nutrient loading around the lake as well as further upstream in the watershed. However, despite the data series comprising 27 years it is still difficult to evaluate the combined effects of recent restoration efforts and climate perturbations. We also found few changes in the long-term trends in plankton phenology. Our analyses depict the ecosystem dynamics during a time period that include a substantial negative PDO phase including a cold temperature regime in the mid-2000s. Thus, it will be an important future task to establish if the nutrient and chlorophyll-a levels will continue to decrease as a result of better ecosystem management, or instead respond to climate and thus increase due to an expected more positive PDO cycle and thus warmer climate in the coming decades.

REFERENCES

- American Public Health Association (APHA). 1985. Standard methods for the examination of water and waste water. 16th Ed. APHA, New York. 1268 p.
- Anderson, M. J. 2001. A new method for non-parametric multivariate analysis of variance. *Austral ecology* 26:32-46.
- Anderson, M. J. and D. C. Walsh. 2013. PERMANOVA, ANOSIM, and the Mantel test in the face of heterogeneous dispersions: What null hypothesis are you testing? *Ecological Monographs* 83:557-574.
- Arhonditsis, G.B., Winder, M., Brett, M.T. and Schindler, D.E. 2004. Patterns and mechanisms of phytoplankton variability in Lake Washington (USA). *Water Research* 38: 4013-4027.
- Banish, N.P., Adams, B.J., Shively, R.S., Mazur, M.M., Beauchamp, D.A., and Wood, T.T. (2009). Distribution and habitat associations of radio-tagged adult Lost River suckers and shortnose suckers in Upper Klamath Lake, Oregon. *Transactions of the American Fisheries Society* 138:153-168.
- Bergquist, A.M. 1985. Effects of herbivory on phytoplankton community composition, size structure and primary production. Ph. D. Dissertation. University of Notre Dame, Notre Dame, Indiana, USA.
- Bradbury, J. P., S. M. Colman, and R. L. Reynolds. 2004. The history of recent limnological changes and human impact on Upper Klamath Lake, Oregon. *Journal of Paleolimnology* 31:151-161.
- Bray, J. R. and J. T. Curtis. 1957. An ordination of upland forest communities of southern Wisconsin. *Ecological Monographs* 27:325-349.
- Brett, M.T. and D.C. Müller-Navarra. 1997. The role of highly unsaturated fatty acids in aquatic food web processes. *Freshwater Biology* 38:483-499.
- Brody, S. R., M. S. Lozier, and J. P. Dunne. 2013. A comparison of methods to determine phytoplankton bloom initiation. *Journal of Geophysical Research: Oceans* 118:2345-2357.
- Carpenter, K.D., Snyder, D.T., Duff, J.H., Triska, F.J., Lee, K. K., Avanzino, R.J. and S. Sobieszczyk (2009). Hydrologic and water-quality conditions during restoration of the Wood River Wetland, Upper Klamath River Basin, Oregon, 2003-05: U.S. Geological Survey Scientific Investigations Report 2009-5004, 67 p. <http://pubs.usgs.gov/sir/2009/5004/>
- Crumpton, W.G. 1987. A simple and reliable method for making permanent mounts of phytoplankton for light and fluorescence microscopy. *Limnol. Oceanogr.* 32:1154-1159.

- Culver, D. A., M. M. Boucherle, D. J. Bean, and J. W. Fletcher. 1985. Biomass of freshwater crustacean zooplankton from length-weight regressions. *Can J. Fish. Aquat. Sci.* 42:1380-1390.
- Day, J. L., J. L. Jacobs, and J. Rasmussen. 2017. Considerations for the propagation and conservation of endangered lake suckers of the western United States. *Journal of Fish and Wildlife Management* 8:301-312.
- DeMott, W. and D. Müller-Navarra. 1997. The importance of highly unsaturated fatty acids in zooplankton nutrition: evidence from experiments with *Daphnia*, a cyanobacterium and lipid emulsions. *Freshwater Biology* 38:649-664.
- DeMott, W. R., R. D. Gulati, and E. Van Donk. 2001. *Daphnia* food limitation in three hypereutrophic Dutch lakes: Evidence for exclusion of large-bodied species by interfering filaments of cyanobacteria. *Limnology and Oceanography* 46:2054-2060.
- Dodds, W.K. et al., 2012. Surprises and insights from long-term aquatic data sets and experiments. *BioScience*, 62:709–721.
- Doney, S. C., M. Ruckelshaus, J. E. Duffy, J. P. Barry, F. Chan, C. A. English, H. M. Galindo, J. M. Grebmeier, A. B. Hollowed, and N. Knowlton. 2012. Climate change impacts on marine ecosystems. *Marine Science* 4:11-37.
- Duff, J.H., Carpenter, K.D., Snyder, D.T., Lee, K.K., Avanzino, R.J. and F.J. Triska (2011). Phosphorus and nitrogen legacy in a restoration wetland, Upper Klamath Lake, Oregon. *Wetlands* 29:735-746.
- Dumont, H. J. F. Guides to the identification of the microinvertebrates of the continental waters of the world, 21. Kenobi Productions, Ghent, Belgium and Backhuys Publishers, Leiden, The Netherlands.
- Eilers, J.M., J. Kann, J.Cornett, K. Moser, and A. St. Amand. 2004. Paleolimnological evidence of a change in a shallow, hypereutrophic lake: Upper Klamath Lake, Oregon. *Hydrobiologia* 520:7-18.
- Eldridge, S.L., T. M. Wood, K. R. Echols, and B. R. Topping. 2013. Microcystins, nutrient dynamics, and other environmental factors during blooms of non-microcystin-producing *Aphanizomenon flos-aquae* in Upper Klamath Lake, Oregon, 2013. *Lake and Reservoir Management* 29:68-81.
- Forkel M, Wutzler T (2015) greenbrown - land surface phenology and trend analysis. A package for the R software. Version 2.2, 2015-04-15.
- Ger, K. A., L. A. Hansson, and M. Lürling. 2014. Understanding cyanobacteria-zooplankton interactions in a more eutrophic world. *Freshwater Biology* 59:1783-1798.
- Hillebrand, H., Dürselen, C.-D., Kirschel, D., Pollinger, U. & Zohary, T. 1999: Biovolume calculation for pelagic and benthic microalgae. *Journal of Phycology* 35:403-424

Hewitt, D.A., Janney, E.C., Hayes, B.S., and Harris, A.C., 2018, Status and trends of adult Lost River (*Deltistes luxatus*) and shortnose (*Chasmistes brevirostris*) sucker populations in Upper Klamath Lake, Oregon, 2017: U.S. Geological Survey Open-File Report 2018-1064, 31 p., <https://doi.org/10.3133/ofr20181064>

Holm, N. P., G. G. Ganf, and J. Shapiro. 1983. Feeding and assimilation rates of *Daphnia pulex* fed *Aphanizomenon flos-aquae*. Limnology and Oceanography 28:677-687.

Jassby, A. and J. Kann. 2010. Upper Klamath Lake monitoring program: preliminary analysis of status and trends for 1990-2009. Prepared for Klamath Tribes Natural Resources Department, Chiloquin, Oregon.

Jassby, A. D., J. E. Cloern, and B. E. Cole. 2002. Annual primary production: Patterns and mechanisms of change in a nutrient-rich tidal ecosystem. Limnology and Oceanography 47:698-712.

Kann J. 2018 Technical Memorandum Prepared by Aquatic Ecosystem Sciences LLC for the Klamath Tribes Natural Resources Department, Chiloquin Oregon. June 2018. 85 pp.

Kann J. 2017. Upper Klamath Lake 2016 data summary report. Prepared by Aquatic Ecosystem Sciences LLC, Ashland, OR for the Klamath Tribes Natural Resources Department, Chiloquin, Oregon. 74 pp.

Kann, J. 1998. Ecology and water quality dynamics of a shallow hypereutrophic lake dominated by Cyanobacteria (*Aphanizomenon flos-aquae*). Doctoral dissertation. University of North Carolina, Curriculum in Ecology, Chapel Hill, North Carolina.

Kann, J. and E. B. Welch. 2005. Wind control on water quality in shallow, hypereutrophic Upper Klamath Lake, Oregon. Lake and Reservoir Management 21:149-158.

Kann, J. and E. B. Welch. 2005. Wind Control on Water Quality in Shallow, Hypereutrophic Upper Klamath Lake, Oregon. Lake and Reservoir Management 21:149-158.

Kann, J. and V.H. Smith. 1999. Estimating the probability of exceeding elevated pH values critical to fish populations in a hypereutrophic lake. Canadian Journal of Fisheries and Aquatic Sciences 56:2262-2270.

Kann, J., J.E. Asarian, A. St. Amand. 2015. Initial Analysis of 1990-2013 Phytoplankton and Zooplankton Data for Upper Klamath Lake (Phase I). Prepared by Aquatic Ecosystem Sciences LLC. for the Klamath Tribes Natural Resources Department. 100p. + appendices.

Klamath Tribes 2013. Standard Operating Procedures (SOP) for Upper Klamath Lake Water Quality Field Sampling. Revision: 2013 v). Klamath Tribes Research Station, Klamath Tribes Natural Resources Department, Chiloquin, OR.

Klamath Tribes 2014. Quality Assurance Project Plan (QAPP). Revision: 01.16.14. Klamath Tribes Research Station, Klamath Tribes Natural Resources Department, Chiloquin, OR.

Kosten, S., V. L. Huszar, E. Bécares, L. S. Costa, E. Donk, L. A. Hansson, E. Jeppesen, C. Kruk, G. Lacerot, and N. Mazzeo. 2012. Warmer climates boost cyanobacterial dominance in shallow lakes. *Global Change Biology* 18:118-126.

Legendre, P. and L. Legendre. 2012. Chapter 8 - Cluster analysis. Pages 337-424 in L. Pierre and L. Louis, editors. *Developments in Environmental Modelling*. Elsevier.

Lindenmayer, D.B. et al., 2012. Value of long-term ecological studies. *Austral Ecology*, 37:745-757.

Lund, J.W.G., C. Kipling and E.D. LeCren. 1958. The inverted microscope method of estimating algal numbers and the statistical basis of estimates by counting. *Hydrobiologia* 11:143-170.

Mantua, N. J., S. R. Hare, Y. Zhang, J. M. Wallace, and R. C. Francis. 1997. A Pacific inter-decadal climate oscillation with impacts on salmon production. *Bulletin of the American Meteorological Society* 78:1069-1079.

Martin-Creuzburg D, Von Elert E & Hoffmann KH (2008) Nutritional constraints at the cyanobacteria-*Daphnia magna* interface: the role of sterols. *Limnol Oceanogr* 53: 456-468.

McCauley, E. 1984. The estimation of the abundance and biomass of zooplankton in samples, pp. 228-265 in: Downing, J. A. and F. H. Rigler, editors. *A manual on methods for the assessment of secondary productivity in fresh waters*. Blackwell Scientific Publication, Oxford.

McCauley, E. 1984. The estimation of the abundance and biomass of zooplankton in samples, pp. 228-265 in: Downing, J. A. and F. H. Rigler, editors. *A manual on methods for the assessment of secondary productivity in fresh waters*. Blackwell Scientific Publication, Oxford.

McNabb, C. D., 1960, Enumeration of freshwater phytoplankton concentrated on the membrane filter. *Limnology and Oceanography*, 5:57–61.

Oksanen, J., F. G. Blanchet, R. Kindt, M. J. Oksanen, and M. Suggs. 2013. Package ‘vegan’. *Community ecology package Version 2:0-0*.

Olrik, K., et. al. 1998. Methods for Quantitative Assessment of Phytoplankton in Freshwaters, part I. Naturvårdsverket, Stockholm.

Pennak, R. W. 1989. Fresh-water invertebrates of the United States, 3rd ed. Protozoa to Mollusca. Wiley, USA.

Perkins, D.L., J. Kann, and Scoppettone, G.G. (2000). The role of poor water quality and fish kills in the decline of endangered Lost River and shortnose suckers in Upper Klamath Lake. U.S. Geological Survey, Biological Resources Division. Prepared for U.S. Bureau of Reclamation, Klamath Falls Project Office, Klamath Falls, OR.
http://www.usbr.gov/mp/kbao/esa/Fish_Kill.pdf

R Development Core Team. 2014. R: A language and environment for statistical computing. R Foundation for Statistical Computing, Vienna, Austria.

Reynolds, C.S. (1994). The long, the short and the stalled: on the attributes of phytoplankton selected by physical mixing in lakes and rivers. *Hydrobiologia* 289: 9-21.
doi.org/10.1007/BF00007405.

Rott, E. 1981. Some results from phytoplankton intercounting calibrations. *Schweiz. Z. Hydrol.* 43:34-62

Rasmussen, J. E., 2011. Status of Lost River and shortnose sucker. *Western North American Naturalist* 71: 442-455

St. Amand, A. 1990. Mechanisms controlling metalimnetic communities and the importance of metalimnetic phytoplankton to whole lake primary productivity. Ph.D. Dissertation. University of Notre Dame, Notre Dame, Indiana, USA.

Thackeray, S., I. Jones, and S. Maberly. 2008. Long-term change in the phenology of spring phytoplankton: Species-specific responses to nutrient enrichment and climatic change. *Journal of ecology* 96:523-535.

Tillmanns, A. R., A. E. Wilson, F. R. Pick, and O. Sarnelle. 2008. Meta-analysis of cyanobacterial effects on zooplankton population growth rate: species-specific responses. *Fundamental and Applied Limnology/Arciv für Hydrobiologie* 171:285-295.

U.S. Bureau of Land Management (USBLM). 2005. Wood River Wetland Monitoring Report, 2003–2005. U.S. Bureau of Land Management, Klamath Falls, Oregon, 51 p.

USFWS (U.S. Fish and Wildlife Service). 2012. Revised recovery plan for the Lost River sucker (*Deltistes luxatus*) and shortnose sucker (*Chasmistes brevirostris*). U.S. Fish and Wildlife Service, Pacific Southwest Region, Sacramento, California. xviii + 122 pp

Utermohl, H. 1958. Zur Vervollkommnung der quantitativen Phytoplankton-Methodik. *Mitt. Int. Ver. Limnol.* 9. 38 p

Walters, A. W., M. d. l. Á. G. Sagrario, and D. E. Schindler. 2013. Species-and community-level responses combine to drive phenology of lake phytoplankton. *Ecology* 94:2188-2194.

White, M. A., P. E. Thornton, and S. W. Running. 1997. A continental phenology model for monitoring vegetation responses to inter-annual climatic variability. *Global Biogeochemical Cycles* 11:217-234.

Willén, E. 1976. A simplified method of phytoplankton counting. *British Phycological Journal* 11:265-278.

Wilson, A. E., O. Sarnelle, and A. R. Tillmanns. 2006. Effects of cyanobacterial toxicity and morphology on the population growth of freshwater zooplankton: Meta-analyses of laboratory experiments. *Limnology and Oceanography* 51:1915-1924.

Winder, M. and D. E. Schindler. 2004. Climatic effects on the phenology of lake processes. *Global Change Biology* 10:1844-1856.

Wong, S.W., Barry, M.J., Aldous, A.R., Rudd, N.T., Hendrixson, H.A., and C.M. Doebring. 2011. Nutrient Release from a Recently Flooded Delta Wetland: Comparison of Field Measurements to Laboratory Results. *Wetlands* 31:433-443.

Wood, T. M., G. R. Hoilman, and M. K. Lindenberg. 2006. Water quality conditions in Upper Klamath Lake, 2002-2004. U.S. Dept. Interior, U.S. Geological Survey. Scientific Investigation Report 2006-5209.

Zuur, A. F., E. N. Ieno, and G. M. Smith. 2007. Principal component analysis and redundancy analysis. *Analyzing ecological data*: 193-224.